The Hong Kong Polytechnic University

Department of Mechanical Engineering

Multi-Objective Optimization of Active Constrained Layer Damping Treatment for Shape Control Application

by

HAU Lap Chi

Thesis submitted in partial fulfillment of the requirements for the degree of

MASTER OF PHILOSOPHY

in

Mechanical Engineering

October 2003

CERTIFICATE OF ORIGINALITY

I hereby declare that this thesis is my own work and that, to the best of my knowledge and belief, it reproduces no material previously published or written nor material which has been accepted for the award of any other degree or diploma, except where due acknowledgment has been made in the text.

_____ (Signed)

HAU LAP CHI (Name of student)

ABSTRACT

Vibration and shape control of structures are common subjects among the engineering community. In vibration control, suppressing the structural vibrations is of primary concern, while shape control means commanding the structure to take a desired shape when both subjected to changes of environment or load conditions. The science and technology developed in the latter topic has found applications in many areas; examples are in the re-adjustment of the focal point of antenna reflectors, and the improvement of aerodynamic and hydrodynamic performances of airfoils and blades respectively.

This thesis presents a study conducted to explore the feasibility of utilizing Active Constrained Layer Damping (ACLD) treatment for shape control of flexible structures. The key idea is to reduce the complexity and enhance the stability of the control system, since ACLD patches can not only change the shapes of flexible structures but also introduce passive damping. The present study deals with the dynamic modeling, analysis and optimization of an ACLD flexible beam for shape control.

First of all, the dynamic model of a flexible beam with distributed ACLD patches is formulated by means of the Finite Element Method (FEM). The Golla-Hughes-McTavish (GHM) model is employed to capture the frequency-dependent characteristic of the viscoelastic materials. With this model, a parametric study of the ACLD flexible beam is conducted by computer simulations to understand the effects of treatment length

and location, the layer physical and geometrical properties, and control gain values on the damping characteristic of the flexible beam.

The optimal performance of the system in this application is defined by several objective functions. Both open and closed-loop performances are taken into account. With respect to open-loop control, certain amount of passive damping is necessary for stability and fail-safe consideration. Meanwhile, a heavy structure is undesirable. For closed-loop control, the minimization of the error between the desired and achieved shapes should be another concern. Based on the previous parametric study, specific design variables in addition to the control gains can be chosen and the inequalities can be set up for the respective constraints. Instead of aggregating the objectives with a weighting function, the Multi-Objective Genetic Algorithm (MOGA) is employed, and a computer code is developed to solve this multi-objective optimization problem.

Pareto solutions are successfully obtained. A clear tradeoff between the total treatment weight and passive damping is found. Transient behavior is analyzed by numerical simulations. Results show the feasibility of using ACLD patches for the shape control of structures. Effects of external disturbances on the shape control system are also examined by applying different types of loadings to the system. It is demonstrated that for the loads under consideration, closed-loop control can regulate the actuator voltages to correct the destroyed shapes. Comparison is also made between open and closed-loop controls. Simulation results confirm that the closed-loop control outperforms the open-loop one in terms of disturbance-rejection ability as well as settling time.

LIST OF PUBLICATIONS

[1] **Hau, L.C.** and Fung, E.H.K. "Performance characteristics of a smart flexible beam with distributed ACLD elements". *Proceedings of 2002 ASME International Mechanical Engineering Congress & Exposition*, 17-22 Nov. 2002, New Orleans, L.A., U.S.A. Paper No. IMECE2002-33980

[2] **Hau, L.C.** and Fung, E.H.K. "Effect of ACLD treatment configuration on damping performance of a flexible beam". *Journal of Sound and Vibration*, Vol. 269, pp.549-567 (2004)

[3] **Hau, L.C.** and Fung, E.H.K. "Integrated optimization of ACLD treatment for shape control of flexible beams using multi-objective genetic algorithm". *Proceedings of 2003 ASME International Mechanical Engineering Congress & Exposition*, 16-21 Nov. 2003, Washington, D.C., U.S.A. Paper No. IMECE2003-41242

[4] **Hau, L.C.** and Fung, E.H.K. "Multi-objective optimization of ACLD treatment for shape control of flexible beams". *Smart Materials and Structures*, (2004) (*Accepted for publication*)

ACKNOWLEDGMENTS

I would like to thank several mentors for their help and guidance. First of all, I sincerely appreciate the guidance, encouragement, and enthusiastic support from my supervisor, Dr. Eric H.K. Fung. He was always available when I needed help and I do not have enough words to express my gratitude for that. Also, I would like to express a special thank to Mr. K.L. Li, the technical staff at the Measurement and Control Laboratory of The Hong Kong Polytechnic University, for his excellent technical support involving computers. Finally, I would like to thank the Research Committee of The Hong Kong Polytechnic University for funding this work in the form of research studentship.

TABLE OF CONTENTS

LIST OF FIGURES

LIST OF TABLES

NOMENCLATURE

b	Width of the base beam
C_a	Capacitance of the piezo-sensor layer
d_{31}	Piezoelectric constant
D	Electrical displacement
$[D]$	Global damping matrix
e	Error function
E	Electric field
E_b	Young's modulus of the base beam
E_p	Young's modulus of the piezoelectric constraining layer
E_s	Young's modulus of the piezo-sensor layer
f_1	Frequency of the first mode
f_2	Frequency of the second mode
f_3	Frequency of the third mode
$\{f_c\}_e$	Nodal piezoelectric force vector
$\{f_d\}$	Global external disturbance force vector
G^∞	Equilibrium value of the shear modulus
G	Shear modulus of the viscoelastic layer
I_b	Moment of inertia about neutral axis of the base beam
I_p	Moment of inertia about neutral axis of the piezoelectric constraining layer
K_{st}	Position sensor gain
K_d	Derivative control gain for vibration control
K_p	Proportional control gain for vibration control

K_P	Proportional control gain for piezo-senor feedback
K_I	Integral control gain for piezo-sensor feedback
K_D	Derivative control gain for piezo-sensor feedback
$k_p^{'}$	Proportional control gain for position sensor feedback
$k_i^{'}$	Integral control gain for position sensor feedback
$k_d^{'}$	Derivative control gain for position sensor feedback
k_p	Equivalent Proportional control gain for position sensor feedback ($=K_{st}k_p^{'}$)
k_i	Equivalent Integral control gain for position sensor feedback ($=K_{is}k_i^{'}$)
k_d	Equivalent Derivative control gain for position sensor feedback ($=K_{is}k_d^{'}$)
$[K]_e$	Element stiffness matrix
$[K]$	Global stiffness matrix
l	Length of ACLD patch for parametric study
L_e	Element length
L	Lagrangian of the system
L_1	Length of the first ACLD patch for shape control
L_2	Length of the second ACLD patch for shape control
L_3	Length of the third ACLD patch for shape control
$[M]_e$	Element mass matrix
$[M]$	Global mass matrix
O_s	Maximum overshoot
P_1	Position of the first ACLD patch for shape control
P_c	Crossover rate
P_m	Mutation rate
$\{q\}_e$	Element nodal displacement vector
$\{q\}$	Global displacement vector
Q	Induced electric charge

s	Laplace operator
S_2	Spacing between the first and second ACLD patches for shape control
S_3	Spacing between the second and third ACLD patches for shape control
t_b	Thickness of the base beam
t_p	Thickness of the piezoelectric constraining layer
t_s	Settling time
t_v	Thickness of the viscoelastic layer
T_e	Total kinetic energy of an ACLD beam element
u_b	Axial displacement of the neutral axis of the base beam
u_p	Axial displacement of the neutral axis of the piezoelectric constraining layer
u_v	Axial displacement of the neutral axis of the viscoelastic layer
U_e	Total potential energy of an ACLD beam element
V_c	Control voltage
V_d	Desired piezo-sensor output
V_{dt}	Desired position sensor output
V_s	Piezo-sensor output voltage
V_{st}	Position sensor output
w_d	Desired transverse displacement
w	Transverse displacement of the base beam
W_d	Virtual work done by external disturbance force
W_p	Virtual work done by the induced strain in the piezoelectric layer
$\{\hat{z}\}_e$	Dissipation coordinates
ε	Mechanical strain
σ	Mechanical stress
S_{11}^{E}	Elastic compliance constant

ε_{33}^{r}	Dielectric constant
ξ	Modal damping
δ	Node error
θ	Rotation of the base beam
γ	Shear strain of the viscoelastic layer
ψ	Shear angle of the viscoelastic layer
ρ_b	Density of the base beam
ρ_p	Density of the piezoelectric constraining layer
ρ_v	Density of the viscoelastic layer
Φ_1	Objective function 1
Φ_2	Objective function 2
Φ_3	Objective function 3
ζ	Desired shape function
$\hat{\alpha}, \hat{\omega}, \hat{\zeta}$	GHM constants

CHAPTER 1

INTRODUCTION

1.1 BACKGROUND

As a consequence of the increasing demand on high-performance system, shape control of structures becomes more and more contributing, and is a topic of current interest. In general, shape control means commanding the positions of a certain number of points on a structure to track the desired values. Most aircraft wings are designed to produce minimum drag under one particular flying condition, while the flying condition actually varies continuously throughout the flight. It is therefore expected that the wing shape should be able to change in response to the change of flying condition. On the other hand, shape control can also be employed to maintain the precise shape of a structure. In some large space systems, such as antenna reflectors, maintaining precise surface shape has been a challenging task. The surface errors are introduced by manufacturing errors, thermal distortion, moisture and material degradation. When these happen, adjustable antennas could simply self-correct. The ability for antennas to change shape can solve another common problem: Earth's atmosphere scatters satellite signals the same way water scatters a beam of light. For this reason, not all transmitted information reaches a target. Standard antennas cannot correct for that, but an adjustable antenna can navigate

signals through turbulent atmospheric conditions like storms. It can deliver more information using the same amount of power [1].

Traditionally, shape control concept employs axial or translational actuators as truss elements of active ribs to reshape the structure by deforming it. However, this has a number of drawbacks. This technique creates discontinuities over the surface. To obtain a smoother surface, a large amount of actuators are required, thus adding weight and redundancy to the system. In view of the drawbacks associated with the conventional actuators, considerable efforts have been devoted to the development of other shape-change techniques. Recently, the use of compliant mechanisms and smart material actuators are two common solutions for achieving a smooth shape change. Compliant mechanisms are one-piece flexible structures, which exploit the inherent mechanical deformation of materials. They are a class of mechanisms that achieve mobility through elastic deformation of one or more of their constituent segments. They are light in weight and generate a variety of precise motions. As for smart material actuators, they produce displacement and forces when exposed to external energy fields, such as electricity input or heat. For instance, when a piezoelectric material is attached to the surface of a flexible structure and expands, the structure surface bends. When it contracts, the structure surface bends to the other direction. With that movement, the overall shape of a structure can be changed.

The above-mentioned systems are made of flexible structures. These structures must sacrifice stiffness in order to achieve the reduced weight requirement. However, low

stiffness can result in structures vulnerable to vibration and hence in reduced precision and performance. They are also lightly damped because of the low internal damping of the materials used in their construction, which will cause large amplitude vibration. As a result, when it comes to flexible structures, another problem necessary to tackle is vibration suppression.

In this research, an alternative approach for shape control of flexible structures is developed. The proposed approach utilizes the Active Constrained Layer Damping (ACLD) treatment idea [2] for shape control of flexible structures. In general, ACLD consists of a viscoelastic layer sandwiched between two piezoelectric layers. This three-layer composite is bonded to the host structure. This smart constraining layer damping treatment, as shown in Figure 1-1, has built-in sensing and actuation capabilities. The sensing is provided by the piezoelectric layer directly bonded to the host structures, whereas the actuation is generated by the other piezoelectric layer which acts as an active constraining layer. As the host structure undergoes bending, the viscoelastic layer undergoes shear deformation and hence provides damping. Based on the sensor feedback, the controller actuates the piezoelectric constraining layer, by application of electric field, to further enhance the shear in the viscoelastic layer as well as to exert active control forces to the host structure.

The advantage of using ACLD treatment for shape control of flexible structures is obvious. It reduces the complexity and enhances the stability of the control system. It is superior to conventional actuators for its simple control architecture, since the actuators

are directly attached to the host structures. It is also better than other smart material actuators, as ACLD patches not only achieve the goal of shape control by providing strain to the host structures, but also introduce passive damping to the system, thus enhancing the stability to the system. In other words, ACLD treatment integrates the vibration and shape control into a single system.

This research also explores the optimization issue of ACLD treatments on flexible structures. The optimal performance of this shape control system can be defined by several objective functions, and there are often tradeoffs between different objective functions. Further, the performance of the system is highly dependent on the selection of design variables. As a result, designing an ACLD shape control system becomes a complicated problem. The current research addresses the multi-objective optimization for the shape control of a flexible beam.

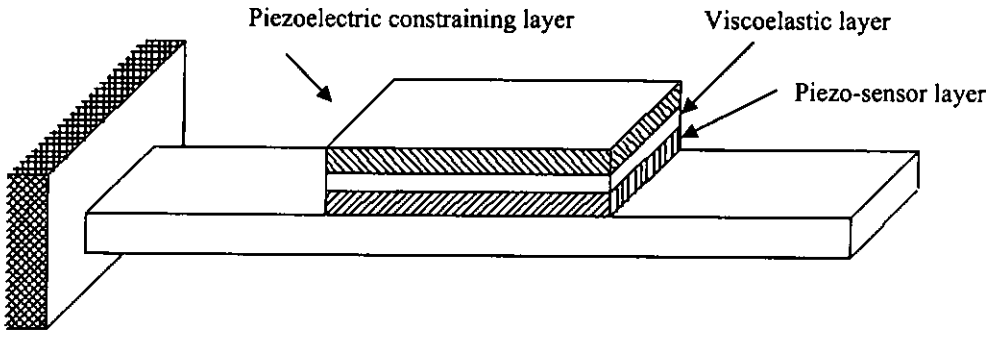

Figure 1-1 Schematic of ACLD treatment

1.2 LITERATURE REVIEW

This literature review is separated into three sections according to the three main aspects of this research, namely: shape control of structures, active constrained layer damping treatment, and optimal design of structures.

1.2.1 Shape Control of Structures

As mentioned above, there are mainly three techniques available to accomplish shape change in structures. These are (1) conventional axial actuators, (2) compliant mechanisms, and (3) smart material actuators.

Austin *et al.* [3-5] did a series of work, both theoretical and experimental, on the static shape control for adaptive wings by employing internal translational actuators. A general method was developed for static shape control of flexible structures with internal actuators, and a physical model of an adaptive rib was constructed. A finite element model of the structure, without the actuators present, was employed to obtain the multiple-input, multiple-output control gains for actuator-load control and actuator-displacement control. Open-loop control experiments of the unloaded structure and closed-loop control experiments of the load structure were conducted.

Although conventional actuators can create a shape change in the wings, the shape achieved is not smooth due to the large separation between the actuators. Other shape-change techniques have thus been developed. The idea of shape change by compliant mechanisms is that the energy from the actuator is transferred via compliant

mechanisms to deform one given shape to another desired shape. The basic premise is to distribute the actuation energy of a remote actuator via compliant transmission (distributed compliance) instead of using a plethora of actuators (distributed actuating systems) [6]. In fact, the use of compliant mechanisms for shape control of structures was first proposed by Saggere and Kota [7]. They used compliant mechanisms, which are powered by a single input actuator, to effectuate desired shape changes in generally curved beam segments. The key design issue in this approach is the synthesis of a suitable compliant mechanism for the task. Hence, a systematic procedure for synthesis of such compliant mechanisms was developed, and was illustrated through an example of camber shaping of an idealized airfoil. Later, Lu and Kota [8] considered the simultaneous optimization of the topology and dimensional aspects of a compliant mechanism for shape-change applications. They proposed a new approach for synthesizing complaint mechanisms that could change an initial curve shape into a desired target shape in the same plane. The design domain was initially discrete with a network of beam elements. Preliminary results were presented for two different reference shapes, and the optimization was done by Genetic Algorithm (GA).

Smart material actuators are another strategy for shape control. Chaudhry and Rogers [9] studied the bending and shape control of beams by Shape Memory Alloy (SMA) actuators. Shape control of Nitinol-reinforced composite beams was studied by Baz *et al.* [10]. The mathematical model developed describes the interaction between the shape memory effect of the composite beams and the thermally induced shape memory effect of the Nitinol strips. Song [11] presented the design and experimental results of active

position control of a SMA wire and a SMA wire actuated composite beam. The beam under consideration was aluminum honeycomb with SMA wires embedded in one of its face sheets for active shape control. Oh *et al.* [12] proposed a method for shape control of double-plate structures by combining the concentrated force from SMA wires and moments from piezoceramic patches. The possibility of shape control was examined by finite element analysis. Numerical and experimental results were presented.

Irschik [13] provided a comprehensive review of shape control of structures by piezoelectric actuation. Donthireddy and Chandrashekhara [14] developed a finite element model to study the shape control of laminated beams with surface bonded or embedded actuators. The formulation was based on a layer-wise theory and was applicable for the analysis of both thin and thick laminated beams. With specified applied voltages, the influences of stacking sequence and boundary conditions on the change in shape were examined. Jenkins [15] designed an intelligent controller based on feedback error learning, which is capable of extracting performance information from precise membrane and subsequently using this information to achieve maximum surface precision. The solutions of the deflection of a beam simultaneously induced by piezoelectric actuators and other external actions for different boundary conditions were given analytically by Yang and Ngoi [16]. It was shown that the piezoelectric actuators could only deform a beam by a quadratic or cubic curve due to their actuation bending moments occurring at the ends of the actuators in a pair form. Kekana [17] proposed a control model simulating the effects of the control potential on the static configuration

of a piezo-elastic structure. A simply supported composite beam attached with collocated piezoelectric elements for measuring and actuating was considered.

Some researchers employed shape control to prevent the structure shapes from being distorted by external disturbances. Wang *et al.* [18] formulated a finite element model for the plate with distributed piezoelectric sensors and actuators. Based on this model, a general method was developed for the static shape control of the intelligent structure. The plate was originally flat and was simply supported along two parallel edges and free on other two edges. The plate was deformed into a curve shape by a force. Also, two cases were given. The first used passive control by directly apply voltages to the piezo-actuators, while the second used active control system by implementing the feedback control law. Tong *et al.* [19] presented analytical models and FEM solution for a thin composite plate with piezoelectric actuators surface embedded or bonded in a bimorph arrangement. Three shape optimization control problems – the applied voltage, actuator layout, and actuator number optimization, were formulated and solved. Two numerical examples were presented as well. Lin and Hsu [20] proposed a novel scheme capable of controlling deflection shape of laminated beam plates without relying on information of external loads and boundary conditions. Layers of piezoelectric sensors and actuators trimmed to sine shapes were embedded in the laminated beam plate. An adaptive control algorithm was used for achieving expected control effects. Clamped-clamped and simply support beam plates under arbitrary loads were used for illustrative purposes. Bruch *et al.* [21] implemented the shape control of beams under general loading conditions by using piezoelectric actuators to provide the control forces. In a paper by

Adali *et al.* [22], the shape of a laminated beam was controlled by an optimally placed piezo-actuator so as to minimize its maximum defection. In their studies, the locations and magnitudes of the external loads were not known a priori and belonged to a specified load uncertainty domain. Numerical results were given to assess the effect of load uncertainty and actuator length on the actuator location and the design efficiency which was defined with respect to the corresponding uncontrolled beam. Sheng and Kapania [23] used piezoelectric actuators to correct the surface thermal distortions, by employing the genetic algorithms to find out the appropriate locations for the piezo-actuators.

On the other hand, some researchers utilized piezoelectric actuators to drive the structures to a given shape. Chandrasekhara and Varadarajan [24] developed a finite element model for beams with piezoelectric actuators. To allow for the effect of transverse shear deformation, the third order shear deformation theory was adopted. Their work included both open and closed loop control of the beam shape. In a follow-up paper [25], they extended their work to consider the plate structures. Agrawal and Treanor [26] presented both analytical and experimental results on optimal placement of piezoelectric actuators for shape control of beam structures. Wang *et al.* [27] used analytical expressions and optimality conditions for determining the input voltages required in shape matching of a cantilevered laminated beam integrated with piezoelectric patch actuators. To cater for the effect of transverse shear deformation, the first order shear deformation beam theory was adopted in the formulation. The

expressions were used to generate bending results and input voltages for shape matching of cantilever beams with various symmetric and non-symmetric lamination designs.

The models developed from the above studies are static. This means that direct application of voltages to the piezoelectric actuators can lead to a successful shape change, but causes transient vibrations of the structures during the shape change process. Fitzpatrick [28] proposed a mathematical framework for the deformation of a flexible beam to a desired shape using piezoceramic patch control. LQR control was applied to obtain a control law for driving the beam from an initial shape to a desired shape. The numerical test was made on an Euler-Bernoulli cantilever beam. Kalaycioglu and Silva [29] proposed a method for the minimization of vibrations of spacecraft appendages during shape control using piezoceramic actuators.

1.2.2 Active Constrained Layer Damping (ACLD) Treatment

Active Constrained Layer Damping (ACLD) treatment is an extension of the original Passive Constrained Layer Damping (PCLD) idea. In a typical ACLD treatment, a viscoelastic layer is sandwiched between a piezoelectric (such as piezoceramic) layer and the host structure. This configuration has been studied by numerous researchers. In this configuration, as shown in Figure 1-2, when the structure vibrates, it introduces passive shear deformation field in the viscoelastic layer. If an active signal is used to control the length of the constraining piezoelectric layer, an active shear field can be introduced. If this active shear deformation is phased such that it adds to the passive shear deformation, the total shear deformation in the viscoelastic layer would become

higher than that of traditional PCLD treatment. This means higher damping performance. Also, the piezoelectric layer applies active forces on the structure and hence could introduce some direct active damping. Benjeddou [30] has given a comprehensive review on hybrid active-passive structural vibration control.

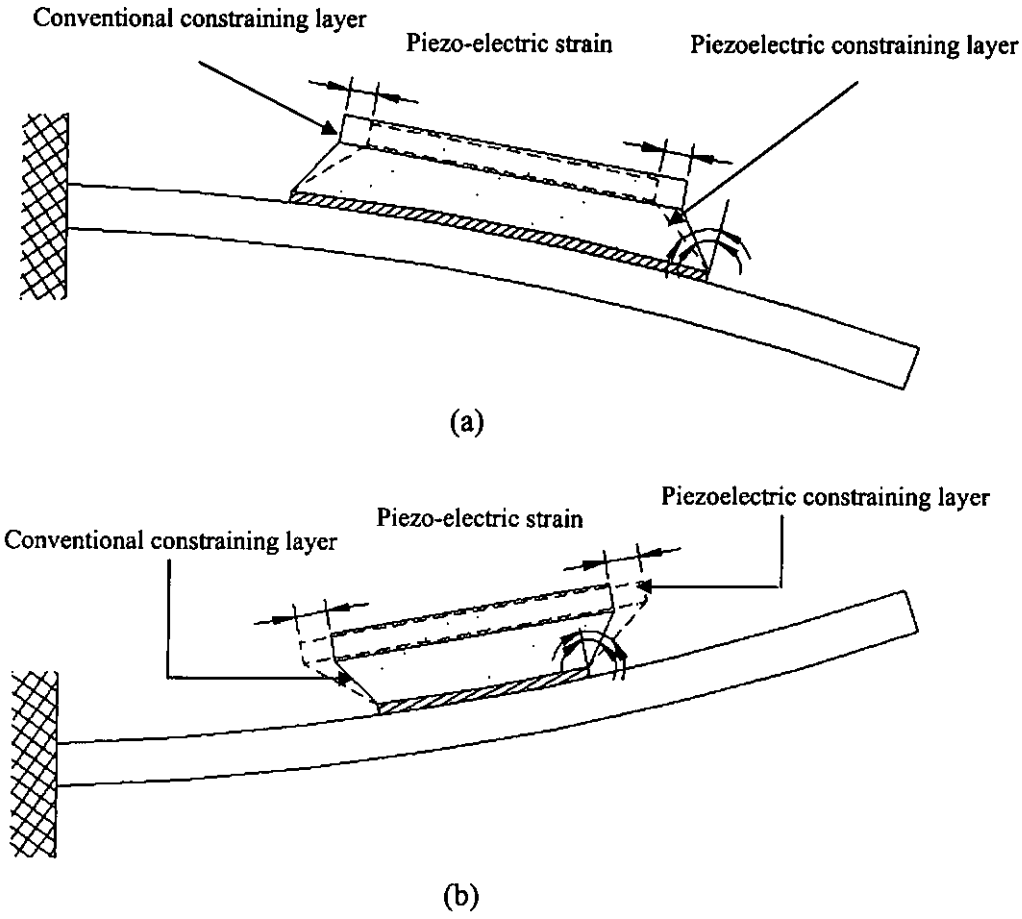

Figure 1-2 Operating principle of ACLD treatment

Plump and Hubbard [31] developed a sixth order partial differential equation (PDE) for an active constrained layer (ACL) damper which used PVF2 as the constraining layer. No analysis and experimental results were presented. Agnes and Napolitano [32] illustrated that the use of an ACL could significantly improve the performance of a passive constrained layer (PCL) damping treatment.

Baz and Ro [33] proposed an ACL configuration with an additional piezoelectric sensor layer between the host structure and the viscoelastic layer. They demonstrated the feasibility and merits of the ACL concepts and indicated that the ACL treatment using proportional and derivative (PD) control was superior to the PCL system. Baz and Ro [34] also developed a beam finite element model, and presented the performance characteristics of the ACL treatment, both analytically and experimentally. Baz and Ro [35] conducted a study on a beam with partial ACLD treatment. The effects of treatment lengths, locations and control gains were investigated. Ray and Baz [36] extended the application of ACLD treatment to control the nonlinear vibration of beams.

Shen [37] derived eighth order differential equations which govern the bending and axial vibrations of a beam. Compared to the PCL treatments, numerical results showed that the ACL could produce significant damping. In addition, the bending vibration control of composite and isotropic plates through the use of ACL treatment was studied by Shen [38]. Shen [38] also formulated ACL systems through a variational approach to study the work-energy relation of ACL and to identify the damping mechanisms of ACL

treatments. The observability, controllability, and stability of ACL systems were also investigated [39].

Nostrand and Inman [40] developed a beam finite element model, using the Augmenting Thermodynamic Fields (ATF) method to model the viscoelastic layer in time domain. Several control schemes applied to the ACL system were examined. Some experiments were implemented to verify the simulation results. Lesieutre and Lee [41] developed a finite element model for beams having segmented ACL treatment. The Anelastic Displacement Fields (ADF) method was used to model the viscoelastic layer in time domain. Trindade *et al.* [42, 43] developed an electromechanically coupled finite element model to handle the active-passive damped multi-layer sandwich beams. The frequency-dependence of the viscoelastic material was captured through the ADF method. Both Lam *et al.* [44] and Liao and Wang [45] used the Golla-Hughes-McTavish (GHM) method to model the viscoelastic behavior in the ACL configuration. Lim *et al.* [46] developed a three-dimensional finite-element closed-loop model to predict the effects of active-passive damping on a vibrating structure. Lee and Kim [47] formulated a spectral finite element model for beams with ACLD treatment. They compared the frequency responses predicted by analytical representation with those by GHM models.

Azvine *et al.* [48] presented a concept for an ACL configuration in which the piezoelectric actuator is bonded to (not replacing) the constraining layer. They considered the effect of actuator location on modal damping of a cantilever beam using velocity feedback. Veley and Rao [49] showed that all of the active, passive, and hybrid

damping techniques could be appropriate when designing a damped structure. Lam *et al.* [50, 51] investigated the treatment of a beam with separate active and passive constrained layer elements. Two new hybrid variations were introduced. Yellin and Shen [52] analyzed the self-sensing ACL treatment originally proposed by Dosch and Inman [53]. In this treatment, the piezoelectric constraining layer was used simultaneously as both a sensor and actuator.

Liao and Wang [54] conducted a study comparing the ACL treatment with the purely active and passive approaches. With a LQR (linear quadratic regulator) optimal control formulation, analysis illustrated that the active piezoelectric action with proper feedback controls will enhance the damping ability of the baseline passive system. On the other hand, it was also shown that the viscoelastic layer would reduce the direct control authorities from the active source to the host structure. With some parameter combinations, the ACL configuration could require more control effort while achieving less vibration reductions as compared to a purely active system. Liao and Wang [45] further investigated the viscoelastic material effects on ACL based structures. Specific interests are on how the viscoelastic parameters would influence the passive damping ability, the active action authority, and their effect on active damping in an ACL configuration. The study identified the viscoelastic parameter regions that would provide the best active-passive hybrid actions. The results of this research could be used to synthesize optimal ACL structures and could outperform both the purely passive and active systems.

The Enhanced Active Constrained Layer (EACL) damping treatment idea was developed to further improve the performance of ACL treatment [55]. In this treatment, the PZT constraining layer is directly connected to the base structure by using a set of edge elements at the end of the treatments. It was demonstrated that these edge elements could increase the transmission of active control forces from the PZT to the base structure. Later, Liu and Wang [56] conducted a non-dimensional parametric study of EACL damping treatments.

1.2.3 Optimal Design of Structures

Extensive efforts have been made to optimally design passive and active constrained layer damping treatments of vibrating structures. These efforts aim to maximize the modal damping ratios and modal strain energies by determining the optimal material and geometric parameters of the treatments, or minimize weight by selecting the optimal length and location. Marcelin *et al.* [57, 58] used genetic algorithms and beam finite elements to maximize the damping factor for partially treated beam. The design variables were the dimensions and locations of the patches. Chen and Huang [59] studied the optimal placement of constrained layer damping (CLD) treatment on a rectangular plate. A restriction of total treatment thickness was assumed. An objective function including structural damping ratios, resonant frequency shift and CLD thickness was designed, where the structural damping was the main performance index and the frequency shift and CLD thickness played as penalties. Topographical and complex optimal solution techniques were employed in searching for the optimal value of CLD treatment. Pau *et al.* [60] compared several optimization algorithms for CLD

patch layout to minimize the maximum vibration response of the odd modes of a simply-support beam. The design variables were the CLD patch location and length. Baz and Ro [61] used Univariate Search Method (USM) to optimize the performance of the ACLD treatments by selecting the optimal thickness and shear modulus of the viscoelastic layer as well as the control gain for a fully treated beam when proportional and derivative controllers are used. In a later study, Ro and Baz [62] extended their previous work to consider the optimum design and control of partial ACLD treatments. Huang *et al.* [63] studied the optimal size, length, and thickness of treatment subjected to a total thickness restriction for cases of ACL, PCL, and pure active control. They showed that the ACL treatment provides better vibration suppression than PCL, and even outperforms pure active control for low gain applications.

On the other hand, in designing piezoelectric active structures, it is known that many factors can affect the system performance. Thus efforts to optimize these parameters are essential to obtain high performance system. Clark and Fuller [64] studied the location of a piezoelectric actuator and both the size and location of a PVDF sensor for active structural acoustic control. An optimization study on design of length and placement of bonded piezo-actuators in active control of a flexible beam was performed by Devasia *et al.* [65] in which collocated actuators and only strain piezo-sensor were used. Wang *et al.* [66] presented a formulation of the optimization problem for the placement and sizing of piezoelectric actuators in adaptive control system. Main *et al.* [67] studied the optimum thickness of a piezo-actuator embedded within or bonded onto a flexible structure, and also studied its optimum distance from structural centre line. They used

the induced moment producing a bending curvature as the cost function. In a paper by Nam *et al.* [68], optimization technique was applied to determine the best geometry (placement, thickness, width and length) of piezo-actuators for flutter suppression. Kapania and Sheng [69] used the genetic algorithm to solve an optimization problem to find the locations of piezoelectric actuators and the corresponding voltages that gave the best correction to the surface thermal distortions under a given type of thermal loads. Kim *et al.* [70] and Varadan *et al.* [71] determined the optimally designed piezoelectric actuators in terms of location, size and applied voltage. Bruch *et al.* [21] determined the optimal locations and lengths of piezo-actuator for the min-max deflection of beams. They showed that the optimal voltage applied to the actuators depends on the actuator length and location. Agrawal and Treanor [26] studied the optimization for the shape control of beam structures. The objective was to determine the optimum piezoceramic actuator locations and voltages to minimize the error between the desired and achieved shapes, using embedded Nader and Mead simplex algorithms.

Regarding the fact that piezoelectric actuator placement affects both the structural parameter and the control parameter, integrated structural and control optimization is indispensable. The optimal design of a smart structure featuring a piezoelectric actuator, sensor and a simple controller was studied by Kim and Ko [72]. The locations and sizes of the piezoelectric actuator and sensor as well as the negative feedback gain were taken as design variables in the optimal design procedure. The objective function was to minimize the total radiated sound power from the structure. Yousefi-koma and Vukovich [73] developed an optimization procedure for finding the optimal location and

dimensions of piezo-actuators in active control systems. Three criteria – (1) maximizing the overall damping ratio of the closed loop system, (2) minimizing the overall real part of the dominant eigenvalues of the controlled system, and (3) minimizing LQR cost function, were used and compared, which led to an optimal configuration of the actuators when the weight and geometry limitations were important. Wang *et al.* [74] presented a new approach for simultaneous optimization of the intelligent structure and the control system to suppress the vibration of the structure. They converted the problem into a multi-objective optimization problem in which the structural variables and the feedback gain were both treated as independent design variables. The vibration control performance index was chosen as the objective function, and the constraints include structural mass, eigenvalues of the closed-loop system, and the actuator force. Zhang *et al.* [75] studied the problem of the integrated optimization of piezoelectric actuator and sensor location and feedback gains for the active control of vibrations. The performance function developed was based on the maximization of the dissipation energy due to a control action. To deal with the nonlinear optimization problem, a float-encoded genetic algorithm (FGA) and the corresponding genetic operations were proposed. Beri et *al.* [76] developed a multi-objective optimization procedure to address the integrated structures/control design of composite plates with surface bonded segmented active constrained layer damping treatment by using the Kresselmeier-Steinhauser (KS) function approach. Objective functions and constraints included damping ratios, structural weight and natural frequencies. Design variables included the ply stacking sequence, dimensions and placement of segmented ACL. The optimal designs showed improved plate vibratory characteristics and led to a reduction in structural weight. Liu

and Wang [77] investigated the feasibility of integrating the EACL and active-passive hybrid constrained layer (HCL) treatments to achieve a better combination of the system closed-loop damping and open-loop (fail-safe) damping. The focus was to maximize the system closed-loop damping while maintaining an open-loop damping margin for fail-safe reasons. Optimization routines were used to search for the best design parameters: the optimal control gain, the stiffness of the edge elements and the active material coverage ratio in the constraining layer. Maxwell and Asokanthan [78] proposed a method to determine the optimal placement and controller design for multiple distributed actuators to reduce the vibrations of flexible structures. In particular, application of piezoceramic patches to a horizontally slewing single-link flexible manipulator was investigated. The optimization method used simulated annealing and allowed placement of any number of distributed actuators of unequal length. They also designed a liner-quadratic-regulator controller as part of the optimization procedure. The measures of performance used were the total mass of the system and the time integral of the absolute values of the hub and tip position errors.

1.3 RESEARCH OBJECTIVE

The overall objective of this research is to explore the feasibility of adding ACLD treatments to flexible structures for shape control application. The studies of ACLD treatments for vibration suppression have shown promising results, but the application of such treatment for shape control is an unexplored topic. Designing such kind of shape control system is challenging, since there are coupling effects and interactions between the structural variables and the controller. In this study, two main issues are investigated. First, the influences of the ACLD treatment parameters as well as the control gains on the system performance are determined. Second, the design of the ACLD treatments is treated as a multi-objective optimization problem such that both the structural and control design objectives are optimized without weighting among them. This combination is challenging, as the two problems often have different criteria, and there exist tradeoffs between them.

To achieve the above-stated objective, the major tasks to be accomplished have been identified and are listed below:

(1) To establish a dynamic model of the flexible beam with distributed ACLD patches.

Predicting dynamic behaviour of a system is indispensable for control design. It is therefore essential to first develop a mathematical model which describes the dynamic behavior of the ACLD flexible beam. Considering the distributed nature of the ACLD patches, and to facilitate time-domain analysis, the finite element method, in conjunction with the Golla-Hughes-McTavish (GHM) viscoelastic model, is employed to formulate the dynamic model.

(2) To study the effects of the ACLD treatment parameters on the system performance.

The effect of treatment patch length and location, the layer physical and geometrical properties as well as the control gains on the system performance are determined by numerical simulations. With this study, specific design variables in addition to the control gains can be chosen and the inequalities can be set up for the respective constraints to be imposed on the design of the system.

(3) To formulate the integrated structural and control optimization problem by using the Multi-Objective Genetic Algorithm (MOGA).

The design is treated as a multi-objective optimization problem. In order to avoid local minima, and weighting the objective functions, a stochastic approach, called MOGA, is used to solve the optimization problem. To implement the optimization, a program, with the commercial software package MATLAB as the working environment, is developed.

(4) To evaluate the feasibility of the design method by numerical simulations.

A parabolic shape function is considered. Static and dynamic loadings are applied separately to the system, so as to show the effects of external disturbances on the control systems.

1.4 THESIS OUTLINE

This thesis consists of six chapters.

Chapter 1 gives the background information, literature review and research objective of this thesis.

Chapter 2 describes the formulation of the finite element based mathematical model of a flexible beam structure with distributed ACLD patches. The mathematical model developed is verified by comparison with other models in the literature and the results are presented.

Chapter 3 presents the results of the parametric study. The effects of the thickness of the viscoelastic and piezoelectric constraining layers, the length and location of the ACLD treatment on the vibration characteristics of the flexible beam are shown and analyzed.

Chapter 4 contains the description of the optimization formulation. It introduces the objective functions, design variables and the constraints used for the design of shape control system as well. The idea and philosophy of MOGA is also outlined.

Chapter 5 presents and discusses the optimization results of the multi-objective design problem. The effects of external loads on the shape control system are studied.

Chapter 6 gives a conclusion summarizing the present study and some suggestions for future work.

CHAPTER 2

MATHEMATICAL MODEL DEVELOPMENT

In this chapter, a finite element model of a flexible beam with distributed Active Constrained Layer Damping (ACLD) treatment is developed, based on the sandwich theory. The energy approach, based on Hamilton's principle, is used to derive the equations of motion. The Golla-Hughes-McTavish (GHM) method is employed to account for the frequency-dependent characteristic of the viscoelastic material. Comparisons are made with other models available in the literature in order to validate the present model.

2.1 ASSUMPTIONS

The finite element model is developed based on the following assumptions:

(1) The shear deformations in both the base beam and piezoelectric layer are negligible.

(2) The rotary inertia is negligible.

(3) The transverse displacement is the same for all layers.

(4) The Young's modulus of the viscoelastic layer is negligible compared to those of the beam and piezoelectric materials.

(5) Linear theories of elasticity, viscoelasticity and piezoelectricity are used.

(6) There is perfect continuity at the interface, and no slip occurs between the layers.

(7) The applied voltage is uniform throughout the piezoelectric constraining layer.

(8) The physical properties are uniform over the beam.

(9) The piezoelectric sensor and the base beam are considered to be perfectly bonded and reduced to a single equivalent layer.

2.2 FINITE ELEMENT FORMULATION

The beam model with distributed ACLD patches is divided into two types of elements (i) ACLD beam elements and (ii) plain beam elements.

2.2.1 Kinematics Relationships

The geometry and deformation of an ACLD beam element is shown in Figure 2-1.

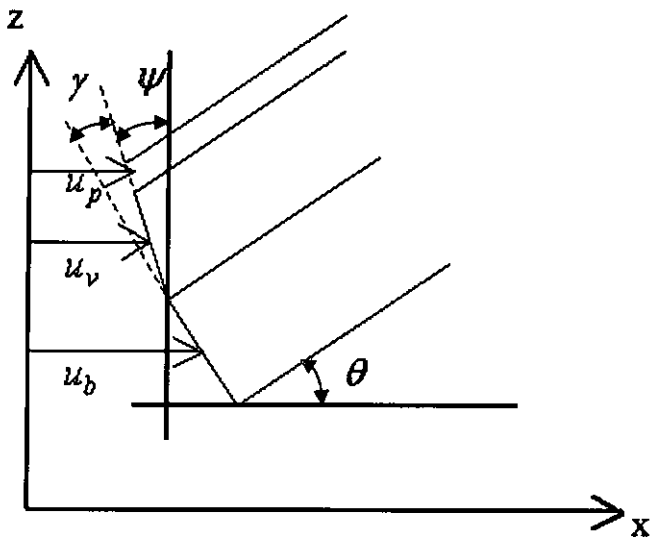

Figure 2-1 Geometry and deformation of a beam with ACLD patch

Let the axial displacements of the neutral axis of the base beam, the viscoelastic layer, and the piezoelectric constraining layer be u_b, u_v, and u_p respectively. The subscripts b, v, and p refer to the base beam, the viscoelastic layer and the piezoelectric constraining layer respectively. The transverse displacement is denoted by w, the rotation by $\theta (= \frac{\partial w}{\partial x})$, the shear angle of the viscoelastic layer $\psi (= \frac{\partial u_v}{\partial z})$, and the shear strain of the viscoelastic layer by γ. They are related by the following equation.

$$\theta = \gamma + \psi \tag{2.1}$$

With perfect bonding conditions, the following kinematics relations can be derived:

$$u_v = u_b - \frac{t_b}{2}\theta - \frac{t_v}{2}\psi \tag{2.2}$$

$$u_p = u_b - \left(\frac{t_b + t_p}{2}\right)\theta - t_v\psi \tag{2.3}$$

Substituting Eq. (2.1) into Eqs. (2.2) and (2.3),

$$u_v = u_b - \left(\frac{t_b + t_v}{2}\right)\theta + \left(\frac{t_v}{2}\right)\gamma \tag{2.4}$$

$$u_v = u_b - \left(\frac{t_b + 2t_v + t_p}{2}\right)\theta + t_v\gamma \tag{2.5}$$

where t_b, t_v, and t_p are the thickness of the base beam, the viscoelastic layer, and the piezoelectric constraining layer respectively.

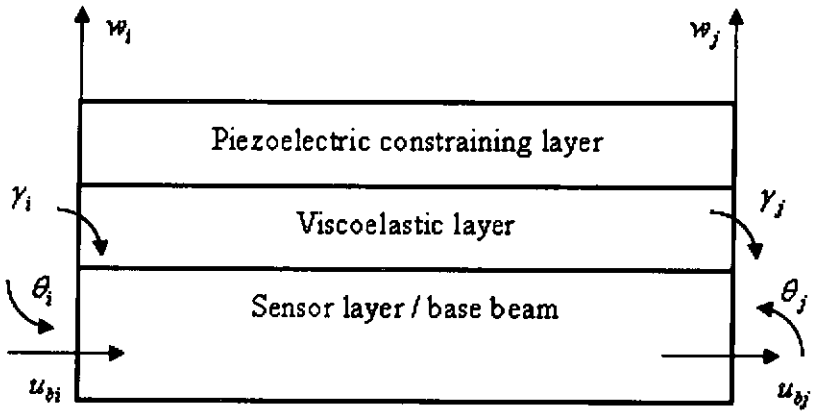

Figure 2-2 Nodal displacements of an ACLD beam element

2.2.2 Shape Functions

Figure 2-2 shows an ACLD beam element. Nodal displacements are given by

$$\{q\}_e = \{u_{bi}\ w_i\ \theta_i\ \gamma_i\ u_{bj}\ w_j\ \theta_j\ \gamma_j\} \tag{2.6}$$

The local shape functions are chosen to be cubic polynomial in x for transverse displacement w and linear polynomial in x for axial displacement u_b and shear angle γ (for satisfying the boundary conditions of a finite element). Therefore, the axial displacement of the base beam u_b, the transverse displacement w, the rotation θ, and the shear strain of the viscoelastic layer γ are expressed in the nodal displacements by finite element shape functions as

$$u_b = [N_{u_b}]\{q\}_e \quad w = [N_w]\{q\}_e \quad \theta = [N_\theta]\{q\}_e \quad \gamma = [N_\gamma]\{q\}_e \tag{2.7a-d}$$

where the shape functions are given by

$$[N_{u_b}] = \left[1 - \frac{x}{L_e} \quad 0 \quad 0 \quad 0 \quad \frac{x}{L_e} \quad 0 \quad 0 \quad 0\right] \quad [N_\gamma] = \left[0 \quad 0 \quad 0 \quad 1 - \frac{x}{L_e} \quad 0 \quad 0 \quad 0 \quad \frac{x}{L_e}\right]$$

$$[N_w]^T = \begin{bmatrix} 0 \\ 1-3(\frac{x}{L_e})^2+2(\frac{x}{L_e})^3 \\ x-2(\frac{x^2}{L_e})+\frac{x^3}{L_e^2} \\ 0 \\ 0 \\ 3(\frac{x}{L_e})^2-2(\frac{x}{L_e})^3 \\ -(\frac{x^2}{L_e})+(\frac{x^3}{L_e^2}) \\ 0 \end{bmatrix} \quad [N_\theta]^T = \begin{bmatrix} 0 \\ -6(\frac{x}{L_e^2})+6(\frac{x^2}{L_e^3}) \\ 1-4(\frac{x}{L_e})+3(\frac{x}{L_e})^2 \\ 0 \\ 0 \\ 6(\frac{x}{L_e^2})-6(\frac{x^2}{L_e^3}) \\ -2(\frac{x}{L_e})+3(\frac{x}{L_e})^2 \\ 0 \end{bmatrix} \tag{2.7e-h}$$

and L_e is the element length. From Eqs. (2.4) and (2.5), u_v and u_p can also be expressed in the nodal displacements as follows:

$$u_v = [N_{u_v}]\{q\}_e \quad u_p = [N_{u_p}]\{q\}_e \tag{2.8a, b}$$

where

$$[N_{u_v}] = [N_{u_b}] - \left(\frac{t_b + t_v}{2}\right)[N_\theta] + \left(\frac{t_v}{2}\right)[N_\gamma]$$

$$[N_{u_p}] = [N_{u_b}] - \left(\frac{t_b + 2t_v + t_p}{2}\right)[N_\theta] + t_v[N_\gamma] \tag{2.8c, d}$$

2.2.3 Potential Energies

Base Beam

The potential energy of the base beam due to axial displacement:

$$\frac{1}{2}\int_0^{L_e} E_b t_b b(\frac{\partial u_b}{\partial x})^2 \, dx = \frac{1}{2}\{q\}_e^T[K_{bu}]\{q\}_e$$

$$[K_{bu}] = E_b t_b b \int_0^{L_e} [N_{u_b}]'^T [N_{u_b}]' \, dx \tag{2.9a, b}$$

The potential energy of the base beam due to transverse displacement:

$$\frac{1}{2}\int_0^{L_e} E_b I_b (\frac{\partial^2 w}{\partial x^2})^2 \, dx = \frac{1}{2}\{q\}_e^T [K_{bw}]\{q\}_e$$

$$[K_{bw}] = E_b I_b \int_0^{L_e} [N_w]''^T [N_w]'' \, dx \tag{2.10a, b}$$

where E_b, I_b, and b are the Young's modulus, the moment of inertia about the neutral axis, and the width of the base beam respectively.

Piezoelectric Constraining Layer

The potential energy of the piezoelectric layer due to axial displacement:

$$\frac{1}{2}\int_0^{L_e} E_p t_p b (\frac{\partial u_p}{\partial x})^2 \, dx = \frac{1}{2}\{q\}_e^T [K_{pu}]\{q\}_e$$

$$[K_{pu}] = E_p t_p b \int_0^{L_e} [N_{u_p}]'^T [N_{u_p}]' \, dx \tag{2.11a, b}$$

The potential energy of the piezoelectric layer due to transverse displacement:

$$\frac{1}{2}\int_0^{L_e} E_p I_p (\frac{\partial^2 w}{\partial x^2})^2 \, dx = \frac{1}{2}\{q\}_e^T [K_{pw}]\{q\}_e$$

$$[K_{pw}] = E_p I_p \int_0^{L_e} [N_w]''^T [N_w]'' \, dx \tag{2.12a, b}$$

where E_p, and I_p are the Young's modulus, and the moment of inertia about the neutral axis of the constraining layer respectively.

Viscoelastic Layer

The potential energy of the viscoelastic layer due to shear:

$$\frac{1}{2}\int_0^{L_e} Gt_v b\gamma^2 \, dx = \frac{1}{2}\{q\}_e^T[K_{v\gamma}]\{q\}_e$$

$$[K_{v\gamma}] = Gt_v b\int_0^{L_e}[N_\gamma]^T[N_\gamma]\,dx \qquad (2.13a, b)$$

where G is the shear modulus of the viscoelastic layer.

The total potential energy of an ACLD beam element:

$$U_e = \frac{1}{2}\{q\}_e^T[K]_e\{q\}_e + \frac{1}{2}\{q\}_e^T[K_{v\gamma}]_e\{q\}_e \qquad (2.14a)$$

$$\text{where } [K]_e = [K_{bu}]+[K_{bw}]+[K_{pu}]+[K_{pw}] \text{ and } [K_{v\gamma}]_e = [K_{v\gamma}] \qquad (2.14b, c)$$

2.2.4 Kinetic Energies

Base Beam

The kinetic energy of the base beam due to axial displacement:

$$\frac{1}{2}\int_0^{L_e} \rho_b t_b b(\frac{\partial u_b}{\partial t})^2 \, dx = \frac{1}{2}\{\dot{q}\}_e^T[M_{bu}]\{\dot{q}\}_e$$

$$[M_{bu}] = \rho_b t_b b\int_0^{L_e}[N_{u_b}]^T[N_{u_b}]\,dx \qquad (2.15a, b)$$

The kinetic energy of the base beam due to transverse displacement:

$$\frac{1}{2}\int_0^{L_e} \rho_b t_b b(\frac{\partial w}{\partial t})^2 \, dx = \frac{1}{2}\{\dot{q}\}_e^T[M_{bw}]\{\dot{q}\}_e$$

$$[M_{bw}] = \rho_b t_b b\int_0^{L_e}[N_w]^T[N_w]\,dx \qquad (2.16a, b)$$

where ρ_b is the density of the base beam.

Piezoelectric Constraining Layer

The kinetic energy of the piezoelectric layer due to axial displacement:

$$\frac{1}{2}\int_0^{L_e}\rho_p t_p b(\frac{\partial u_p}{\partial t})^2\,dx=\frac{1}{2}\{\dot{q}\}_e^T[M_{pu}]\{\dot{q}\}_e$$

$$[M_{pu}]=\rho_p t_p b\int_0^{L_e}[N_{u_p}]^T[N_{u_p}]\,dx \qquad (2.17a, b)$$

The kinetic energy of the piezoelectric layer due to transverse displacement:

$$\frac{1}{2}\int_0^{L_e}\rho_p t_p b(\frac{\partial w}{\partial t})^2\,dx=\frac{1}{2}\{\dot{q}\}_e^T[M_{pw}]\{\dot{q}\}_e$$

$$[M_{pw}]=\rho_p t_p b\int_0^{L_e}[N_w]^T[N_w]\,dx \qquad (2.18a, b)$$

where ρ_p is the density of the piezoelectric layer.

Viscoelastic Layer

The kinetic energy of the viscoelastic layer due to axial displacement:

$$\frac{1}{2}\int_0^{L_e}\rho_v t_v b(\frac{\partial u_v}{\partial t})^2\,dx=\frac{1}{2}\{\dot{q}\}_e^T[M_{vu}]\{\dot{q}\}_e$$

$$[M_{vu}]=\rho_v t_v b\int_0^{L_e}[N_{u_v}]^T[N_{u_v}]\,dx \qquad (2.19a, b)$$

The kinetic energy of the viscoelastic layer due to transverse displacement:

$$\frac{1}{2}\int_0^{L_e}\rho_v t_v b(\frac{\partial w}{\partial t})^2\,dx=\frac{1}{2}\{\dot{q}\}_e^T[M_{vw}]\{\dot{q}\}_e$$

$$[M_{vw}] = \rho_v t_v b \int_0^{L_e} [N_w]^T [N_w]\, dx \qquad \text{(2.20a, b)}$$

where ρ_v is the density of the viscoelastic layer.

The total kinetic energy of an ACLD beam element: $T_e = \frac{1}{2}\{\dot{q}\}_e^T [M]_e \{\dot{q}\}_e$ (2.21a)

where $[M]_e = [M_{bu}] + [M_{bw}] + [M_{pu}] + [M_{pw}] + [M_{vu}] + [M_{vw}]$ (2.21b)

2.2.5 Work Done

Piezoelectric Constraining Layer

For one-dimensional structures with uni-axial loading, the constitutive equations of piezoelectric materials can be written as [79]:

$$\begin{bmatrix} \varepsilon \\ D \end{bmatrix} = \begin{bmatrix} s_{11}^E & d_{31} \\ d_{31} & \varepsilon_{33}^\tau \end{bmatrix} \begin{bmatrix} \sigma \\ E \end{bmatrix} \qquad (2.22)$$

where D is the electrical displacement (charge per unit area in the beam vertical direction), E is the electric field, ε is the mechanical strain in the x direction, and σ is the mechanical stress in the x direction. s_{11}^E is the elastic compliance constant, ε_{33}^τ is the dielectric constant, and d_{31} is the piezoelectric constant. Based on the above constitutive equations, the stress-strain relation is given by

$$\varepsilon = s_{11}^E \sigma + d_{31} E \qquad (2.23)$$

$$\Rightarrow \quad \sigma = E_p(\varepsilon - d_{31} E) \qquad (2.24a)$$

where $E_p = \frac{1}{s_{11}^E}$, $E = \frac{V_c(t)}{t_p}$ (2.24b, c)

and $V_c(t)$ is the voltage applied to the piezoelectric constraining layer.

The work done by the induced strain in the piezoelectric layer:

$$W_p = \int_0^{L_e} E_p d_{31} b V_c(t) \left(\frac{\partial u_p}{\partial x} \right) dx = \{q\}_e^T \{f_c\}_e \tag{2.25}$$

where $\{f_c\}_e$ is the nodal piezoelectric force vector and is given by:

$$\{f_c\}_e = E_p d_{31} b V_c(t) \int_0^{L_e} [N_{u_p}]'^T \, dx$$

External Load

The work done by external disturbance force $\{f_d\}$:

$$W_d = \int_0^{L_e} f_d(x,t) w(x,t) \, dx = \{q\}^T \{f_d\} \tag{2.26}$$

Note that it is usually more convenient to consider the effects of such force at the global level.

2.2.6 Sensor Equation

Assume that there is no external electric field applied to the piezoelectric sensor layer. From Eq. (2.22), the charge induced is:

$$D = d_{31} \sigma \tag{2.27}$$

$$D = d_{31} E_s \varepsilon_s \tag{2.28}$$

where E_s and ε_s are the Young's modulus and the strain of the piezoelectric sensor layer respectively. If a piezoelectric sensor layer is extending on the beam from $x = x_1$ to $x = x_2$

$(x_1 < x_2)$, the corresponding electric charge Q induced is equal to the integral of the electric displacement over the piezoelectric sensor layer, i.e.

$$Q = \int_{x_1}^{x_2} Db\, dx \tag{2.29}$$

$$Q = \int_{x_1}^{x_2} E_s d_{31} \varepsilon_s b\, dx \tag{2.30}$$

$$Q = \int_{x_1}^{x_2} -E_s d_{31} bh \frac{\partial^2 w}{\partial x^2}\, dx \tag{2.31a}$$

where $h = \left(\frac{t_b + t_s}{2}\right)$ (2.31b)

The output voltage from the piezoelectric sensor layer is given by:

$$V_s = -\frac{Q}{C_a} \tag{2.32}$$

$$V_s = \frac{E_p d_{31} hb}{C_a}\left(w'(x_2) - w'(x_1)\right) \tag{2.33}$$

where C_a is the capacitance of the piezoelectric sensor layer.

2.2.7 Equations of Motion of an ACLD Beam Element

Defining the quantity $(T_e - U_e + W_p)$ as the Lagrangian of the system and expressing it as L, i.e. $L = T_e - U_e + W_p$, the Lagrange's equations of motion are:

$$\frac{\partial L}{\partial \{q\}_e} - \frac{d}{dt}\frac{\partial L}{\partial \{\dot{q}\}_e} = 0 \tag{2.34}$$

From Eqs (2.14), (2.21) & (2.25),

$$L = -\frac{1}{2}\{q\}_e^T[K]_e\{q\}_e - \frac{1}{2}\{q\}_e^T[K_{v\gamma}]_e\{q\}_e + \frac{1}{2}\{\dot{q}\}_e^T[M]_e\{\dot{q}\}_e + \{q\}_e^T\{f_c\}_e \tag{2.35}$$

Therefore,

$$\frac{\partial L}{\partial\{q\}_e} = \frac{\partial}{\partial\{q\}_e}\left(-\frac{1}{2}\{q\}_e^T[K]_e\{q\}_e - \frac{1}{2}\{q\}_e^T[K_{v\gamma}]_e\{q\}_e + \frac{1}{2}\{\dot{q}\}_e^T[M]_e\{\dot{q}\}_e + \{q\}_e^T\{f_c\}_e\right)$$

$$= -[K]_e\{q\}_e - [K_{v\gamma}]_e\{q\}_e + \{f_c\}_e \tag{2.36a, b}$$

and

$$\frac{\partial L}{\partial\{\dot{q}\}_e} = \frac{\partial}{\partial\{\dot{q}\}_e}\left(-\frac{1}{2}\{q\}_e^T[K]_e\{q\}_e - \frac{1}{2}\{q\}_e^T[K_{v\gamma}]_e\{q\}_e + \frac{1}{2}\{\dot{q}\}_e^T[M]_e\{\dot{q}\}_e + \{q\}_e^T\{f_c\}_e\right)$$

$$= [M]_e\{\dot{q}\}_e \tag{2.37a, b}$$

Consequently,

$$\frac{\partial L}{\partial\{q\}_e} - \frac{d}{dt}\frac{\partial L}{\partial\{\dot{q}\}_e} = \left(-[K]_e\{q\}_e - [K_{v\gamma}]_e\{q\}_e + \{f_c\}_e\right) - [M]_e\{\ddot{q}\}_e = 0 \tag{2.38}$$

Finally, the equations of motion are:

$$[M]_e\{\ddot{q}\}_e + [K]_e\{q\}_e + [K_{v\gamma}]_e\{q\}_e = \{f_c\}_e \tag{2.39}$$

2.2.8 Golla-Hughes-McTavish (GHM) Method

The Golla-Hughes-McTavish (GHM) [80, 81] approach is now used to account for the damping due to the frequency-dependent viscoelastic layer. This is achieved by adding internal dissipation coordinates to the system. The GHM method represents the shear modulus of viscoelastic materials as a series of mini-oscillator terms in the Laplace domain:

$$s\tilde{G}(s) = G^{\infty}\left[1 + \sum_{k=1}^{N}\hat{\alpha}_k\frac{s^2 + 2\hat{\zeta}_k\hat{\omega}_k s}{s^2 + 2\hat{\zeta}_k\hat{\omega}_k s + \hat{\omega}_k^2}\right] \tag{2.40}$$

The factor G^{∞} corresponds to the equilibrium value of the modulus – the final value of the relaxation function $G(t)$. The positive constants $\hat{\alpha}_k$, $\hat{\omega}_k$ and $\hat{\zeta}_k$ govern the shape of the modulus function over the complex s-domain. The number of terms, N, retained in the expression is determined from the degree of frequency dependence of the modulus. Also, the GHM parameters (G^{∞}, $\hat{\alpha}_k$, $\hat{\omega}_k$ and $\hat{\zeta}_k$) are determined by curve fitting of the experimental data (shear storage modulus and loss factor against frequency).

From Eq. (2.39),

$$[M]_e\{\ddot{q}(t)\}_e + [K]_e\{q(t)\}_e + G[\hat{K}_{v\gamma}]_e\{q(t)\}_e = \{f(t)_c\}_e \tag{2.41a}$$

where $[\hat{K}_{v\gamma}]_e = t_v b \int_0^{L_e} [N_\gamma]^T [N_\gamma]\, dx$. (2.41b)

Eq. (2.41) is now generalized to the case of viscoelasticity by replacing the constant shear modulus G by a linear stress-strain law [82]. i.e.: Replace $G[\hat{K}_{v\gamma}]_e\{q(t)\}_e$ by $\int_0^t G(t-\tau)[\hat{K}_{v\gamma}]_e\{\dot{q}(\tau)\}_e\, d\tau$, which is a standard convolution integral. $G(t)$ is the material relaxation function – the stress response to a unit-step strain input. This stress relaxation represents energy loss from the material, hence damping. When taking Laplace transform, it becomes: $[\hat{K}_{v\gamma}]_e\tilde{G}(s)s\{\tilde{q}\}_e$ or $s\tilde{G}(s)[\hat{K}_{v\gamma}]_e\{\tilde{q}\}_e$. The GHM method in fact represents the term $s\tilde{G}(s)$ as a series of mini-oscillator terms in the Laplace domain, as Eq. (2.40). Therefore, Eq. (2.41a) becomes:

$$[M]_e\{\ddot{q}(t)\}_e + [K]_e\{q(t)\}_e + G(t)[\hat{K}_{v\gamma}]_e\{q(0)\}_e + \int_0^t G(t-\tau)[\hat{K}_{v\gamma}]_e\{\dot{q}(\tau)\}_e\, d\tau = \{f_c(t)\}_e \tag{2.42}$$

Eq (2.42) can be expressed in the Laplace domain as:

$$s^2[M]_e\{\tilde{q}\}_e + [K]_e\{\tilde{q}\}_e + s\tilde{G}(s)[\hat{K}_{v\gamma}]_e\{\tilde{q}\}_e = \{\tilde{f}_c\}_e \tag{2.43}$$

For demonstration, consider a GHM material modulus function with a single mini-oscillator term, i.e.

$$s\tilde{G}(s) = G^{\infty}\left(1+\hat{\alpha}\frac{s^2+2\hat{\zeta}\hat{\omega}s}{s^2+2\hat{\zeta}\hat{\omega}s+\hat{\omega}^2}\right) \tag{2.44}$$

Eq (2.43) then becomes:

$$s^2[M]_e\{\tilde{q}\}_e + [K]_e\{\tilde{q}\}_e + G^{\infty}\left(1+\hat{\alpha}\frac{s^2+2\hat{\zeta}\hat{\omega}s}{s^2+2\hat{\zeta}\hat{\omega}s+\hat{\omega}^2}\right)[\hat{K}_{v\gamma}]_e\{\tilde{q}\}_e = \{\tilde{f}_c\}_e \tag{2.45}$$

Introduce a column vector of dissipation coordinates,

$$\{\tilde{\tilde{z}}\}_e = \frac{\hat{\omega}^2}{s^2+2\hat{\zeta}\hat{\omega}s+\hat{\omega}^2}\{\tilde{q}\}_e \tag{2.46a}$$

$$\Rightarrow\ s^2\{\tilde{\tilde{z}}\}_e + 2\hat{\zeta}\hat{\omega}s\{\tilde{\tilde{z}}\}_e + \hat{\omega}^2\{\tilde{\tilde{z}}\}_e - \hat{\omega}^2\{\tilde{q}\}_e = \{0\} \tag{2.46b}$$

From Eq (2.45),

$$s^2[M]_e\{\tilde{q}\}_e + [K]_e\{\tilde{q}\}_e + G^{\infty}\left(1+\hat{\alpha}-\hat{\alpha}\frac{\hat{\omega}^2}{s^2+2\hat{\zeta}\hat{\omega}s+\hat{\omega}^2}\right)[\hat{K}_{v\gamma}]_e\{\tilde{q}\}_e = \{\tilde{f}_c\}_e \tag{2.47}$$

$$s^2[M]_e\{\tilde{q}\}_e + [K]_e\{\tilde{q}\}_e + (1+\hat{\alpha})G^{\infty}[\hat{K}_{v\gamma}]_e\{\tilde{q}\}_e - \hat{\alpha}G^{\infty}[\hat{K}_{v\gamma}]_e\left(\frac{\hat{\omega}^2}{s^2+2\hat{\zeta}\hat{\omega}s+\hat{\omega}^2}\{\tilde{q}\}_e\right) = \{\tilde{f}_c\}_e \tag{2.48}$$

Using Eqs (2.46a) and (2.48),

$$s^2[M]_e\{\tilde{q}\}_e + [K]_e\{\tilde{q}\}_e + G^{\infty}(1+\hat{\alpha})[\hat{K}_{v\gamma}]_e\{\tilde{q}\}_e - \hat{\alpha}G^{\infty}[\hat{K}_{v\gamma}]_e\{\tilde{\tilde{z}}\}_e = \{\tilde{f}_c\}_e \tag{2.49}$$

Multiplying Eq. (2.46b) by $\frac{\hat{\alpha}}{\hat{\omega}^2}[\bar{K}_{v\gamma}]_e$, where $[\bar{K}_{v\gamma}]_e = G^{\infty}[\hat{K}_{v\gamma}]_e$:

$$s^2\frac{\hat{\alpha}}{\hat{\omega}^2}[\bar{K}_{v\gamma}]_e\{\tilde{\hat{z}}\}_e + s\frac{2\hat{\alpha}\hat{\zeta}}{\hat{\omega}}[\bar{K}_{v\gamma}]_e\{\tilde{\hat{z}}\}_e + \hat{\alpha}[\bar{K}_{v\gamma}]_e\{\tilde{\hat{z}}\}_e - \hat{\alpha}[\bar{K}_{v\gamma}]_e\{\tilde{q}\}_e = \{0\} \tag{2.50}$$

Hence, the governing equations become:

$$s^2[M]_e\{\tilde{q}\}_e + [K]_e\{\tilde{q}\}_e + (1+\hat{\alpha})[\bar{K}_{v\gamma}]_e\{\tilde{q}\}_e - \hat{\alpha}[\bar{K}_{v\gamma}]_e\{\tilde{\hat{z}}\}_e = \{\tilde{f}_c\}_e \tag{2.51}$$

$$s^2\frac{\hat{\alpha}}{\hat{\omega}^2}[\bar{K}_{v\gamma}]_e\{\tilde{\hat{z}}\}_e + s\frac{2\hat{\alpha}\hat{\zeta}}{\hat{\omega}}[\bar{K}_{v\gamma}]_e\{\tilde{\hat{z}}\}_e + \hat{\alpha}[\bar{K}_{v\gamma}]_e\{\tilde{\hat{z}}\}_e - \hat{\alpha}[\bar{K}_{v\gamma}]_e\{\tilde{q}\}_e = \{0\} \tag{2.52}$$

In matrix form,

$$\left\{ s^2\begin{bmatrix}[M]_e & [0]\\ [0] & \frac{\hat{\alpha}}{\hat{\omega}^2}[\bar{K}_{v\gamma}]_e\end{bmatrix} + s\begin{bmatrix}[0] & [0]\\ [0] & \frac{2\hat{\alpha}\hat{\zeta}}{\hat{\omega}}[\bar{K}_{v\gamma}]_e\end{bmatrix} + \begin{bmatrix}[K]_e + [\bar{K}_{v\gamma}]_e(1+\hat{\alpha}) & -\hat{\alpha}[\bar{K}_{v\gamma}]_e\\ -\hat{\alpha}[\bar{K}_{v\gamma}]_e & \hat{\alpha}[\bar{K}_{v\gamma}]_e\end{bmatrix}\right\}\begin{Bmatrix}\{\tilde{q}\}_e\\ \{\tilde{\hat{z}}\}_e\end{Bmatrix} = \begin{Bmatrix}\{\tilde{f}_c\}_e\\ \{0\}\end{Bmatrix} \tag{2.53}$$

In time-domain,

$$[\bar{M}]_e\{\ddot{\bar{q}}\}_e + [\bar{D}]_e\{\dot{\bar{q}}\}_e + [\bar{K}]_e\{\bar{q}\}_e = \{\bar{f}_c\} \tag{2.54a}$$

where

$$[\bar{M}]_e = \begin{bmatrix}[M]_e & [0]\\ [0] & \frac{\hat{\alpha}}{\hat{\omega}^2}[\bar{K}_{v\gamma}]_e\end{bmatrix} \quad [\bar{D}]_e = \begin{bmatrix}[0] & [0]\\ [0] & \frac{2\hat{\alpha}\hat{\zeta}}{\hat{\omega}}[\bar{K}_{v\gamma}]_e\end{bmatrix}$$

$$[\bar{\mathrm{K}}]_e = \begin{bmatrix}[K]_e + [\bar{K}_{v\gamma}]_e(1+\hat{\alpha}) & -\hat{\alpha}[\bar{K}_{v\gamma}]_e\\ -\hat{\alpha}[\bar{K}_{v\gamma}]_e & \hat{\alpha}[\bar{K}_{v\gamma}]_e\end{bmatrix} \quad \{\bar{q}\}_e = \begin{Bmatrix}\{q\}_e\\ \{\hat{z}\}_e\end{Bmatrix} \quad \{\bar{f}_c\}_e = \begin{Bmatrix}\{f_c\}_e\\ \{0\}\end{Bmatrix}. \tag{2.54b-f}$$

Since the elastic element stiffness matrix $[\bar{K}_{v\gamma}]_e$ is usually positive semi-definite (one or more zero eigenvalues represents rigid body motion), the "mass" matrix in this formulation will not usually be positive definite. To remedy this situation, spectral decomposition of the elastic stiffness matrix $[\bar{K}_{v\gamma}]_e$ is used [81].

$$[\bar{K}_{v\gamma}]_e = G^{\infty}[\hat{K}_{v\gamma}]_e = G^{\infty}[\hat{R}][\hat{\Lambda}][\hat{R}]^T \tag{2.55}$$

Here, $[\hat{\Lambda}]$ is a diagonal matrix of the non-zero (necessarily positive) eigenvalues of matrix $[\hat{K}_{v\gamma}]_e$. The corresponding orthonormalized eigenvectors form the columns of the matrix $[\hat{R}]$, and $[\hat{R}]^T[\hat{R}] = I$. To achieve the objective of fewer dissipation coordinates and a positive-definite mass matrix, it is necessary to factor the equilibrium modulus G^∞ back into the diagonal eigenvalue matrix $[\hat{\Lambda}]$, i.e. $[\Lambda] = G^\infty[\hat{\Lambda}]$. Then, let $\{z\}_e = [\hat{R}]^T\{\hat{z}\}_e$ and $[R] = [\hat{R}][\Lambda]$. Substituting these into Eq. (2.54), and pre-multiplying the bottom row by $[\hat{R}]^T$:

$$\begin{bmatrix}[M]_e & [0] \\ [0] & \dfrac{\hat{\alpha}}{\hat{\omega}^2}[\hat{R}]^T[\bar{K}_{v\gamma}]_e\end{bmatrix}\begin{Bmatrix}\{\ddot{q}\}_e \\ \{\ddot{\hat{z}}\}_e\end{Bmatrix}+\begin{bmatrix}[0] & [0] \\ [0] & \dfrac{2\hat{\alpha}\hat{\zeta}}{\hat{\omega}}[\hat{R}]^T[\bar{K}_{v\gamma}]_e\end{bmatrix}\begin{Bmatrix}\{\dot{q}\}_e \\ \{\dot{\hat{z}}\}_e\end{Bmatrix}+ \\ \begin{bmatrix}[K]_e+[\bar{K}_{v\gamma}]_e(1+\hat{\alpha}) & -\hat{\alpha}[\bar{K}_{v\gamma}]_e \\ -\hat{\alpha}[\hat{R}]^T[\bar{K}_{v\gamma}]_e & \hat{\alpha}[\hat{R}]^T[\bar{K}_{v\gamma}]_e\end{bmatrix}\begin{Bmatrix}\{q\}_e \\ \{\hat{z}\}_e\end{Bmatrix}=\begin{Bmatrix}\{f_c\}_e \\ \{0\}\end{Bmatrix} \tag{2.56}$$

$$\begin{bmatrix}[M]_e & [0] \\ [0] & \dfrac{\hat{\alpha}}{\hat{\omega}^2}[\hat{R}]^T G^\infty[\hat{R}][\hat{\Lambda}][\hat{R}]^T\end{bmatrix}\begin{Bmatrix}\{\ddot{q}\}_e \\ \{\ddot{\hat{z}}\}_e\end{Bmatrix}+\begin{bmatrix}[0] & [0] \\ [0] & \dfrac{2\hat{\alpha}\hat{\zeta}}{\hat{\omega}}[\hat{R}]^T G^\infty[\hat{R}][\hat{\Lambda}][\hat{R}]^T\end{bmatrix}\begin{Bmatrix}\{\dot{q}\}_e \\ \{\dot{\hat{z}}\}_e\end{Bmatrix}+ \\ \begin{bmatrix}[K]_e+[\bar{K}_{v\gamma}]_e(1+\hat{\alpha}) & -\hat{\alpha}G^\infty[\hat{R}][\hat{\Lambda}][\hat{R}]^T \\ -\hat{\alpha}[\hat{R}]^T G^\infty[\hat{R}][\hat{\Lambda}][\hat{R}]^T & \hat{\alpha}[\hat{R}]^T G^\infty[\hat{R}][\hat{\Lambda}][\hat{R}]^T\end{bmatrix}\begin{Bmatrix}\{q\}_e \\ \{\hat{z}\}_e\end{Bmatrix}=\begin{Bmatrix}\{f_c\}_e \\ \{0\}\end{Bmatrix} \tag{2.57}$$

$$\begin{bmatrix}[M]_e & [0] \\ [0] & \dfrac{\hat{\alpha}}{\hat{\omega}^2}[\Lambda][\hat{R}]^T\end{bmatrix}\begin{Bmatrix}\{\ddot{q}\}_e \\ \{\ddot{\hat{z}}\}_e\end{Bmatrix}+\begin{bmatrix}[0] & [0] \\ [0] & \dfrac{2\hat{\alpha}\hat{\zeta}}{\hat{\omega}}[\Lambda][\hat{R}]^T\end{bmatrix}\begin{Bmatrix}\{\dot{q}\}_e \\ \{\dot{\hat{z}}\}_e\end{Bmatrix}+ \\ \begin{bmatrix}[K]_e+[\bar{K}_{v\gamma}]_e(1+\hat{\alpha}) & -\hat{\alpha}[\hat{R}][\Lambda][\hat{R}]^T \\ -\hat{\alpha}[\Lambda][\hat{R}]^T & \hat{\alpha}[\Lambda][\hat{R}]^T\end{bmatrix}\begin{Bmatrix}\{q\}_e \\ \{\hat{z}\}_e\end{Bmatrix}=\begin{Bmatrix}\{f_c\}_e \\ \{0\}\end{Bmatrix} \tag{2.58}$$

$$\begin{bmatrix}[M]_e & [0] \\ [0] & \dfrac{\hat{\alpha}}{\hat{\omega}^2}[\Lambda]\end{bmatrix}\begin{Bmatrix}\{\ddot{q}\}_e \\ \{\ddot{z}\}_e\end{Bmatrix}+\begin{bmatrix}[0] & [0] \\ [0] & \dfrac{2\hat{\alpha}\hat{\zeta}}{\hat{\omega}}[\Lambda]\end{bmatrix}\begin{Bmatrix}\{\dot{q}\}_e \\ \{\dot{z}\}_e\end{Bmatrix}+ \\ \begin{bmatrix}[K]_e+[\bar{K}_{v\gamma}]_e(1+\hat{\alpha}) & -\hat{\alpha}[R] \\ -\hat{\alpha}[R]^T & \hat{\alpha}[\Lambda]\end{bmatrix}\begin{Bmatrix}\{q\}_e \\ \{z\}_e\end{Bmatrix}=\begin{Bmatrix}\{f_c\}_e \\ \{0\}\end{Bmatrix} \tag{2.59}$$

$$[\hat{M}]_e\{\ddot{\hat{q}}\}_e+[\hat{D}]_e\{\dot{\hat{q}}\}_e+[\hat{K}]_e\{\hat{q}\}_e=\{\hat{f}_c\}_e \tag{2.60a}$$

where

$$[\hat{M}]_e=\begin{bmatrix}[M]_e & [0]\\ [0] & \dfrac{\hat{\alpha}}{\hat{\omega}^2}[\Lambda]\end{bmatrix}\quad [\hat{D}]_e=\begin{bmatrix}[0] & [0]\\ [0] & \dfrac{2\hat{\alpha}\hat{\zeta}}{\hat{\omega}}[\Lambda]\end{bmatrix}$$

$$[\hat{\mathrm{K}}]_e=\begin{bmatrix}[K]_e+[\bar{K}_{vy}]_e(1+\hat{\alpha}) & -\hat{\alpha}[R]\\ -\hat{\alpha}[R]^T & \hat{\alpha}[\Lambda]\end{bmatrix}\quad \{\hat{q}\}_e=\begin{Bmatrix}\{q\}_e\\ \{z\}_e\end{Bmatrix}\ \{\hat{f}_c\}_e=\begin{Bmatrix}\{f_c\}_e\\ \{0\}\end{Bmatrix}. \tag{2.60b-f}$$

The above case of single mini-oscillator can easily be extended to a multi-oscillator model. The general form of the mass, damping and stiffness matrices are given by:

$$[\hat{M}]_e=\begin{bmatrix}[M]_e & 0 & \cdots & 0\\ 0 & \dfrac{\hat{\alpha}_1}{\hat{\omega}_1^2}[\Lambda] & 0 & \vdots\\ \vdots & 0 & \ddots & 0\\ 0 & \cdots & 0 & \dfrac{\hat{\alpha}_N}{\hat{\omega}_N^2}[\Lambda]\end{bmatrix}\quad [\hat{D}]_e=\begin{bmatrix}0 & 0 & \cdots & 0\\ 0 & \dfrac{2\hat{\alpha}_1\hat{\zeta}_1}{\hat{\omega}_1}[\Lambda] & 0 & \vdots\\ \vdots & 0 & \ddots & 0\\ 0 & \cdots & 0 & \dfrac{2\hat{\alpha}_N\hat{\zeta}_N}{\hat{\omega}_N}[\Lambda]\end{bmatrix}$$

$$[\hat{K}]_e=\begin{bmatrix}[K]_e+[\bar{K}_{vy}]_e(1+\sum_{k=1}^{N}\hat{\alpha}_k) & -\hat{\alpha}_1[R] & \cdots & -\hat{\alpha}_N[R]\\ -\hat{\alpha}_1[R]^T & \hat{\alpha}_1[\Lambda] & 0 & 0\\ \vdots & 0 & \ddots & 0\\ -\hat{\alpha}_N[R]^T & 0 & 0 & \hat{\alpha}_N[\Lambda]\end{bmatrix}$$

$$\{\hat{q}\}_e=\begin{Bmatrix}\{q\}_e\\ \{z_1\}_e\\ \vdots\\ \{z_N\}_e\end{Bmatrix}\quad \{\hat{f}_c\}_e=\begin{Bmatrix}\{f_c\}_e\\ \{0\}\\ \vdots\\ \{0\}\end{Bmatrix}. \tag{2.61a-e}$$

2.2.9 Curve Fitting of GHM Parameters

After expressing Eq. (2.44) – the GHM material modulus function, into a frequency-dependent complex modulus form, the GHM parameters can be found by using the nonlinear least squares method. When $s\tilde{G}(s)$ is evaluated along the imaginary axis of the s-plane, it yields the complex modulus: $G^*(\omega) \equiv i\omega\tilde{G}(i\omega) = G'(1+i\eta)$, where $G'(\omega)$ and $\eta(\omega)$ are the shear storage modulus and loss factor of the viscoelastic material. They can be expressed in terms of the GHM parameters as:

$$G'(\omega) = \mathrm{Re}\{i\omega\tilde{G}(i\omega)\}$$

$$= G^{\infty}\left[1 + \sum_{k=1}^{N} \hat{\alpha}_k \frac{\omega^4 + (4\hat{\zeta}_k^2 - 1)\hat{\omega}_k^2\omega^2}{\omega^4 + 2(2\hat{\zeta}_k^2 - 1)\hat{\omega}_k^2\omega^2 + \hat{\omega}_k^4}\right] \tag{2.62}$$

$$\eta(\omega) = \frac{\mathrm{Im}\{i\omega\tilde{G}(i\omega)\}}{G'(\omega)}$$

$$= \sum_{k=1}^{N} \hat{\alpha}_k \frac{2\hat{\zeta}_k\hat{\omega}_k^3\omega}{(1+\hat{\alpha}_k)\omega^4 + [4(1+\hat{\alpha}_k)\zeta_k^2 - 1]\hat{\omega}_k^2\omega^2 + \hat{\omega}_k^4} \tag{2.63}$$

Now, considering three-term GHM (N=3), the curve fitting tool box of MATLAB is used to fit the measured data of the 3M viscoelastic material ISD 112 at 27 °C from 20 to 5000 Hz. As a result of the computation, the GHM parameters are: G^{∞} = 5.032 x 10^5; $\hat{\alpha}_1$ =0.786; $\hat{\alpha}_2$ =4.027; $\hat{\alpha}_3$ =43.354; $\hat{\zeta}_1$ =6.27; $\hat{\zeta}_2$ =5.81; $\hat{\zeta}_3$ =2.66; $\hat{\omega}_1$ =6309.23; $\hat{\omega}_2$=50788.2 and $\hat{\omega}_3$=338422.17. The curve fit for the storage modulus and loss factor is shown in Figure 2-3. It can be seen that the found GHM parameters yields a good approximation to the measured material curves within the frequency range of interest.

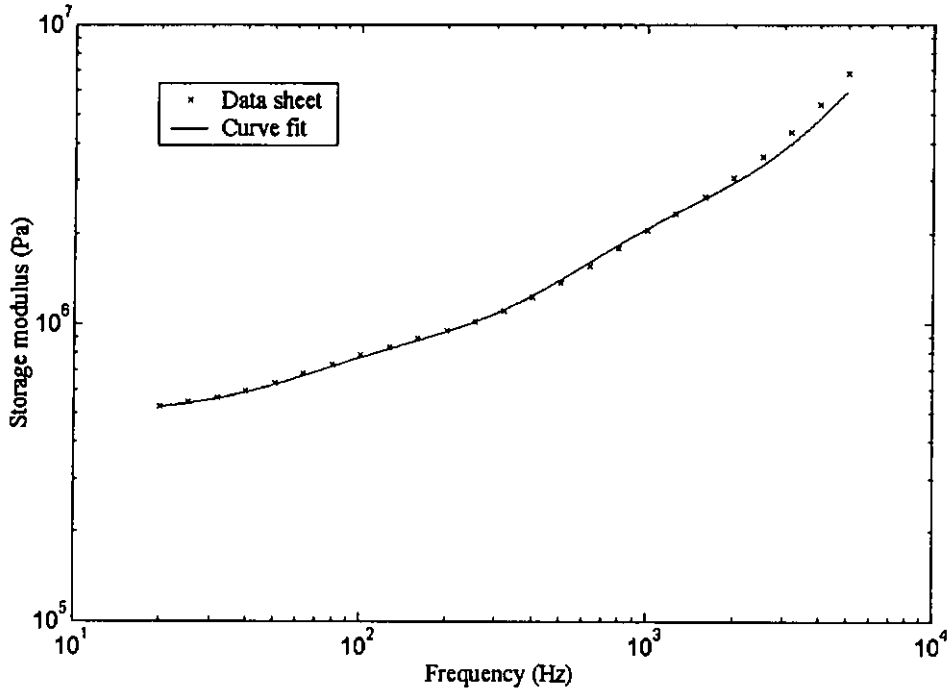

Figure 2-3(a) Curve fitting of GHM parameters – storage modulus

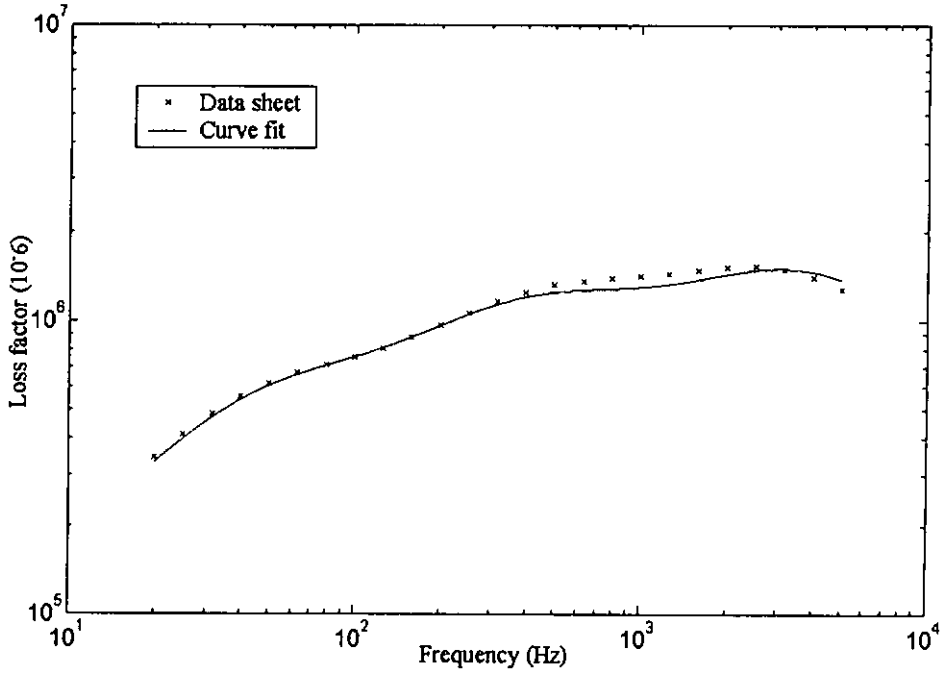

Figure 2-3(b) Curve fitting of GHM parameters – loss factor

2.2.10 Global Equations of Motion

Plain Beam Elements

The stiffness and mass matrices of plain beam elements have dimensions of 6 x 6, and are similar to those given by Eqs. (2.9), (2.10), (2.15) and (2.16).

Boundary Condition

For a clamped-free beam, the equations of motion are subjected to the following boundary conditions: $\text{At } x = 0, \quad w = 0; \quad \frac{\partial w}{\partial x} = 0; \quad u_b = 0.$

Assembly

In assembling ACLD beam element, compatibility constraints are applied only to the physical coordinates ($\{q\}_e$), exactly as in the corresponding elastic case [80]. There are no additional compatibility constraints for the dissipation coordinates ($\{z_1\}_e, \cdots \{z_N\}_e$). In fact, all dissipation coordinates are retained in the assembled system. Besides, a rearrangement of the coordinates at the element level is needed before assembly. Lastly, boundary conditions are only applied to the physical coordinates, exactly as in the corresponding elastic case.

The following global equations of motion can be obtained:

$$[M]\{\ddot{q}\} + [D]\{\dot{q}\} + [K]\{q\} = \{f_c\} + \{f_d\} \tag{2.64}$$

where $[M]$, $[D]$ and $[K]$ are the global mass, damping, and stiffness matrix respectively. $\{f_c\}$ is the global piezoelectric force vector, and $\{f_d\}$ is the global load vector.

2.3 MODEL VALIDATION

To validate the present model, comparisons with the results available in literature (Shi *et al.* [83]; Lee and Kim [47]) are given in this section. An aluminum beam (261.6 mm x 12.7 mm x 2.286 mm) is considered and an ACLD patch (101.6 mm x 12.7 mm) is bonded at 27 mm from the fixed end. The ACLD patch consists of a viscoelastic damping layer (3M ISD 112) and a piezoelectric constraining layer (PKI 502) with thickness of 0.254 mm and 0.762 mm respectively. Other system parameters are given in Table 2-1. Shi *et al.* [83] used this patched ACLD beam in their studies. For the purpose of comparison, a one-term GHM model is first considered, as done by the above authors. The first five eigenvalues calculated using the present model and those given in Shi *et al.* [83] are listed in Table 2-2. It can be found that all the five eigenvalues obtained by using the present model (one-term GHM) are close to those by Shi *et al.* [83]. Table 2-3 shows the relative percentage difference of the real and imaginary parts between the two models. However, in the above models, a single-term GHM model is considered, leading to unreal material behaviour [43]. It is thus necessary to use multi-term GHM model to enhance the accuracy of the present model. Using the spectral element method, Lee and Kim [47] established a model for the above patched ACLD beam, in which the same parameters are used, except the Young's modulus of the piezoelectric constraining layer is 64.9 GPa instead of 74 GPa. Since the spectral element model (SEM) is developed in the frequency domain, the analytical damping representation (expressing the complex modulus as a function of frequency) introduced by Soovere and Drake [84] can directly be used in conjunction with the SEM. Besides, in general SEM provides accurate dynamic characteristics for both

passive and active ACLD beams, compared with the conventional finite element model (FEM). As a result, comparisons are made with the SEM with analytical damping model. The frequency response functions (FRFs) obtained by using the present model with three GHM terms and Young's modulus of 64.9 GPa for the piezoelectric constraining layer for the patched (Figure 2-4) and fully covered (Figure 2-5) ACLD beams are close to those by Lee and Kim [47] (Appendix A). For both ACLD beams, the FRFs by one-term GHM model are found to deviate significantly from those by three-term GHM model, especially at high frequency. In general, the three-term GHM model is found to yield the FRFs of lower peaks with lower natural frequencies, compared to one-term GHM model. Thus, the results confirm that a single internal dissipation coordinate (i.e. one-term GHM) is not enough for the GHM model to fully represent the damping characteristics of the viscoelastic layer. Table 2-4 presents the first five modal frequencies and modal damping ratios of the patched ACLD beam and fully covered ACLD beam. In short, all the above results presented are not only a reflection of the validity but also an indication of the accuracy of the present model to predict the dynamic behaviour of an ACLD treated beam.

Table 2-1 System parameters of the ACLD beam

ρ_p	7600 kg/m^3	E_p	74 x 10^9 Pa	$\hat{\alpha}$	6.0
ρ_v	1250 kg/m^3	E_b	71 x 10^9 Pa	$\hat{\omega}$	10000 rad/s
ρ_b	2700 kg/m^3	G^∞	5 x 10^5 Pa	$\hat{\zeta}$	4.0

Table 2-2 The first five eigenvalues obtained by the present model (one-term GHM) and those given in Shi *et al.* (2001)

Modes	Eigenvalues	
	Present model	Shi *et al.*, 2001
1	-2.2474±175.184	-2.2424±175.124
2	-13.082±944.724	-13.006±944.466
3	-39.725±2778.641	-39.206±2776.994
4	-24.514±5209.34	-24.368±5207.037
5	-22.248±8936.316	-22.105±8932.071

Table 2-3 Relative percentage difference of the real and imaginary parts between the present model (one-term GHM) and Shi *et al.* (2001)

Modes	Relative difference (%)	
	Real part	Imaginary part
1	0.214	0.034
2	0.584	0.027
3	1.324	0.059
4	0.599	0.044
5	0.647	0.048

Table 2-4 Modal frequencies and damping ratios of the first five modes of the patched and fully covered ACLD beams

Modes	Modal frequencies (Hz)		Modal damping (%)	
	Full	Patched	Full	Patched
1	27.846	27.859	3.8333	0.7361
2	149.825	149.026	7.2013	0.8654
3	402.917	432.286	8.2296	2.8935
4	781.880	821.735	6.9087	1.8765
5	1309.511	1418.125	5.5616	2.1437

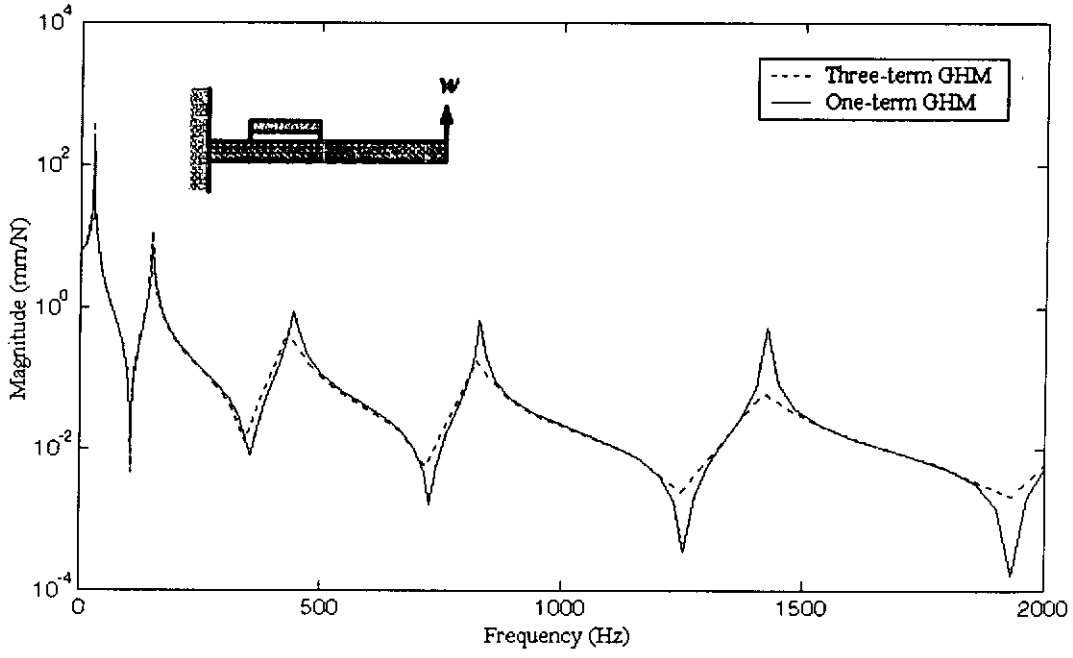

Figure 2-4 Frequency response functions of a patched ACLD beam

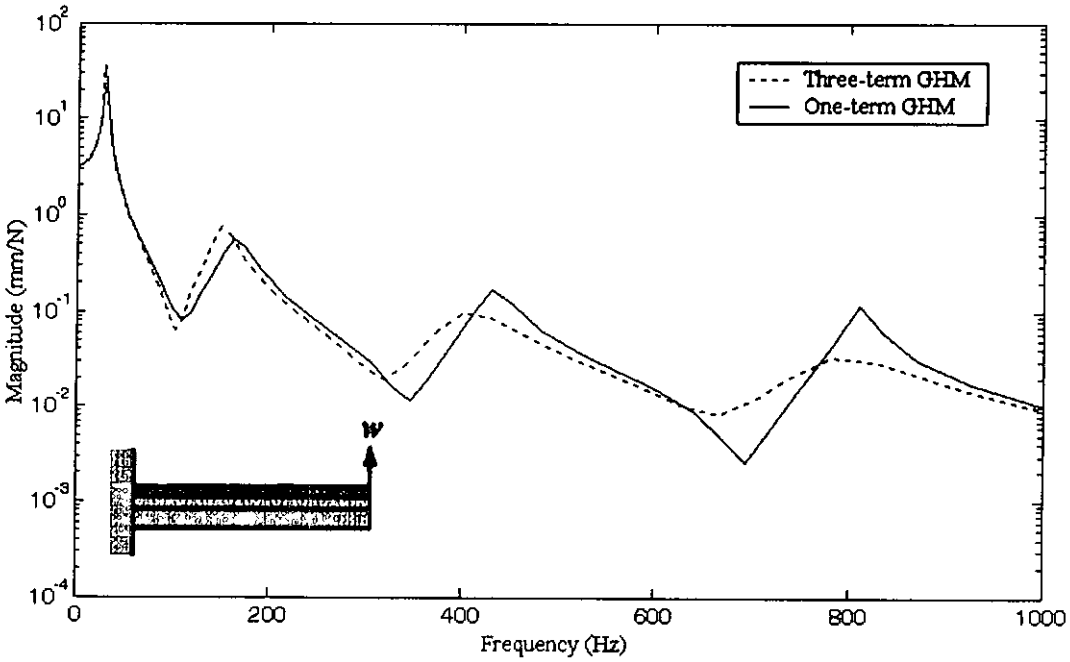

Figure 2-5 Frequency response functions of a fully covered ACLD beam

CHAPTER 3

PARAMETRIC STUDY OF ACLD TREATMENTS

In this chapter, a parametric study is conducted to determine the effects of different ACLD treatment parameters on the damping performance of the system. The variables considered include the control gains, K_p (proportional) and K_d (derivative), the thicknesses of the constraining and viscoelastic layers, t_p and t_v, the equilibrium value of the shear modulus, G^{∞}, as well as the treatment length, l, and location, P – the distance between the fixed-end and the left hand side of the ACLD patch. Both passive and hybrid damping of the system are studied for the first three modes of vibration.

3.1 SYSTEM DESCRIPTION AND ANALYSIS

For the purpose of this study, an aluminum beam (300 mm x 15 mm x 2 mm) is considered. An ACLD patch (100 mm x 15 mm) is bonded at 30 mm from the fixed end (Figure 3-1). The ACLD patch consists of a viscoelastic damping layer (3M ISD 112) sandwiched between two piezoelectric layers (PKI 502). The upper one acts as the active constraining layer, while the lower one serves as the sensor layer. Other system parameters are given in Table 3-1. The present study focuses on the first three vibration modes. Table 3-2 presents the first three modal frequencies and modal damping ratios of the ACLD beam.

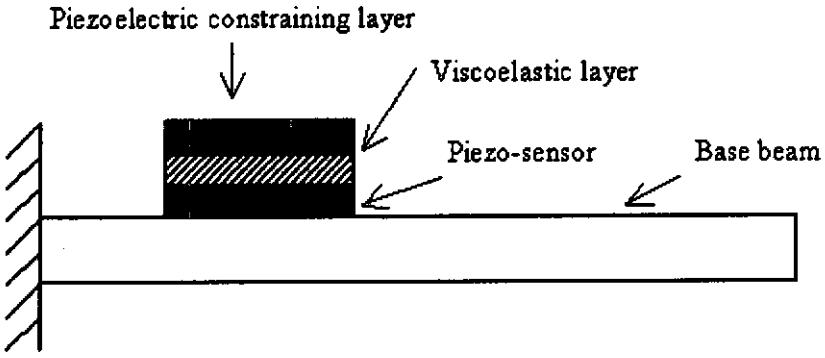

Figure 3-1 A patched ACLD beam

Table 3-1 System parameters of patched ACLD beam

ρ_p	7600 kg/m^3	t_v	0.25 mm	$\hat{\alpha}_2$	3.237
ρ_v	1250 kg/m^3	t_z	0.025 mm	$\hat{\omega}_2$	50618.8 rad/s
ρ_b	2700 kg/m^3	G^∞	5 x 10^5 Pa	$\hat{\zeta}_2$	5.38
E_p	74 x 10^9 Pa	$\hat{\alpha}_1$	0.742	$\hat{\alpha}_3$	41.654
E_b	71 x 10^9 Pa	$\hat{\omega}_1$	6502.9 rad/s	$\hat{\omega}_3$	352782 rad/s
t_p	1 mm	$\hat{\zeta}_1$	6.97	$\hat{\zeta}_3$	2.56

Table 3-2 Modal frequencies and damping ratios of the first three modes of the ACLD beam

Modes	Modal frequencies (Hz)	Modal damping (%)
1	19.032	0.6331
2	98.02	0.5221
3	278.314	2.9167

To examine the actuating ability of the system, the ACLD beam is excited by the actuator. The beam response at the free end is observed (Figure 3-2). It is obvious that large amplitude indicates higher actuator authority [85]. Similarly, to examine the sensing ability of the system, the ACLD beam is excited by a force in transverse direction at the free end. The sensing voltage from the piezoelectric sensor layer is measured. Figure 3-3 shows the frequency response of the sensor voltage over the applied force. The open loop system response, as shown in Figure 3-4, is obtained by applying a disturbance to the beam tip, and the output is transverse displacement there as well. Figure 3-5 is the impulse response of the open loop system.

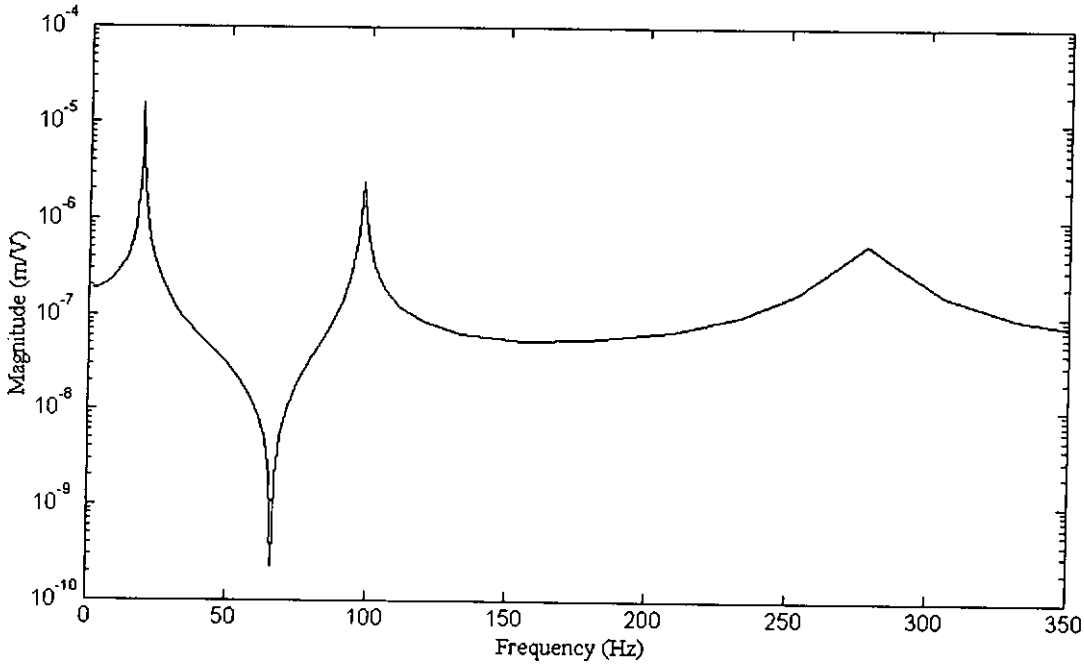

Figure 3-2 Frequency response for actuating ability

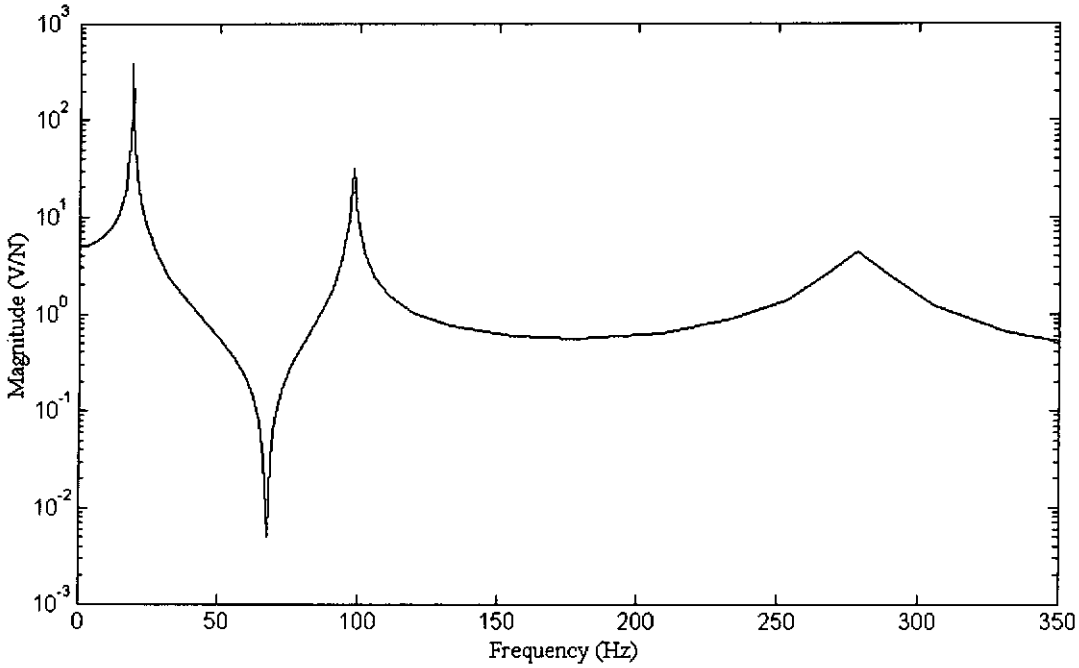

Figure 3-3 Frequency response for sensing ability

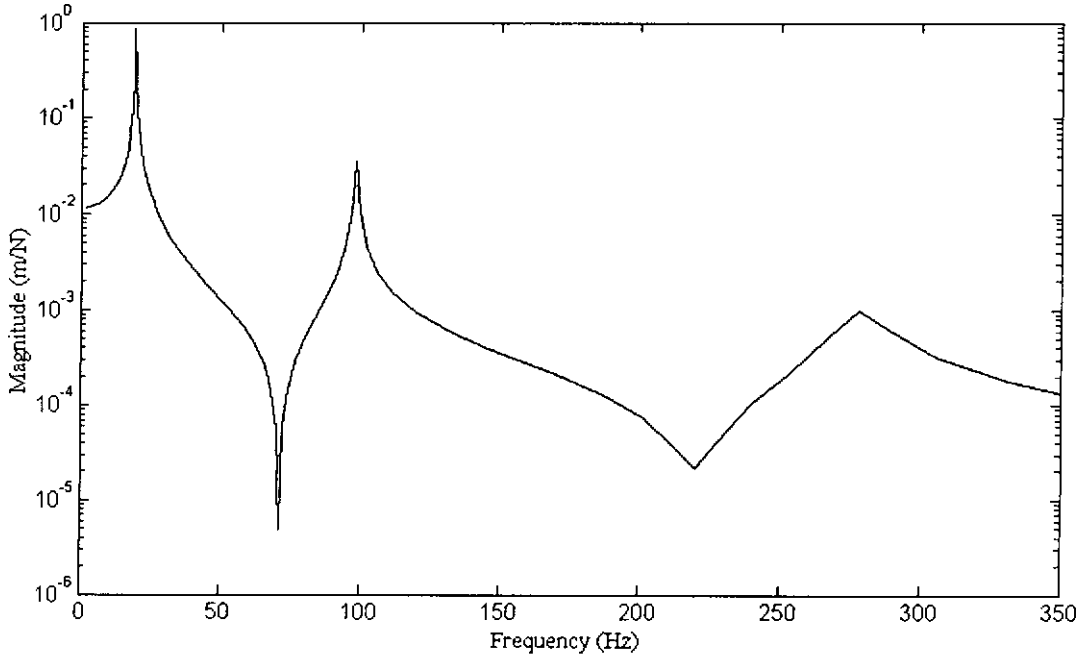

Figure 3-4 Frequency response of open loop system

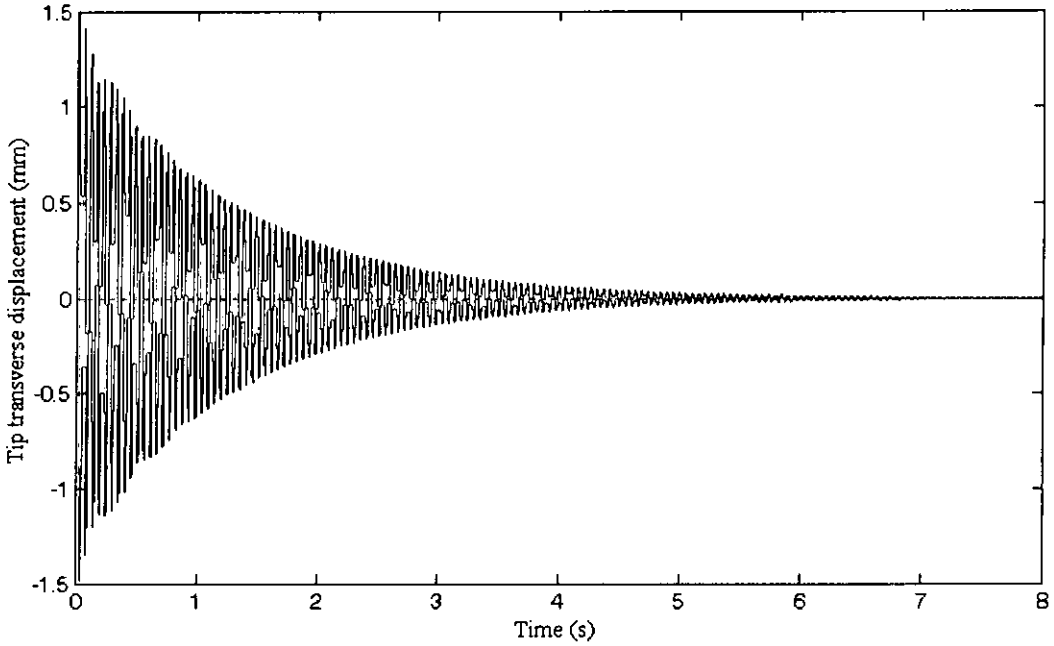

Figure 3-5 Impulse response of beam tip transverse displacement

3.2 DAMPING CHARACTERISTICS

3.2.1 Effect of Control Gains

Figure 3-6 and 3-7 show the root locus diagrams of the first three modes of the system for proportional control ($V_c = -K_p V_s$) and derivative control ($V_c = -K_d \dot{V}_s$) respectively. It is clear that as the control gains (both K_p and K_d) increase from zero to infinity, the open loop poles move toward the open loop zeros. The decrease of the angle ϕ, as defined in Figure 3-6(b), implies the increase of modal dampings. The closed-loop poles for $K_p = 500$ and $K_d = 5$ are also presented in the figures.

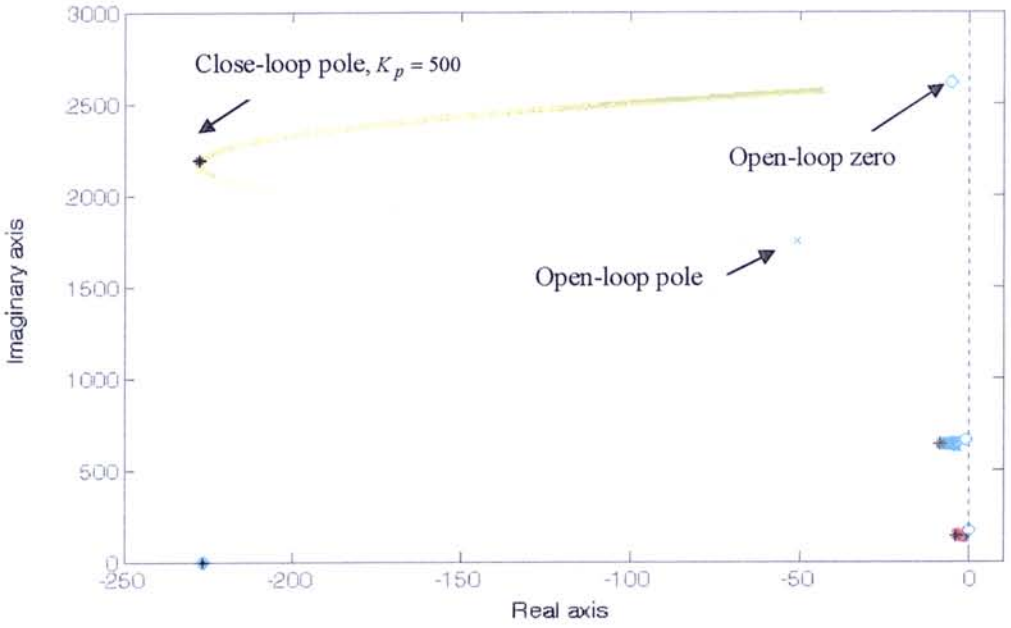

(a)

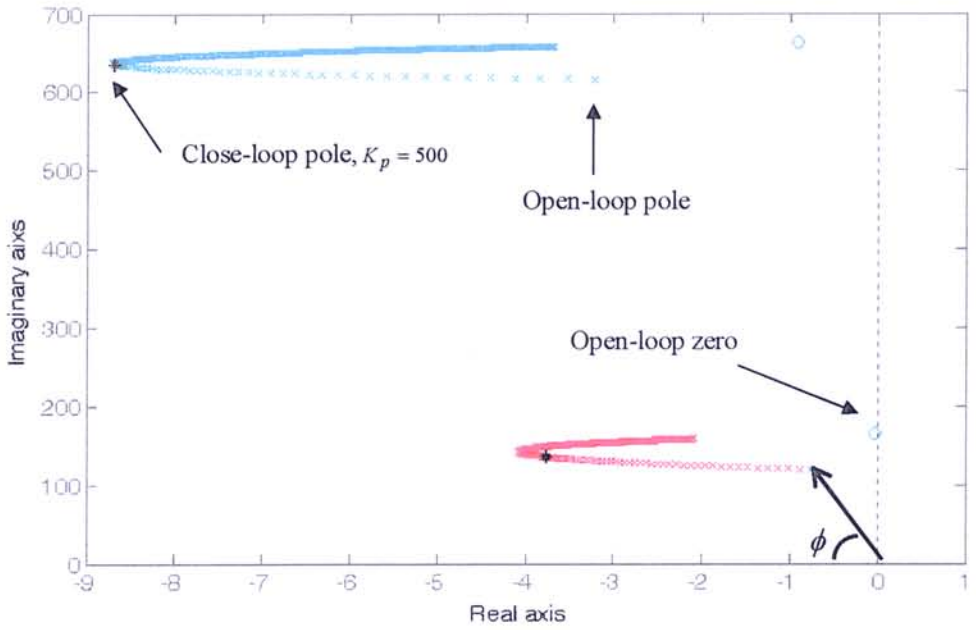

(b)

Figure 3-6 Root locus diagram for proportional control

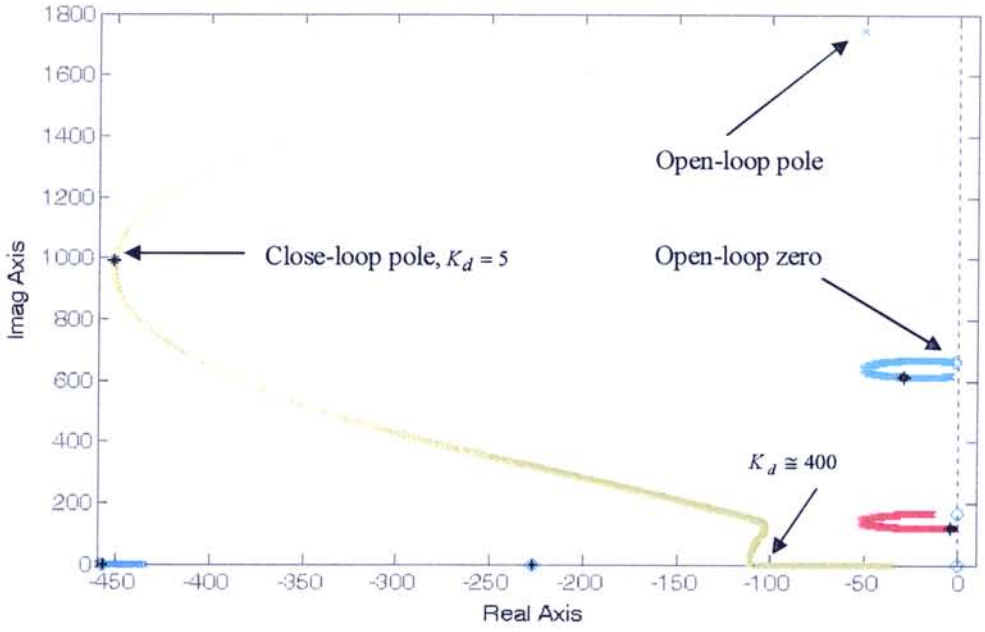

(a)

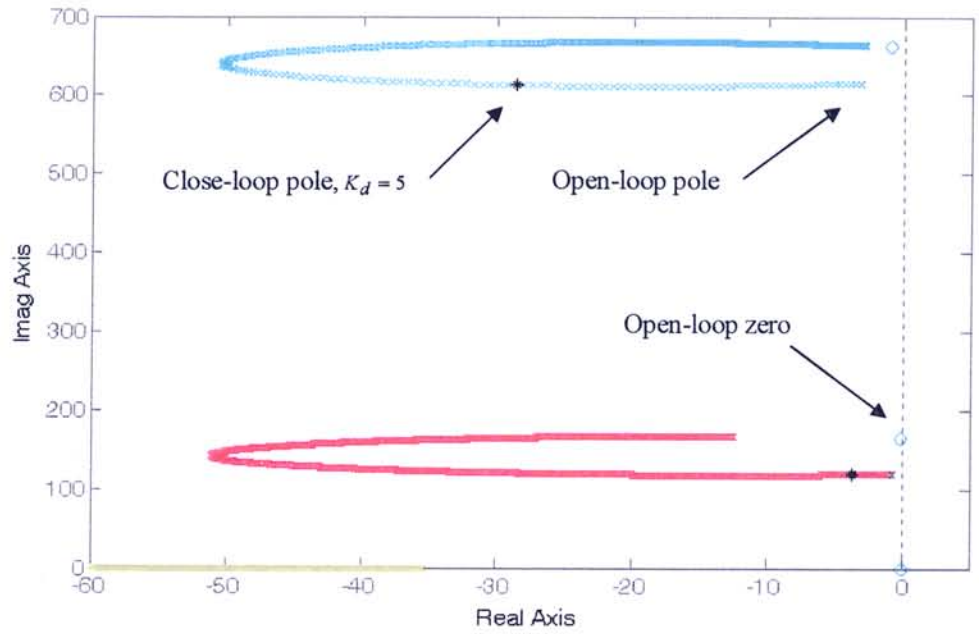

(b)

Figure 3-7 Root locus diagram for derivative control

It can be seen that for proportional control, the dampings of all the three modes can be enhanced with the increase of gain value. However, when the proportional control gain is increased beyond 500, the dampings of the first and second modes will decrease on further increasing K_p. As for the derivative control (Figure 3-7), the effects of K_d on the first and second modes are similar to those of K_p. For the third mode, since ϕ decreases monotonically with K_d, the increase of K_d will always enhance the third mode damping. However, large derivative control gain can overdamp the third mode. As shown in Figure 3-7, the third mode becomes an overdamped mode when K_d is greater than 400.

In the practical implementation of ACLD structures, the control gains are limited to prevent voltage saturation of the piezoelectric actuators. Also, spillover problem is also necessary to be taken into account. In order to demonstrate the effectiveness of ACLD treatments, an arbitrary combination of proportional and derivative gains is selected (K_p= 300 and K_d=3). Figure 3-8 shows that with active control, the peak values are reduced, without exciting the fourth and fifth modes. It means that the dampings of the first three modes are increased, as compared to PCLD. Figure 3-9 shows the impulse responses of PCLD treated and ACLD treated beam. It is obvious that the ACLD outperforms the PCLD. It is worth mentioning that due to stability consideration, the values of K_p and K_d are not kept the same for the study of the effects of layer physical and geometrical properties.

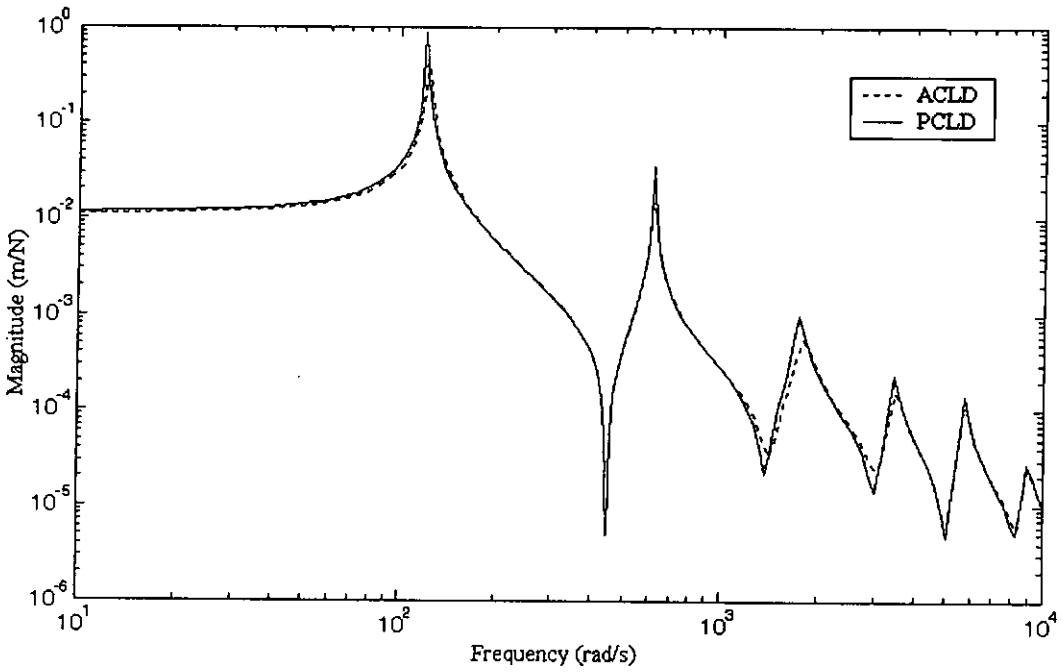

Figure 3-8 Comparison of frequency response functions between PCLD and ACLD

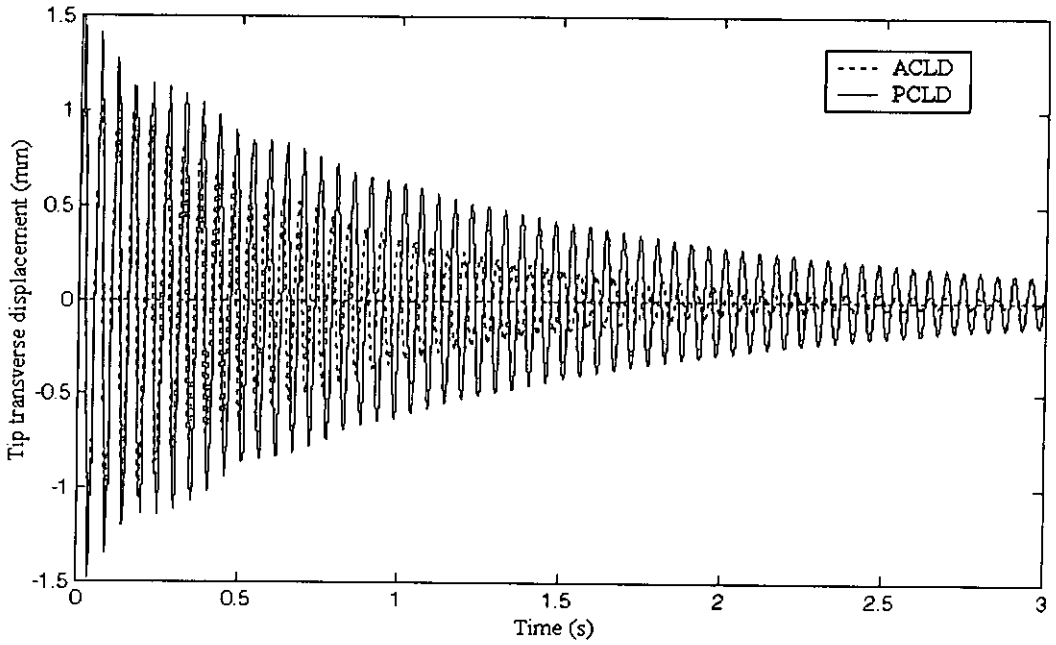

Figure 3-9 Comparison of impulse responses of beam tip transverse displacements between PCLD and ACLD

3.2.2 Effect of Layer Physical and Geometrical Properties

Constraining Layer Thickness

K_p: 5 t_v : 0.25 mm P : 30 mm

K_d: 0.01 l : 100 mm G^∞: $5x10^5$ Pa

It is found from Figure 3-10 that reducing the constraining layer thickness toward zero leads to a decrease in the damping of all the three modes. This is in agreement with the existing knowledge on the passive constrained layer damping treatment [86]. A thick piezoelectric layer increases the stiffness of the constraining layer and hence increases the passive damping. As for the hybrid damping, a thick piezoelectric layer means better active control authority, thus improving the hybrid damping. Although an increase in constraining layer thickness monotonically increases the damping, meaning that the thicker the layer, the higher the damping, it should be noted that there is a tradeoff between the increase in constraining layer and weight.

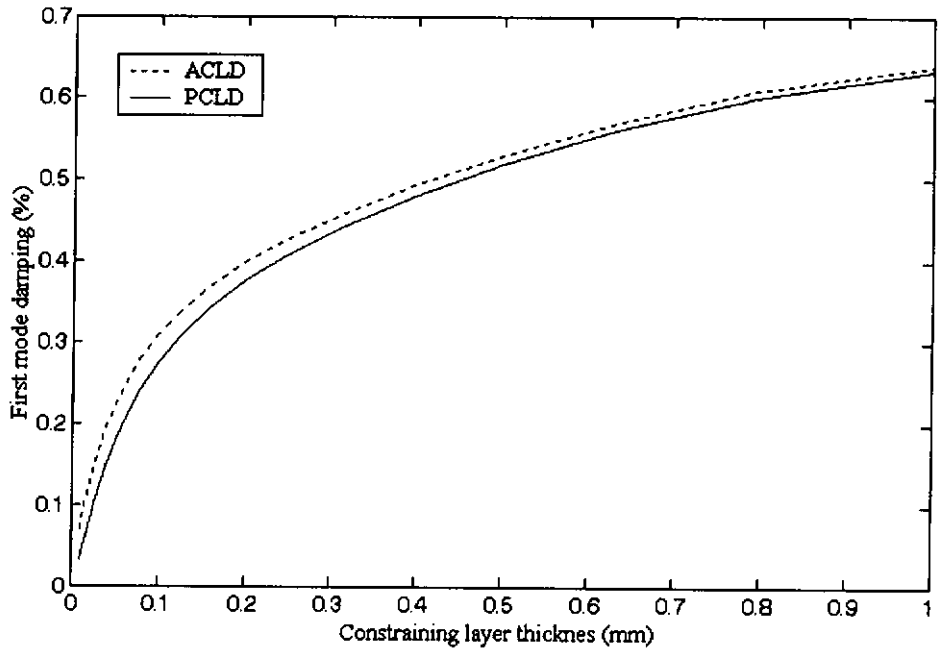

Figure 3-10(a) Effect of constraining layer thickness on the first mode damping

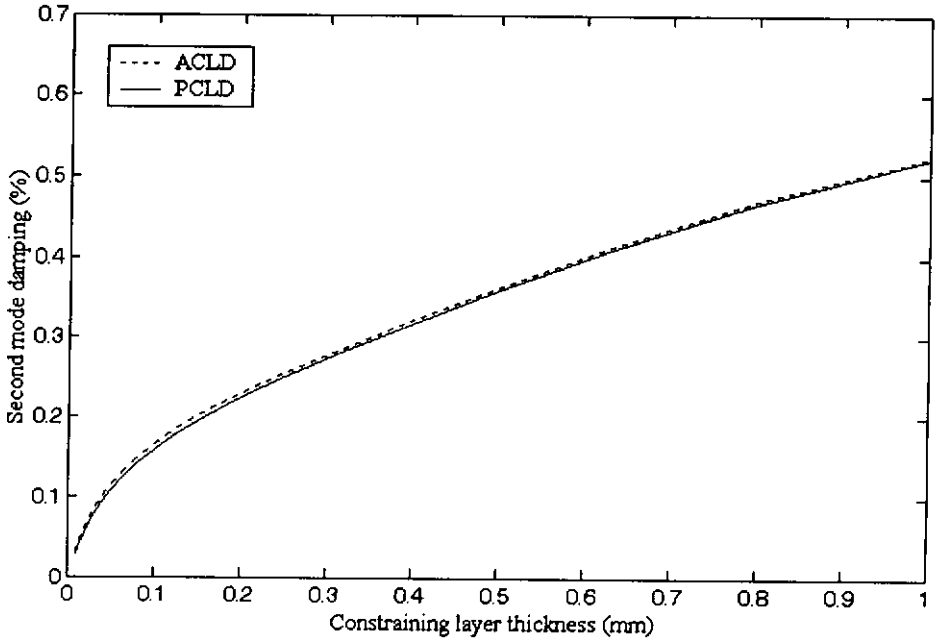

Figure 3-10(b) Effect of constraining layer thickness on the second mode damping

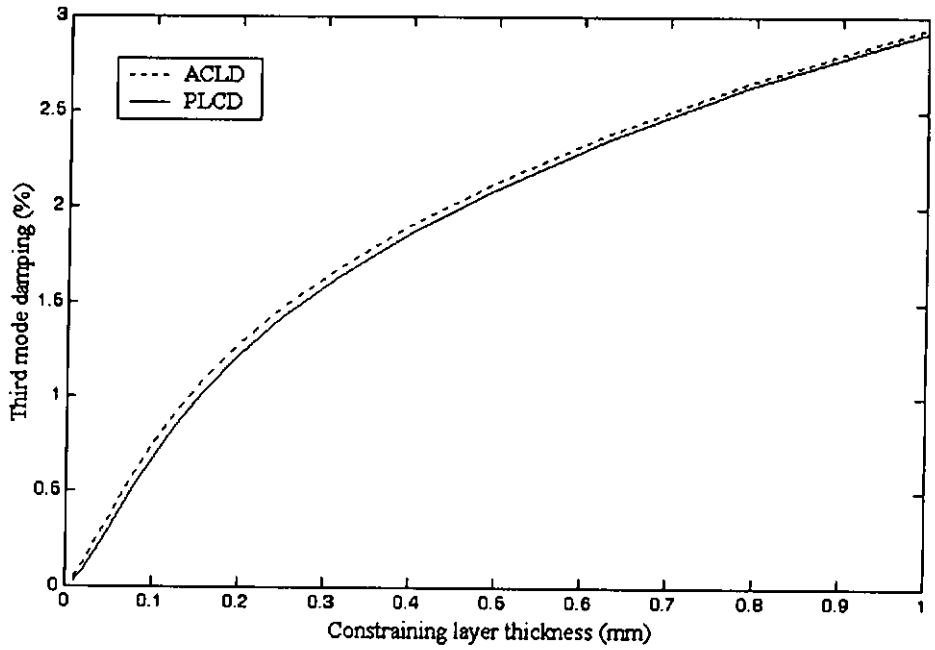

Figure 3-10(c) Effect of constraining layer thickness on the third mode damping

Viscoelastic Layer Thickness

K_p: 30 t_p : 1 mm P : 30 mm

K_d: 0.01 l : 100 mm G^{∞}: 5×10^5 Pa

Results, presented in Figure 3-11, indicate that for thin viscoelastic layer, the increase of layer thickness increases the damping rapidly. However, the damping reaches a maximum value and further increase of viscoelastic layer thickness causes a decrease in damping. In other words, there is an optimal thickness of viscoelastic layer, meaning that neither too thin nor too thick viscoelastic layers leads to effective hybrid damping.

It can also be seen that for the first and second modes, the modal dampings are optimal for relatively thin cores, while for the third mode, the optimal thickness is higher. Figure 3-11 also illustrates that increasing the viscoelastic layer thickness reduces the transmissibility between the piezoelectric constraining layer and the base beam. This is the reason for the decrease in the ACLD performance with the increase of viscoelastic layer thickness.

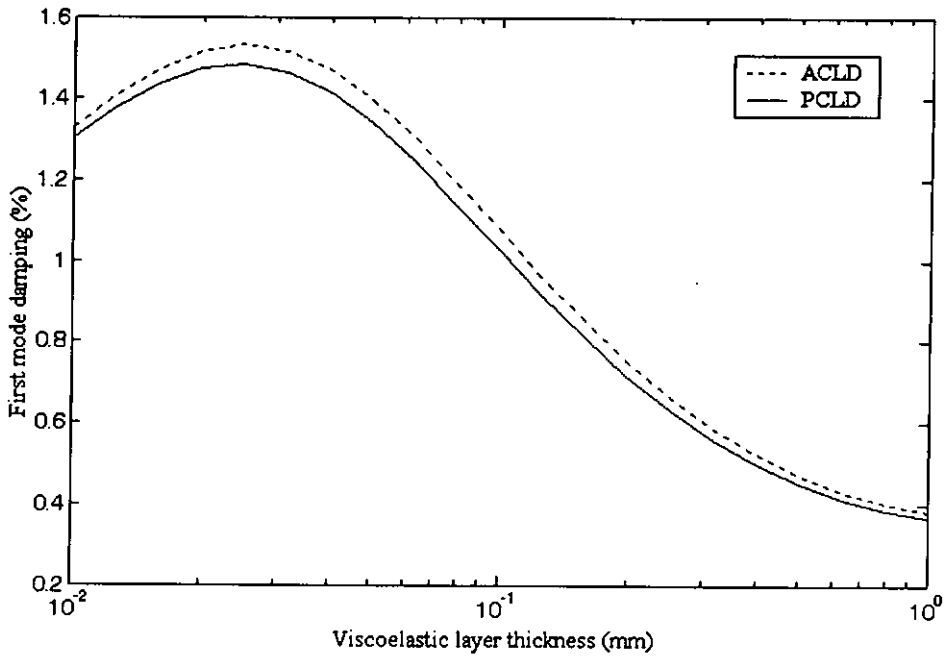

Figure 3-11(a) Effect of viscoelastic layer thickness on the first mode damping

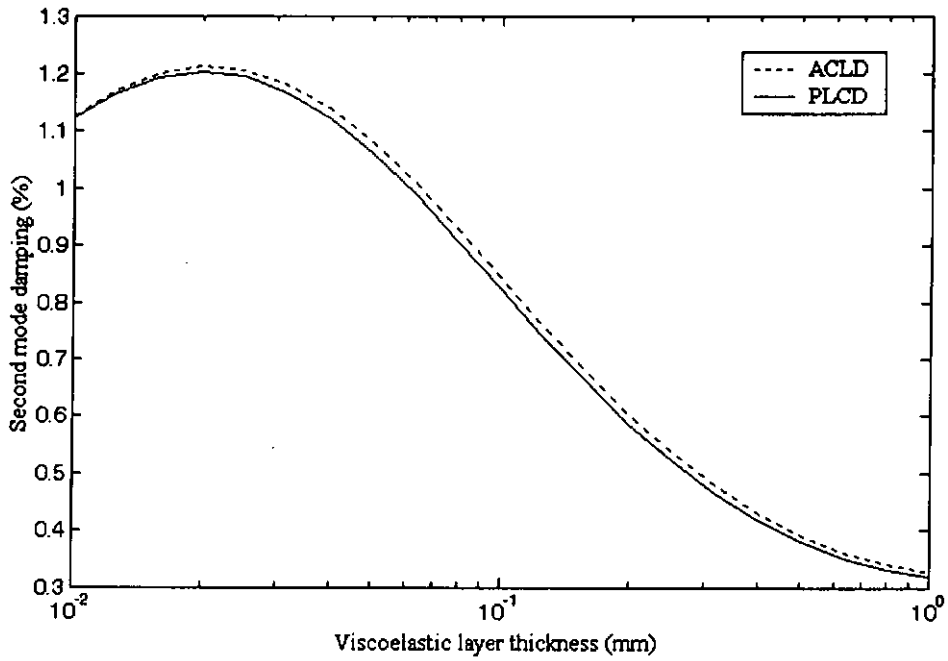

Figure 3-11(b) Effect of viscoelastic layer thickness on the second mode damping

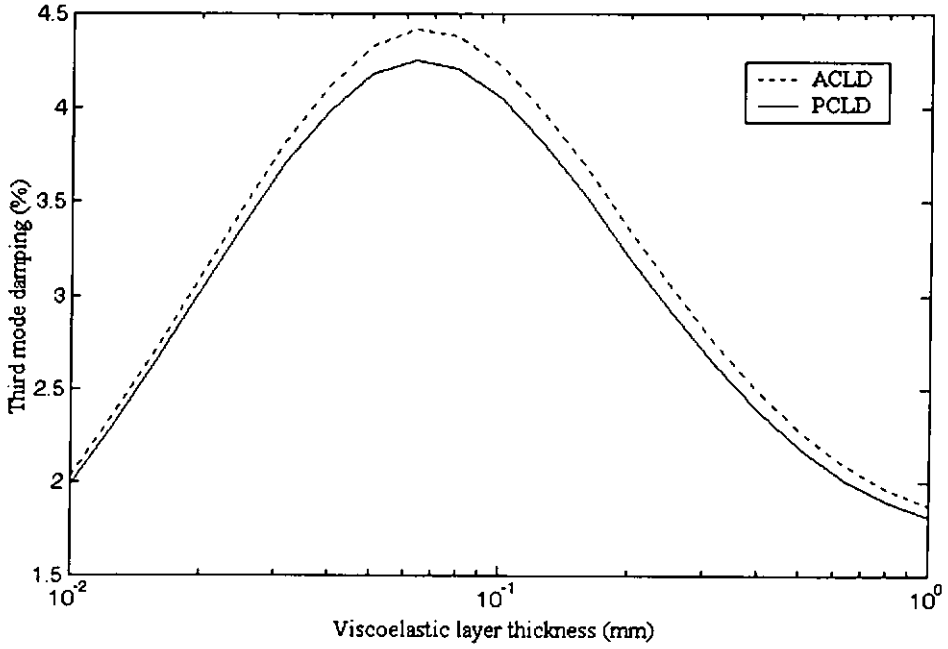

Figure 3-11(c) Effect of viscoelastic layer thickness on the third mode damping

The first mode passive damping of the system is presented in Figure 3-12 for various viscoelastic and constraining layer thickness. It can be seen that the optimal value of the viscoelastic layer disappears as the constraining layer thickness approaches to zero. The reason for this is that an unconstrained layer damping treatment is forming, as the thickness of the constraining layer is reducing. For unconstrained layer damping treatment, the thicker the viscoelastic layer, the higher the damping is obtained.

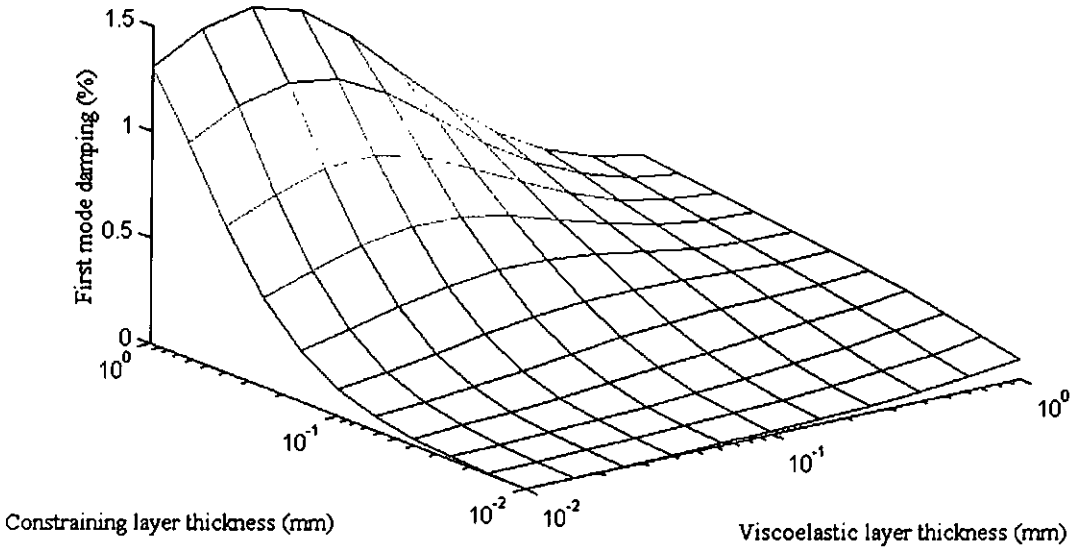

Figure 3-12 Passive damping of the first mode for various viscoelastic and constraining layer thicknesses

Shear Modulus

K_p: 160 t_p : 1 mm l : 100 mm

K_d: 0.01 t_v : 0.25 mm P : 30 mm

It has been shown that the shear modulus is proportional to G^∞ [45]. It means that varying the equilibrium value of shear modulus G^∞ is equivalent to varying the shear modulus. It can be observed from Figure 3-13 that both the passive and active damping increase with G^∞ up to certain level and afterwards decrease with further increase in G^∞. In other words, there exits an optimal G^∞ value for maximum damping. It can be attributed to the fact that for a given shear stress and a constant material loss factor, the energy dissipation in the viscoelastic layer is proportional to the magnitude of G^∞ as well as to the square of the shear strain amplitude. For a compliant viscoelastic layer (low G^∞ value), shear strain amplitude is high, yet there is little energy dissipation due to the low shear modulus. On the other hand, for a stiff viscoelastic layer (high G^∞ value), owing to the low shear strain amplitude; there is still little energy dissipation. Only intermediate values of G^∞ can give both sufficiently large shear loss modulus and shear strain amplitude to provide a large damping. The first mode passive damping of the system is presented in Figure 3-14 for various viscoelastic layer thicknesses and the equilibrium value of shear modulus. It can be seen that the optimal value of shear modulus shifts to a higher value as the viscoelastic layer thickness increases.

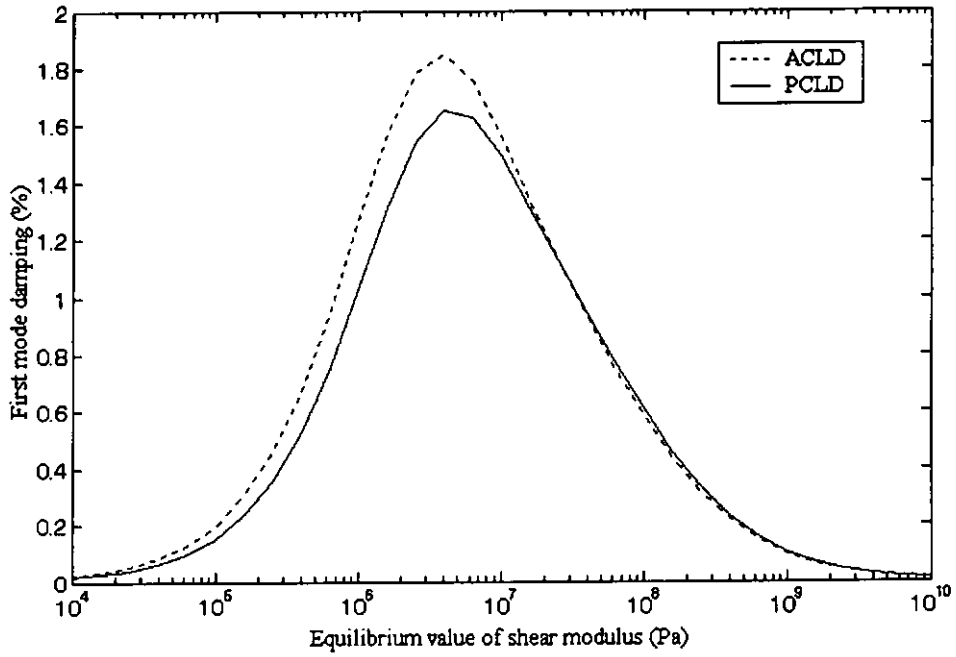

Figure 3-13(a) Effect of equilibrium value of shear modulus on the first mode damping

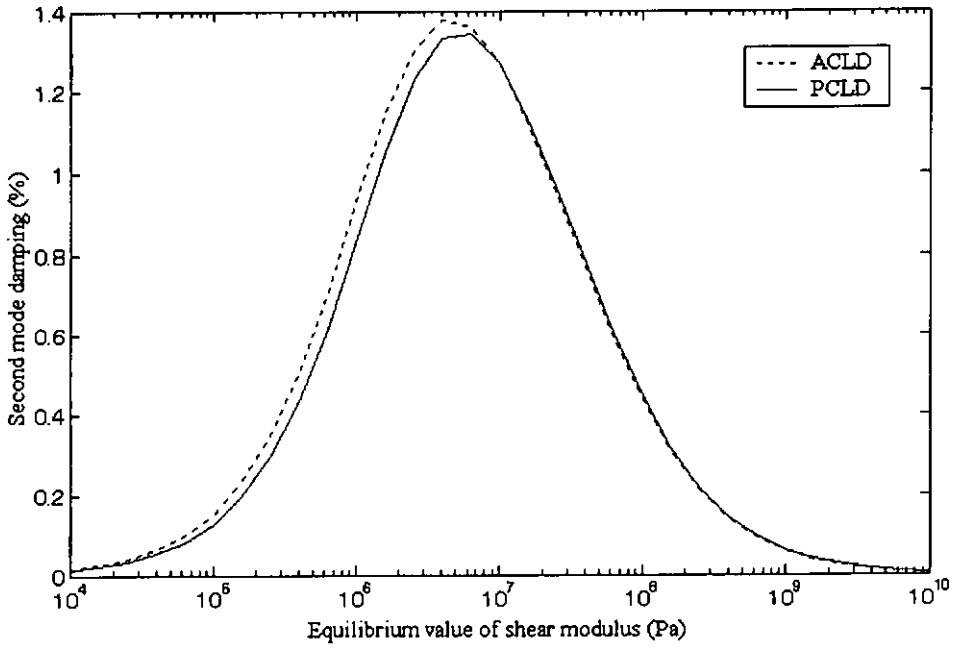

Figure 3-13(b) Effect of equilibrium value of shear modulus on the second mode damping

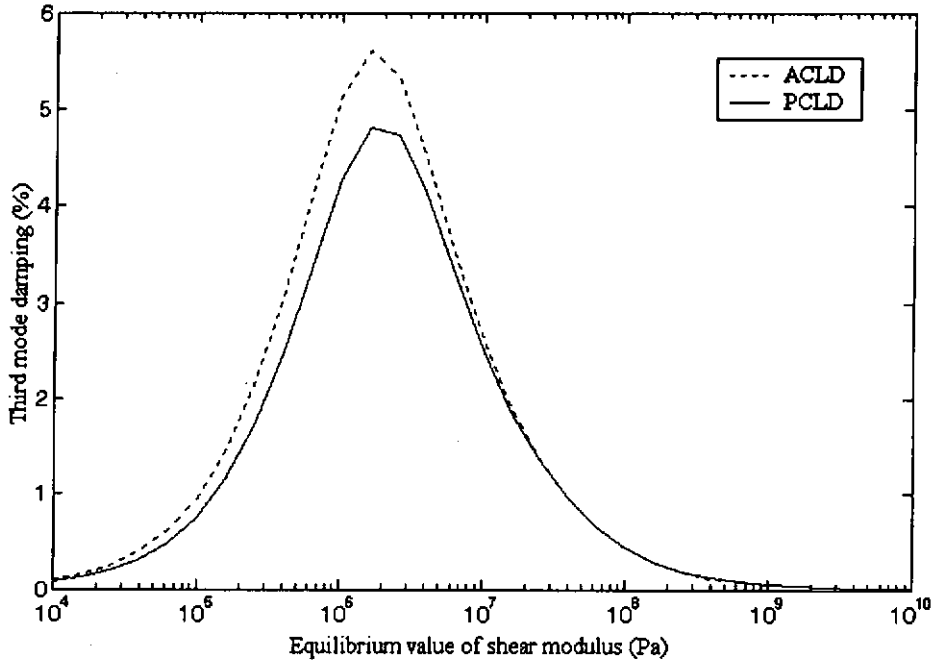

Figure 3-13(c) Effect of equilibrium value of shear modulus on the third mode damping

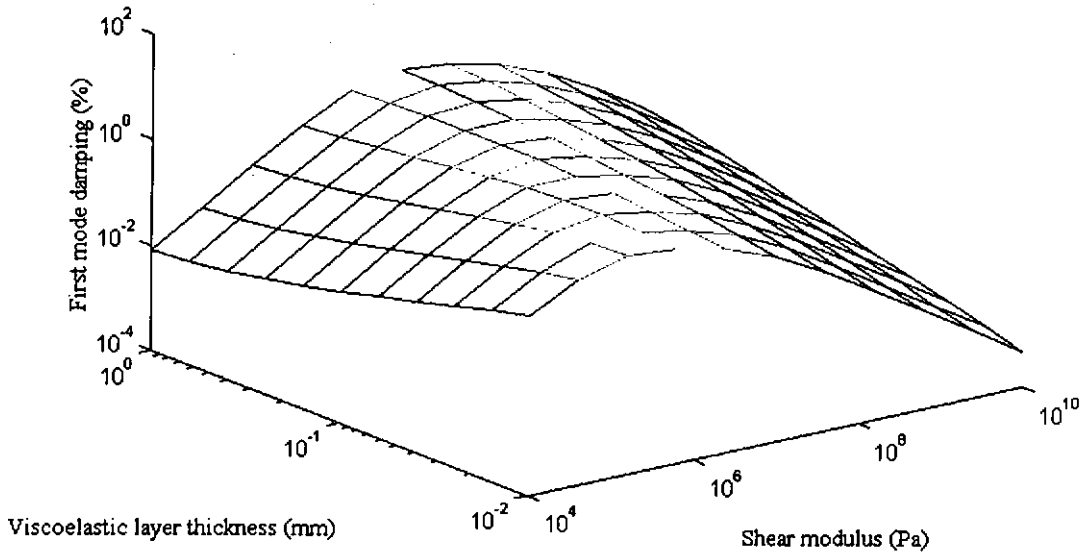

Figure 3-14 Passive damping of the first mode for various equilibrium value of shear modulus and viscoelastic layer thickness

3.2.3 Effect of ACLD Patch Arrangements

Treatment Location

K_p: 300 t_p : 1 mm l : 100 mm

K_d: 0.01 t_v : 0.25 mm G^{∞}: $5x10^5$ Pa

It can be observed from Figure 3-15(a) that for the first mode, as the ACLD patch moves from the root of the beam to the tip, both the passive and hybrid damping simply decrease. For the second mode, as shown in Figure 3-15(b), the damping ratio initially increases with the departure of the patch, and then decreases with further departure. It can be seen from Figure 3-15(c) that the third mode damping oscillates through out the movement of the ACLD patch. In fact, the damping of all the three modes show characteristics of their mode shapes as the patch is moved along the length of the beam. This is due to the fact that high damping is best achieved when the viscoelastic layer is subjected to large bending stress. Besides, for all the modes, it can be found that the hybrid damping is more effective for a patch location with higher passive damping. It can also be concluded that the degree of improvement in damping of individual modes depends on the ACLD patch location.

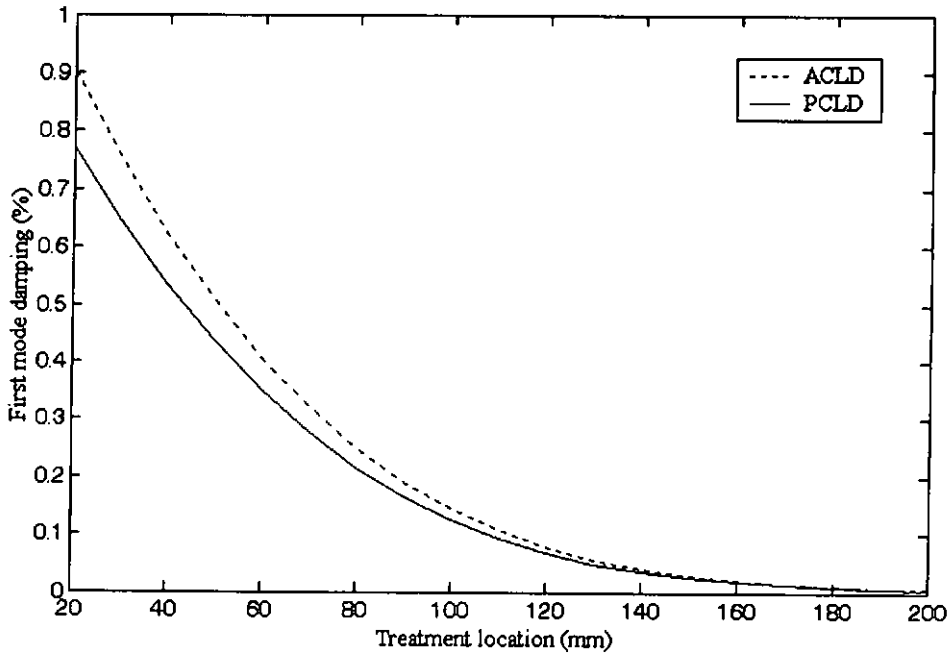

Figure 3-15(a) Effect of treatment location on the first mode damping

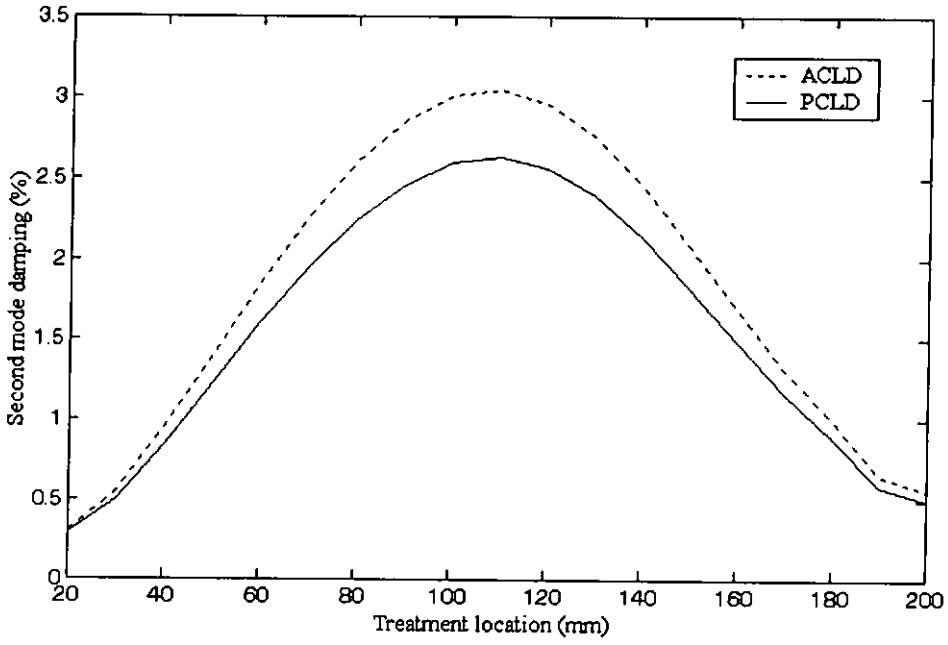

Figure 3-15(b) Effect of treatment location on the second mode damping

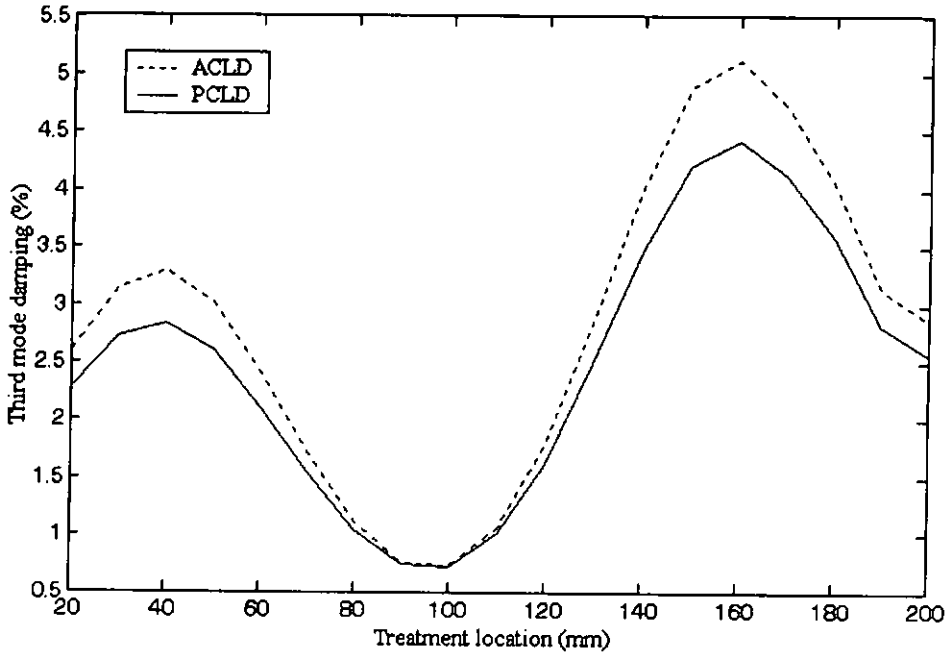

Figure 3-15(c) Effect of treatment location on the third mode damping

Treatment Length

K_p: 300 t_p : 1 mm P : 30 mm

K_d: 0.01 t_v : 0.25 mm G^{∞}: $5\text{x}10^5$ Pa

The effects of varying the length of the ACLD patch on the first three dampings are shown in Figure 3-16. It is evident that short treatments generally are not effective in vibration reduction. Increasing the length results in enhancing the damping ratios, especially for hybrid damping. As far as a clamped-free beam is concerned, the highest bending strains (proportional to the value of curvature) occur near the root and center of

the beam for the first and second modes respectively (Figure 3-15(a) and (b)). This is the reason why once the largest damping is reached, further enhancement in the treatment length makes no improvement to the damping. For the third mode, the high bending strains distribute over the entire beam (Figure 3-15(c)). Therefore, increasing the ACLD treatment coverage means covering more high bending strain regions, thus increasing damping. However, it can also be seen from Figure 3-16 that there are slightly decreases in hybrid dampings in both the first and second modes, when the hybrid dampings attain their highest values. It is due to the fact that an increase in treatment length causes an increase in weight of the structure, which in turn, increases the modal frequencies. Hence, the hybrid damping performance is deteriorated.

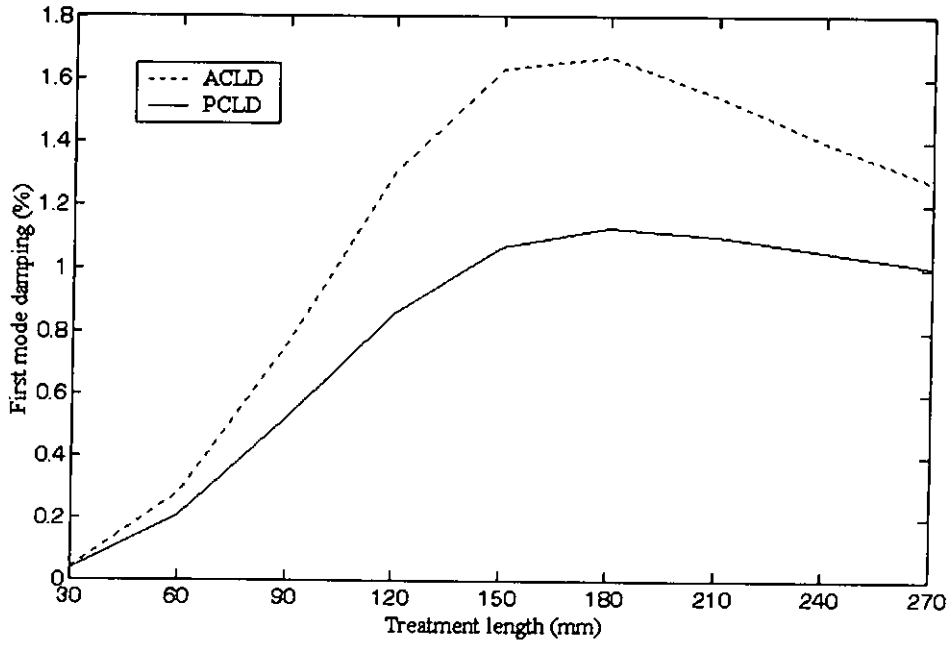

Figure 3-16(a) Effect of treatment length on the first mode damping

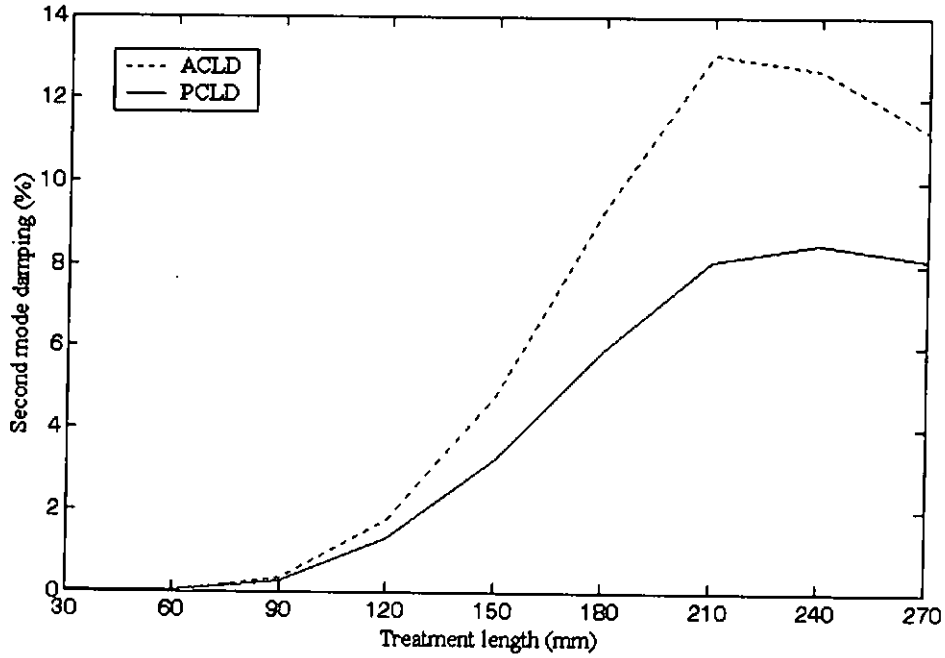

Figure 3-16(b) Effect of treatment length on the second mode damping

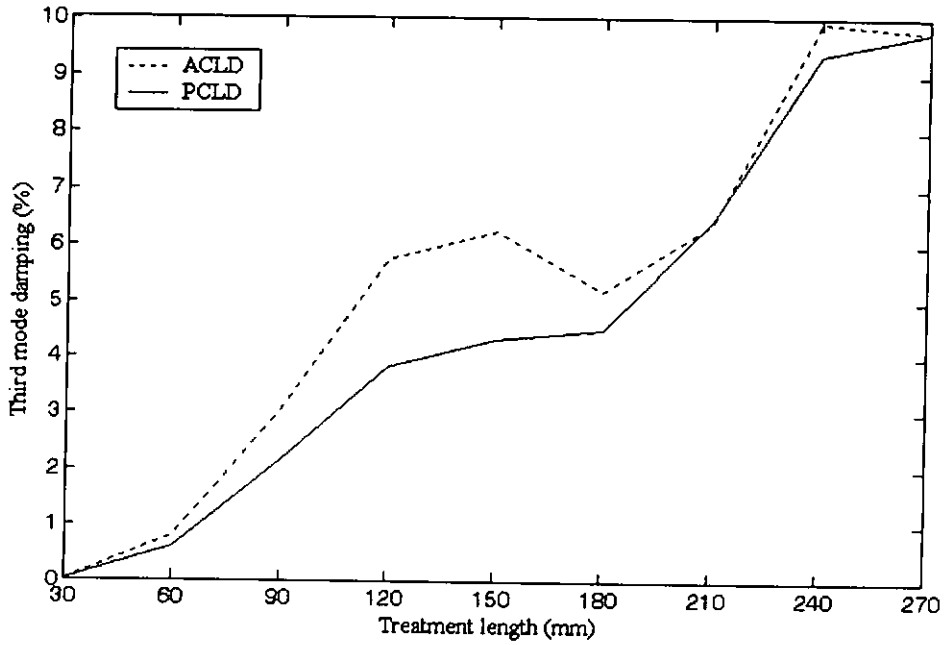

Figure 3-16(c) Effect of treatment length on the third mode damping

3.3 SUMMARY

The above findings can be summarized as follows:

(i) The selection of control gains is important since improper gain values can decrease the modal dampings, and even lead to destabilization of systems.

(ii) The best location for the damping treatment is the one with the highest bending strains.

(iii) The most effective location of the damping treatment is mode dependent.

(iv) An increase in the constraining layer thickness increases both the passive and hybrid dampings.

(v) There is an optimal thickness of the viscoelastic layer to obtain maximum damping.

(vi) There exists an optimal value of shear modulus for maximum damping.

CHAPTER 4

OPTIMIZATION OF ACLD TREATMENT FOR SHAPE CONTROL USING MULTI-OBJECTIVE GENETIC ALGORITHM

In this chapter, based on the previous parametric study of ACLD treatment, the shape control system design is formulated. The design is treated as a multi-objective optimization problem. The solution is done in an integrated manner to give optimal values of both the design variables and the control gains, by using Multi-objective Genetic Algorithm (MOGA) searching technique [87].

4.1 SHAPE CONTROL PROBLEM

In this study, the shape control problem under consideration is to drive the structure from its initial shape to the desired shape and prevent it from being distorted by external disturbances. The shape of the beam is described by the shape of the mid-plane of the beam, which in turn is described by the transverse displacement w of beam nodes [27]. The desired shape of the mid-plane is given by:

$$w_d = \zeta(x) \tag{4.1}$$

where w_d is the desired transverse displacement at a point on the beam and ζ defines the desired shape as a function of x. $\zeta(x)$ is continuous and differentiable.

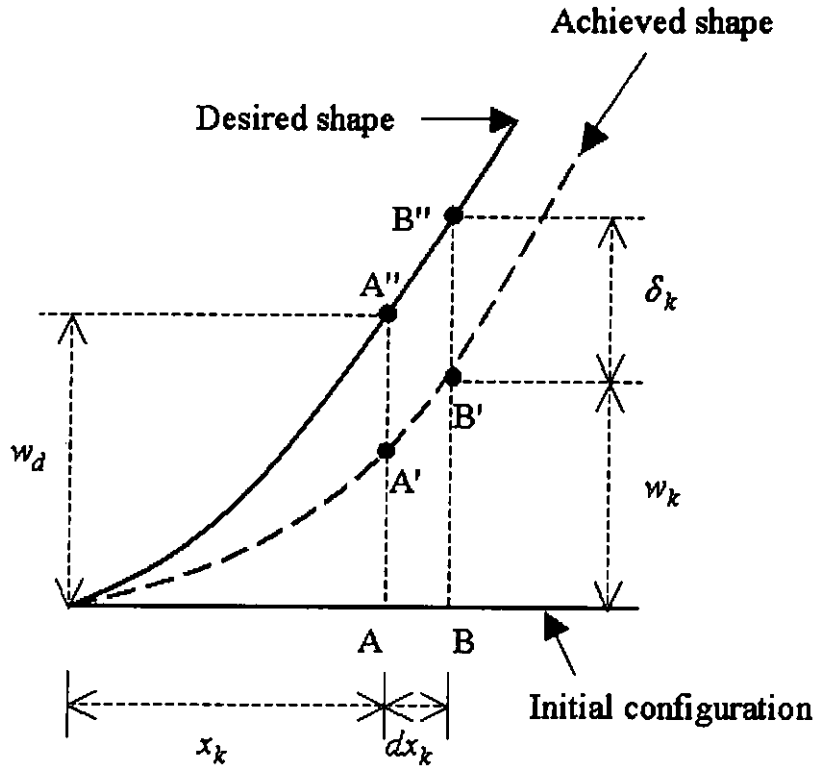

Figure 4-1 Beam shape configuration

4.1.1 Error Function

The error function is defined as:

$$e = \sum_{k=1}^{n} (\zeta_k - w_k)^2 = \sum_{k=1}^{n} \delta_k^2 \tag{4.2}$$

where n is the total number of nodes; w_k is the actual transverse displacement of the k^{th} node; ζ_k is the corresponding desired displacement and δ_k is the displacement error at the k^{th} node. However, the error function defined in Eq. (4.2) does not consider the extension of the middle plane, i.e. u. To allow for this extension, consider a node A

on the original mid-plane at x_k, as shown in Figure 4-1. On the application of voltages, point A on the original surface moves to point B' on the achieved surface. BB' is the z-coordinate of the point B' and B'' is the point on the desired surface which corresponds to point B' on the achieved surface. BB'' is the z-coordinate of the point B'' and $(x_k + dx_k)$ is the x-coordinate of both B' and B''. Thus the error is given by:

$$\delta_k = \mathrm{BB}^{''} - \mathrm{BB}^{'} \tag{4.3}$$

or

$$\delta_k = \zeta(x_k) + (\zeta'(x_k)u_k) - w_k \tag{4.4}$$

where u_k or (dx_k) is the axial displacement of the k^{th} node.

In the present study, the desired shape function under consideration is a parabolic shape function [88], given by:

$$w_d(x) = Cx^2 \tag{4.5}$$

It is selected due to its mathematical simplicity and its applicability to common structures such as antennas. This shape function has uniform curvature C over the length of the beam.

4.1.2 Control Law

The block diagram for the whole system with two ACLD patches (for illustration) is shown in Figure 4-2.

The control laws are given by:

$$\begin{pmatrix} V_{c1} \\ V_{c2} \end{pmatrix} = \begin{bmatrix} K_{P1} & 0 \\ 0 & K_{P2} \end{bmatrix} \begin{pmatrix} \Delta V_{s1} \\ \Delta V_{s2} \end{pmatrix} + \begin{bmatrix} K_{I1} & 0 \\ 0 & K_{I2} \end{bmatrix} \begin{pmatrix} \int \Delta V_{s1}\, dt \\ \int \Delta V_{s2}\, dt \end{pmatrix} + \begin{bmatrix} K_{D1} & 0 \\ 0 & K_{D2} \end{bmatrix} \begin{pmatrix} \Delta \dot{V}_{s1} \\ \Delta \dot{V}_{s2} \end{pmatrix}$$

$$+ \begin{pmatrix} k_{p1}^{'} \\ k_{p2}^{'} \end{pmatrix} \Delta V_{st} + \begin{pmatrix} k_{i1}^{'} \\ k_{i2}^{'} \end{pmatrix} \int \Delta V_{st}\, dt + \begin{pmatrix} k_{d1}^{'} \\ k_{d2}^{'} \end{pmatrix} \Delta \dot{V}_{st} \qquad (4.6)$$

where V_c is the control voltage, K_P, K_I and K_D are respectively the proportional, integral and derivative gains for the piezoelectric sensor feedback; $k_p^{'}$, $k_i^{'}$ and $k_d^{'}$ are respectively the proportional, integral and derivative gains for the tip position sensor feedback; ΔV_s is the difference between the actual piezo-sensor output and the desired sensor output V_d, which is obtained by using Eq. (2.31). Suffices 1 and 2 denote patch number 1 and 2 respectively. For instance, for the first patch, $V_{d1} = \frac{E_p d_{31} hb}{C_a}\left(w_d'(x_2) - w_d'(x_1)\right)$ (x_1 and x_2 are the two edge positions of the first patch); ΔV_{st} is the difference between the position sensor output and the desired position sensor output, V_{dt} .

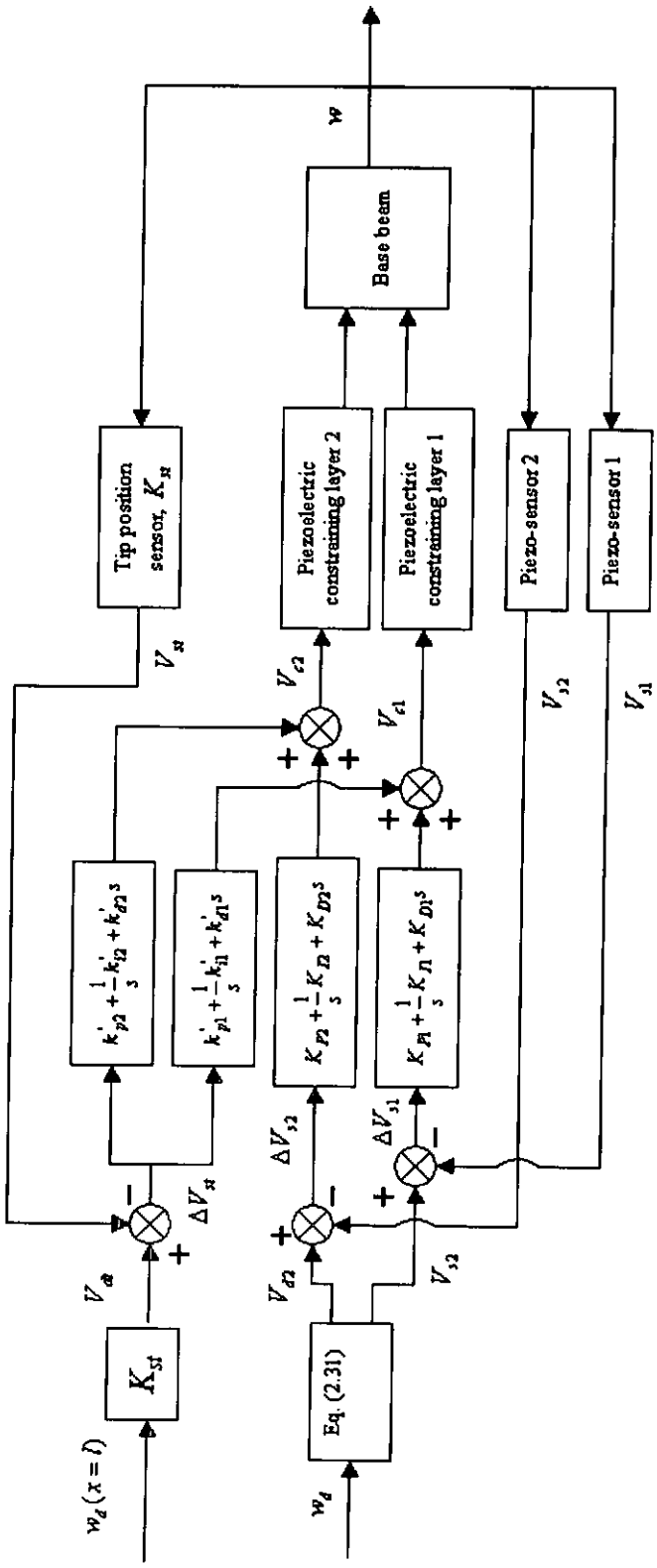

Figure 4-2 Block diagram of shape control system with two ACLD patches

4.2 MULTI-OBJECTIVE DESIGN PROBLEM AND GENETIC ALGORITHM

4.2.1 Concept of Multi-objective Optimization

A general constrained multi-objective optimization problem can be defined mathematically as:

Minimize $f(d) = \{f_1(d),...,f_i(d),...,f_m(d)\}$

subject to $d \in D$ (4.7)

$D = \{d : g_j(d) \le 0,\ \ j = 1,...,J,\ \ h_k(d) = 0,\ \ k = 1,...,K\}$,

where d is an n x 1 design variable vector, $f(d)$ is an m x 1 vector of design objectives that are at least partly conflicting, $g_j(d)$ is the j^{th} inequality constraint and $h_k(d)$ is the k^{th} equality constraint. The set of design vectors that satisfies all equality and inequality constraints constitutes the feasible domain D. Mathematically, a design solution $d^* \in D$ is said to be Pareto optimal if there does not exist another solution $d \in D$ such that $f_i(d) \le f_i(d^*)$ for all $i = 1,...,m$ with strict inequality for at least one i. Any other feasible solution $d \in D$ with $f_i(d^*) \le f_i(d)$ for all $i = 1,...,m$, is an inferior solution.

4.2.2 Background of Genetic Algorithm

Genetic Algorithms (GA) were invented and developed, initially by J. Holland and his associates at the University of Michigan in the 1960s and 1970s [89], to mimic some of the processes observed in natural selection. GAs are a form of randomized search, in that the way in which strings are chosen and combined is a stochastic process. This is a radically different approach to the problem solving methods used by more traditional algorithms, which tend to be more deterministic in nature, such as the gradient methods

used to find minima in graph theory. GA exploits the idea of "survival of the fittest" and an interbreeding population to create a novel and innovative search strategy. A population of strings (or chromosomes), representing solutions to a specified problem, is maintained by the GAs. The GAs then iteratively create new populations from the old by ranking the strings and interbreeding the fittest to create new strings, which are probably closer to the optimum solution of the problem at hand. So in each generation, the GAs create a set of strings from the bits and pieces of the previous strings, occassionally adding random new data to prevent the population from stagnating. The end result is a search strategy that is tailored for vast, complex, multimodal search spaces. The idea of survival of the fittest is of great importance to GAs. GAs use a fitness function in order to select the fittest string that will be used to create new, and conceivably better, populations of strings. The fitness function takes a string and assigns a relative fitness value to the string. The method by which it does this and the nature of the fitness value do not matter. The only thing that the fitness function must do is to rank the strings in some way by producing the fitness value. These values are then used to select the fittest strings.

GAs start with a random creation of a population of strings and then generates successive populations of string that improve over time (evolution). Traditionally, strings (chromosomes) are simple binary vectors. The processes involved in the generation of new populations mainly consist of the followings:

Reproduction: it is a process in which individual strings are copied according to their fitness (objective) function values. Strings with a higher fitness value have a probability of contributing one or more offspring in the next generation. The reproduction operator may be implemented in an algorithmic form in a number of ways such as roulette wheel selection [90] and stochastic universal sampling [91]. Once a string has been selected for reproduction, an exact replica of the string is made. This string is then entered into the mating pool, a tentative new population for further genetic operator action.

Crossover: it is considered as the primary operator that makes GAs converge to an optimum. After reproduction, simple crossover may proceed in two steps. First, members of newly reproduced strings in the mating pool are mated at random. Second, each pair of strings undergoes crossing over as follows: an integer k along the string is selected uniformly at random between 1 and string length l minus one. Two new strings are crested by swapping all the characters between positions $(k+1)$ and l inclusively, as illustrated in Figure 4-3(a). This crossover operation is not necessarily performed on all strings in the population. Instead, it is applied with a probability P_c (or crossover rate) when the pairs are chosen for breeding.

Mutation: it is a complementary operator that prohibits converging to a local optimum. Mutation is a random alteration of the value of a string position. In binary coding, this means changing a 1 to 0 and vice versa (Figure 4-3(b)). Like crossover, mutation is applied to the chromosomes with a probability P_m (or mutation rate). In GAs, its

probability of occurrence rate would lead to a loss of important data. GAs, with 100% mutation rate, become random search in the solution space.

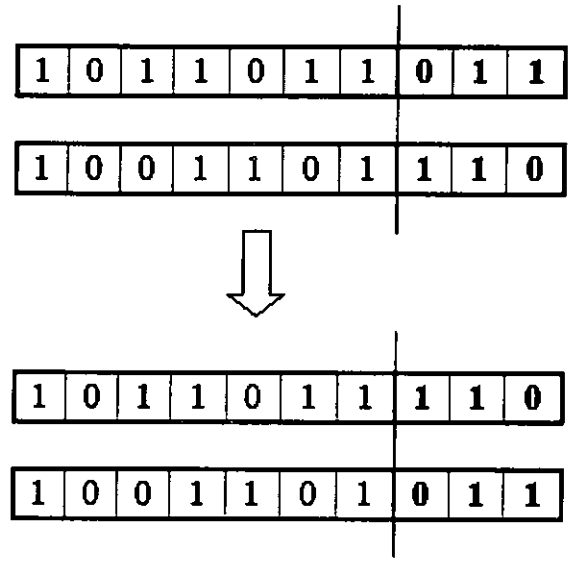

(a)

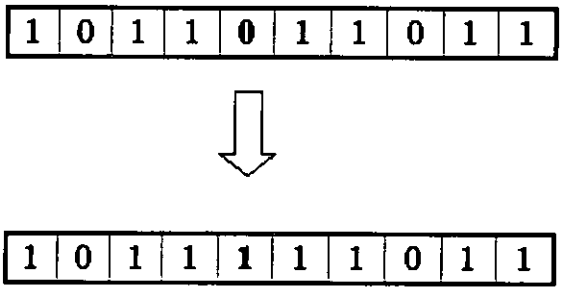

(b)

Figure 4-3 Schematic representations of basic genetic algorithm operations

4.2.3 Multi-objective Genetic Algorithm

In fact, GAs have been mainly applied to single-objective optimization problems. However, in real-world optimization, the multi-objective optimization is often required rather than the single-objective optimization since there exist tradeoffs between various objectives in general. As described in the previous section, the solution to a multi-objective optimization problem is not a single point. It consists of a family of points, the Pareto-optimal set, which describes the trade-offs available in the problem. Each point in this set is such that no improvement can be achieved in any one objective without degrading in at least one of the remaining objectives.

GAs have many attractive advantages to solve multi-objective problems. Since GAs seek optimal solutions in parallel, multiple Pareto solutions can be obtained simultaneously without specifying weights between objectives. The multi-objective genetic algorithms (MOGAs) were first introduced by Fonseca and Fleming [87]. The main difference between a conventional GA and a MOGA resides in the assignment of fitness. Once fitness has been assigned to individuals, selection can be performed and genetic operators applied as usual.

For each generation, the dominant value of an individual or a point in the population is calculated as follows. For a set of points in the objective space, $P = (p_1, ..., p_{np})$, the dominant value of a point $p_k (p_k \in P)$ is defined as the number of all other points in the set P that dominates p_k. For example, if n points in the set P dominate the point p_k,

the dominant value of the point p_k is quantified as n (Figure 4-4). The individuals with zero dominant value are identified. These individuals are called the non-inferior individuals. Note that while these individuals are non-inferior for the current population, they are most likely non-Pareto for the problem in an absolute sense. These non-inferior individuals are given the highest rank in the current population. With the highest probability, these non-inferior individuals will become parents to produce offspring, and the process is repeated. As such, the population is gradually improved as it approaches the final population and the corresponding Pareto set for the problem.

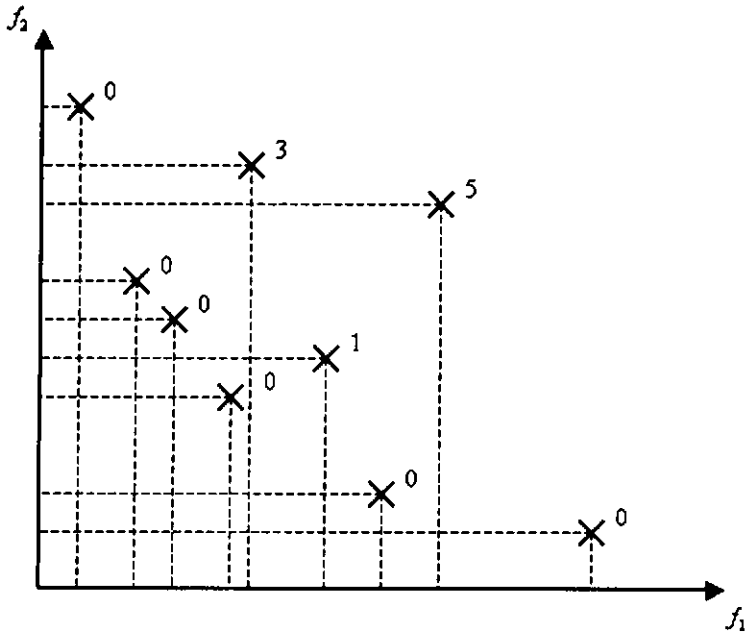

Figure 4-4 Examples of dominant value assignment

4.3 OPTIMIZATION PROBLEM FORMULATION

4.3.1 Objective Functions

When selecting the proper design objectives, both open and closed-loop requirements are considered. With respect to open-loop, certain amount of passive damping is necessary for stability and fail-safe consideration. Thus, it is reasonable that the maximization of the passive damping should be a design objective. Meanwhile, a heavy structure is undesirable, so the minimization of treatment weight is necessary. On the other hand, when it comes to closed-loop, the minimization of the error between the desired and achieved shapes is another concern. As a result, the objective functions used in this study can be stated as follows:

(1) Minimizing the error function at steady state.

Objective function $1\,\Phi_1$: e

(2) Minimizing the total weight of treatment on the structure.

Objective function $2\,\Phi_2$: $(\rho_p t_p b(L_1 + L_2 + L_3)) + (\rho_v t_v b(L_1 + L_2 + L_3))$

(3) Minimizing the reciprocal of the weighted damping of the first three modes.

Objective function $3\,\Phi_3$: $\dfrac{1}{\dfrac{\xi_1}{f_1} + \dfrac{\xi_2}{f_2} + \dfrac{\xi_3}{f_3}}$

where ξ, f are the damping ratio and frequency, and the suffices 1, 2 and 3 denote the first, second and third mode respectively.

4.3.2 Design Variables

From the previous parametric study, it is known that the thicknesses of both the piezoelectric constraining (t_p) and viscoelastic layers (t_v) have contribution to the treatment weight and directly affect the damping performance of the structure. Besides, in addition to the control gains (K_P, K_I, K_D, k_p, k_i and k_d), the locations (P), spacing (S) and length (L) of the ACLD patches also have influences on the precision of shape change. Thus, it is obvious that they should be chosen as the design variables.

4.3.3 Constraints

The transient behavior of the beam is specified by the constraints on the maximum overshoot (O_s) and the settling time (t_s) of the beam tip transverse response, which in turn, is a constraint on system stability. Another constraint is imposed on the applied electric field.

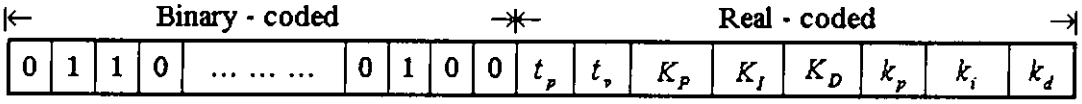

Figure 4-5 Chromosome representation

4.4 OPTIMIZATION USING MULTI-OBJECTIVE GENETIC ALGORITHM

4.4.1 Chromosome Representation

In the present work, both binary encoding and real encoding are used to form the chromosome, as shown in Figure 4-5. The former is used to represent the patch

arrangement (P and S), since they are discrete values. On the other hand, considering the wide searching ranges of the thickness of the constraining and the viscoelastic layers as well as the control gains, the length of the chromosome will have to be made sufficiently long so as to preserve a certain degree of precision, thus degrading the performance of GA. To overcome this difficulty, these variables are encoded in real numbers.

4.4.2 Fitness Assignment and Constraints Handling

The following procedure, proposed by Kurpati *et al.* [92], is used to handle constraints during the fitness assignment stage of the present MOGA.

Step1: Evaluate the constraints for every chromosome.

Step2: Identify feasible and infeasible chromosomes in the current population.

Step3: Assign a high (i.e. bad) rank to all infeasible chromosomes (r = 0.95 x N, where r is the rank and N is the population size).

Step4: Assign a moderate rank to all feasible chromosomes (r = 0.5 x N).

Step5: Evaluate the objective functions for all feasible chromosomes.

Step6: Identify the non-inferior chromosomes among the feasible chromosomes.

Step7: Assign a low (i.e. good) rank to feasible non-inferior chromosomes (r = 1).

Step8: Obtain fitness values for all chromosomes using the following equation.

$$F = C_{\max} - (C_{\max} - C_{\min})(r-1)/(N-1), \tag{4.8}$$

where $C_{\max} = 1.2$; $C_{\min} = 0.8$.

4.4.3 Reproduction

Once the fitness values are assigned, the roulette-wheel-selection procedure is adopted to select the chromosomes for reproduction. The following genetic operations [91, 93] are executed.

4.4.4 Crossover

For the case where crossover occurs in the binary-coded region, the conventional crossover executes. Let the randomly selected parents s_b^1 and s_b^2 participate in crossover to produce their offsprings $s_b^{1\prime}$ and $s_b^{2\prime}$ in a random position. The following change occurs:

$$s_b^1 = (b_1^1 \cdots b_m^1 \mid b_{(m+1)}^1 \cdots b_{l_b}^1)$$

$$s_b^2 = (b_1^2 \cdots b_m^2 \mid b_{(m+1)}^2 \cdots b_{l_b}^2)$$

$$\Downarrow$$

$$s_b^{1\prime} = (b_1^1 \cdots b_m^1 \mid b_{(m+1)}^2 \cdots b_{l_b}^2)$$

$$s_b^{2\prime} = (b_1^2 \cdots b_m^2 \mid b_{(m+1)}^1 \cdots b_{l_b}^1),$$

where l_b is the total number of binary bits of the string and b_m (0 or 1) is the m^{th} bit.

For the case where crossover occurs in real-coded region, the modified simple crossover is used and described as follows:

$$s_r^1 = (r_1^1 \cdots r_n^1 \mid r_{n+1}^1 \cdots r_{l_r}^1)$$

$$s_r^2 = (r_1^2 \cdots r_n^2 \mid r_{n+1}^2 \cdots r_{l_r}^2)$$

$$\Downarrow$$

$$s_r^{1\,\prime} = (r_1^1 \cdots \tilde{r}_n^1 \mid r_{n+1}^2 \cdots r_{l_r}^2)$$

$$s_r^{2\,\prime} = (r_1^2 \cdots \tilde{r}_n^2 \mid r_{n+1}^1 \cdots r_{l_r}^1),$$

where $\tilde{r}_n^1 = \lambda_1 r_n^1 + (1-\lambda_1) r_n^2$; $\tilde{r}_n^2 = \lambda_2 r_n^2 + (1-\lambda_2) r_n^1$, and r_n represents the n^{th} parameter, l_r is the total number of real-coded parameters, and λ_1, λ_2 are uniformly distributed random numbers between 0 and 1.

4.4.5 Mutation

For the case where mutation occurs in the binary-coded region, the standard mutation is enforced and the mechanism of it in a string is illustrated as follows:

$$(b_1 \cdots b_m \cdots b_{l_b}) \Rightarrow (b_1 \cdots \overline{b}_m \cdots b_{l_b}),$$

where $\overline{b}_m$ represents the flipped bit of b_m, i.e. from 0 to 1 or from 1 to 0.

For the case where mutation occurs in real-coded region, the principle of uniform mutation is used.

$$(r_1 \cdots r_n \cdots r_{l_r}) \Rightarrow (r_1 \cdots \overline{r}_n \cdots r_{l_r}),$$

where $\overline{r}_n = \lambda(r_n^U - r_n^L) + r_n^L$, and $\overline{r}_n \in [r_n^L, r_n^U]$ is a mutated n^{th} gene and $\lambda \in [0,1]$ is a random number. r_n^L and r_n^U are the lower and upper limit of r_n respectively.

4.5 COMPUTER CODE DEVELOPMENT AND VALIDATION

It is necessary to develop a program to implement the principle of MOGA, as explained in Section 4.3. The finite element model, which is used to simulate the dynamic behavior of the ACLD treated beam, is established with the commercial software package, MATLAB. To allow the MOGA and the finite element analysis running in the same computation environment, the MOGA is also developed with MATLAB by using the built-in commands and programming logic of it. Figure 4-6 is the flowchart of the MOGA process.

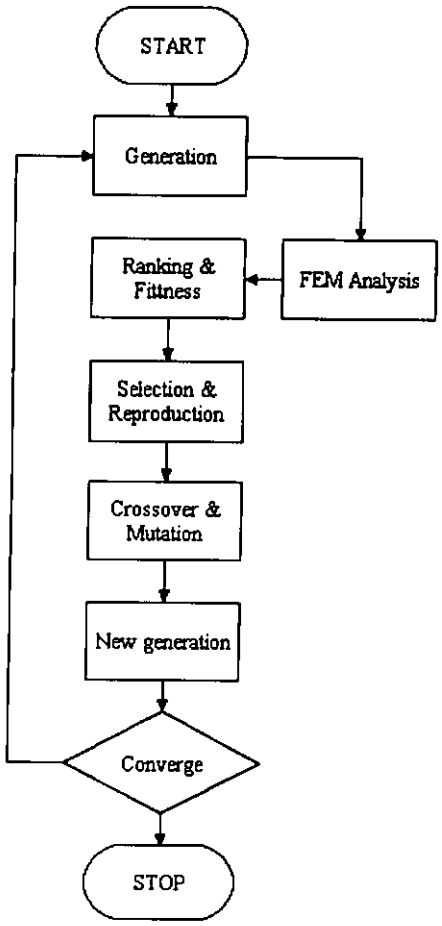

Figure 4-6 Flowchart of MOGA operations

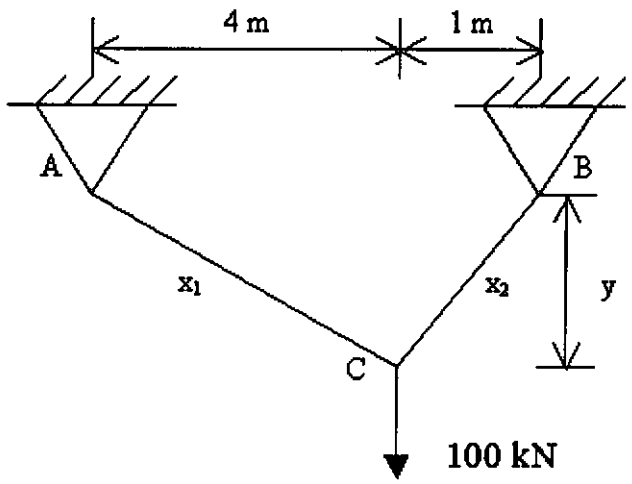

Figure 4-7 Two-bar truss

To demonstrate the searching ability, the developed program is applied to an engineering design problem adopted from Kalyanmoy [94], in which the penalty function approach was used to handle the constraints. A truss (Figure 4-7) has to carry a certain load without elastic failure. Thus, in addition to the objective of designing the truss for minimum volume (V), there are additional objectives of minimizing the stress in AC. Given constraints: the stresses in AC and BC (σ_{AC} and σ_{BC}) should not exceed 100,000 kPa and the total volume of materials should not exceed 0.1 m^3. The following two-objective optimization problem, for three variables – y (vertical distance between B and C in m), and x_1 and x_2 (cross-sectional areas of AC and BC respectively, m^2), is constructed.

Minimize $V(x_1, x_2, y) = x_1(16+y^2)^{0.5} + x_2(1+y^2)^{0.5}$

Minimize $\sigma_{AC}(x_1, y) = \dfrac{20(16+y^2)^{0.5}}{yx_1}$

Subject to $V \leq 0.1$, $\sigma_{AC} \leq 100000$, $\sigma_{BC} \leq 100000$, where $\sigma_{BC} = \dfrac{80(1+y^2)^{0.5}}{yx_2}$.

This problem is solved by the program developed in the present work with the following MOGA parameters. Population size: 200, crossover probability: 0.8, mutation probability: 0.05, number of generation: 200. Results are shown in Figure 4-8. As can be seen from Figure 4-8(a), the population starts with a non-uniform set. After 200 generations, the Pareto set seems to have been reached, and the values of both objectives have been improved. Moreover, the Pareto-optimal solutions obtained by Kalyanmoy [94] for the same two-bar truss problem are included in Appendix B. As shown in the figure, apart from the uniformity, the optimum solutions obtained by the present MOGA code and those by Kalyanmoy [94] are very similar in terms of extreme value. In other words, the present MOGA code can be used to find out the Pareto optimum solutions.

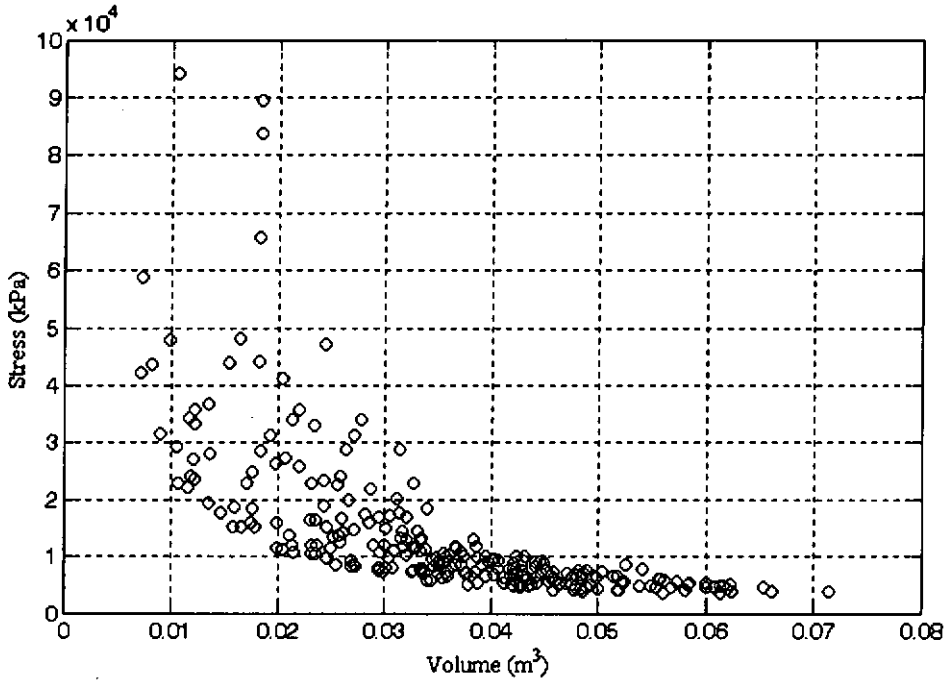

Figure 4-8(a) Randomly generated initial-solutions using the program developed in the present work for the two-bar truss problem

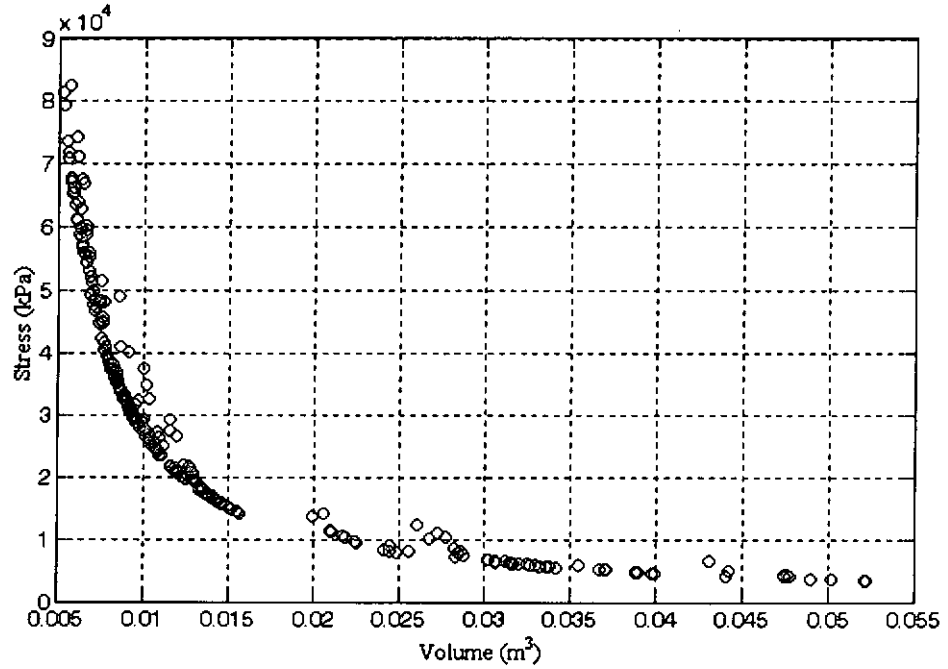

Figure 4-8(b) Optimized solutions obtained using the program developed in the present work for the two-bar truss problem

CHAPTER 5

OPTIMIZATION RESULTS AND DISCUSSIONS

This chapter presents the results of the implementation of the multi-objective optimization formulated in the previous chapter. The Pareto solutions are discussed. For a given solution, the shape control problem is studied numerically and its transient behavior is analyzed. Effects of external disturbances on the shape control systems are also examined by applying different types of loadings (static/impulsive and point/distributed loads) to the system. Comparison is also made between open loop and closed loop controls.

5.1 SYSTEM DESCRIPTION

A graphite/epoxy beam (1000 mm x 20 mm x 2 mm) is considered. It is necessary to perform a transient analysis for every chromosome in every generation so that the MOGA can work according to its philosophy. Therefore, the computation load required is heavy. With respective to this, the beam is evenly divided into twenty finite elements. It is obvious that neither one nor two ACLD patches are enough to give a fine parabolic shape. On the other hand, the more patches are used, the more redundant the control system will be. Besides, for a twenty-finite-element beam, if four or more ACLD patches are used, the choices of lengths and locations of the patches will be limited. In

other words, it is meaningless to optimize these variables. As a result, three ACLD patches are used to accomplish the shape change. The coefficient C in Eq. (4.5) is chosen to be 0.0001. Other system parameters and material properties are given in Table 5-1. The structural design variables include the position of the first patch, P_1, the spacing between patches – S_2 (first and second), S_3 (second and third), the lengths of the three patches (L_1 , L_2 and L_3), the thickness of the piezoelectric constraining (t_p) and viscoelastic (t_v) layers. The control variable are the gain values $-K_P, K_I, K_D$ and k_p, k_i, k_d. The former group of gains is for piezo-sensor feedback while the latter one is for tip position sensor feedback. Since there are three ACLD patches, the total number of control gains is eighteen. Constraints on the system and ranges of design variables are described in Table 5-2. In this study, the following MOGA parameters are used. The population size is 200. The crossover and mutation probability are 0.8 and 0.05 respectively. The MOGA is terminated when the number of generation reaches 100.

Table 5-1 System parameters

ρ_p	7600 kg/m^3	d_{31}	-0.175 x 10^{-9} m/V	$\hat{\alpha}_2$	3.237
ρ_v	1250 kg/m^3	t_s	0.025 mm	$\hat{\omega}_2$	50618.8 rad/s
ρ_b	1600 kg/m^3	G^∞	5 x 10^5 Pa	$\hat{\zeta}_2$	5.38
E_p	64.9 x 10^9 Pa	$\hat{\alpha}_1$	0.742	$\hat{\alpha}_3$	41.654
E_b	150 x 10^9 Pa	$\hat{\omega}_1$	6502.9 rad/s	$\hat{\omega}_3$	352782 rad/s
ε	15 x 10^{-9} F/m	$\hat{\zeta}_1$	6.97	$\hat{\zeta}_3$	2.56

Table 5-2 Constraints on shape control system

Electric field	< 1000 (V/mm)
Settling time	< 3 (s)
Maximum overshoot	< 10 (%)
Number of ACLD patch	3
Length of ACLD patch	0.1 – 0.25 (m)
Position of 1st patch	0 – 0.15 (m)
Spacing between patches	0.05 – 0.4 (m)
Thickness of constraining layer	0.01 – 1 (mm)
Thickness of viscoelastic layer	0.01 – 1 (mm)
Proportional gains (piezo-sensor)	0 – 500
Integral gains (piezo-sensor)	0 – 10
Derivative gains (piezo-sensor)	0 – 500
Proportional gains (position sensor)	0 – 500
Integral gains (position sensor)	0 – 10
Derivative gains (position sensor)	0 – 500

5.2 PARETO SOLUTIONS

In this section, the derived Pareto optimum solutions are discussed. In Figures 5-1, 5-2 and 5-3, the derived solutions are projected on weight-damping ($\Phi_2 - \Phi_3$), damping-error ($\Phi_3 - \Phi_1$) and error-weight ($\Phi_1 - \Phi_2$) surfaces respectively. From figure 5-1, a clear tradeoff relation is found. It means that there exists a conflict between the treatment weight and summation of passive damping. It is worth mentioning that the tradeoff relation between them is convex. It means that the change of damping with the

change of treatment weight is not constant. There exists a critical point, below which the change of damping with the change of weight is drastic, beyond which the change of damping with the change of weight is minor. According to the findings in Chapter 3, this convex relationship is due to the fact that initially when the patch length increases, the dampings of all the three modes increase. Consequently, the increase of weight makes a rapid enhancement of the damping. On the other hand, after the length has extended to a certain value and increases further, the damping of the first and second mode decrease and only the third mode damping increases. The overall effect is that the increase of weight only leads to a little change of damping. For the remaining surfaces (damping-error and error-weight), results show that the tradeoffs are not as clear as that of weight-damping surface.

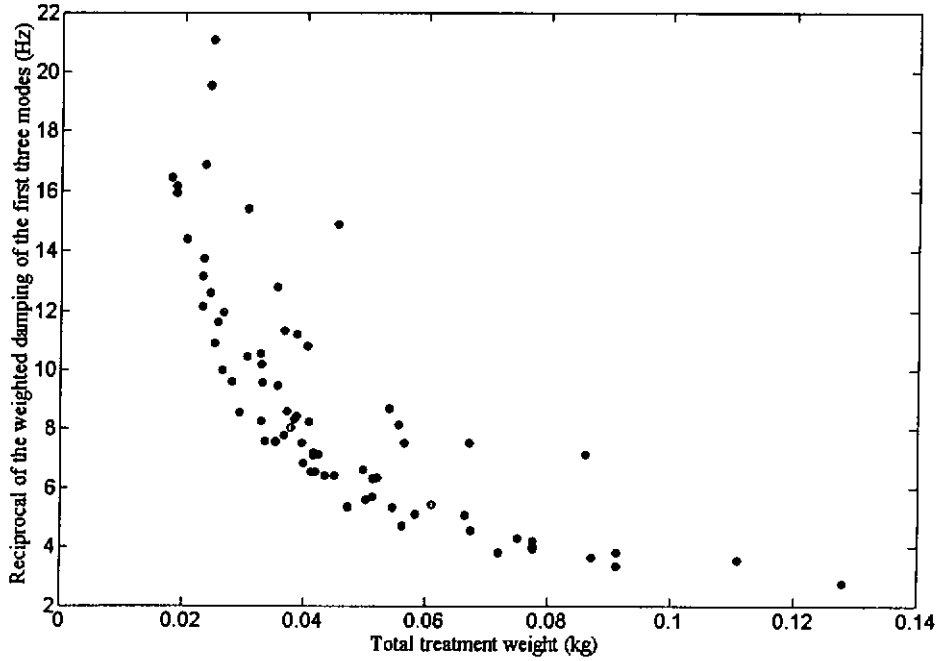

Figure 5-1 Projection of Pareto solutions on weight and damping ($\Phi_2 - \Phi_3$) surfaces

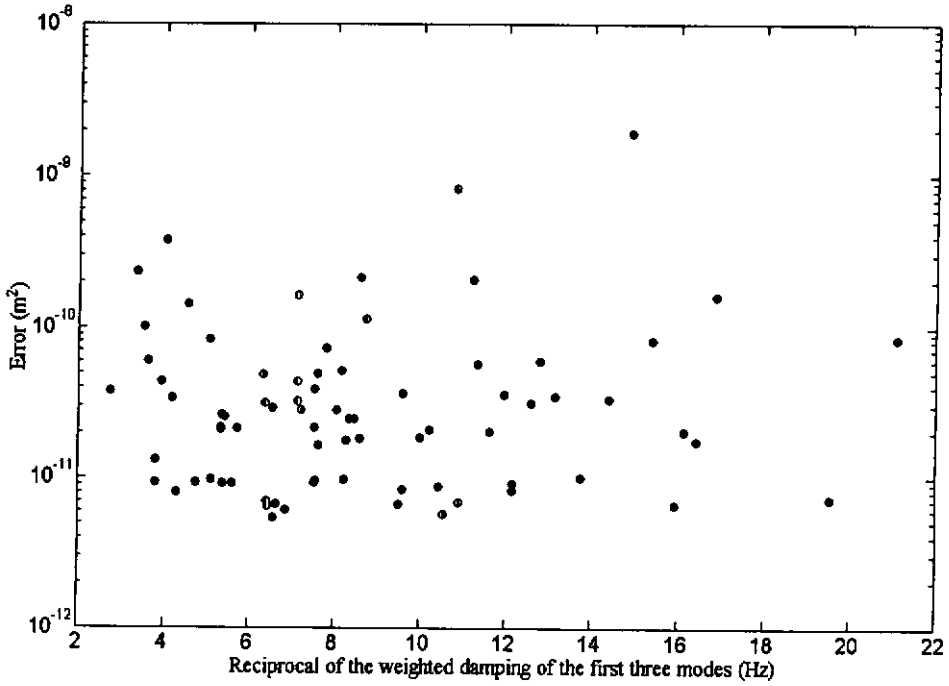

Figure 5-2 Projection of Pareto solutions on damping and error ($\Phi_3 - \Phi_1$) surfaces

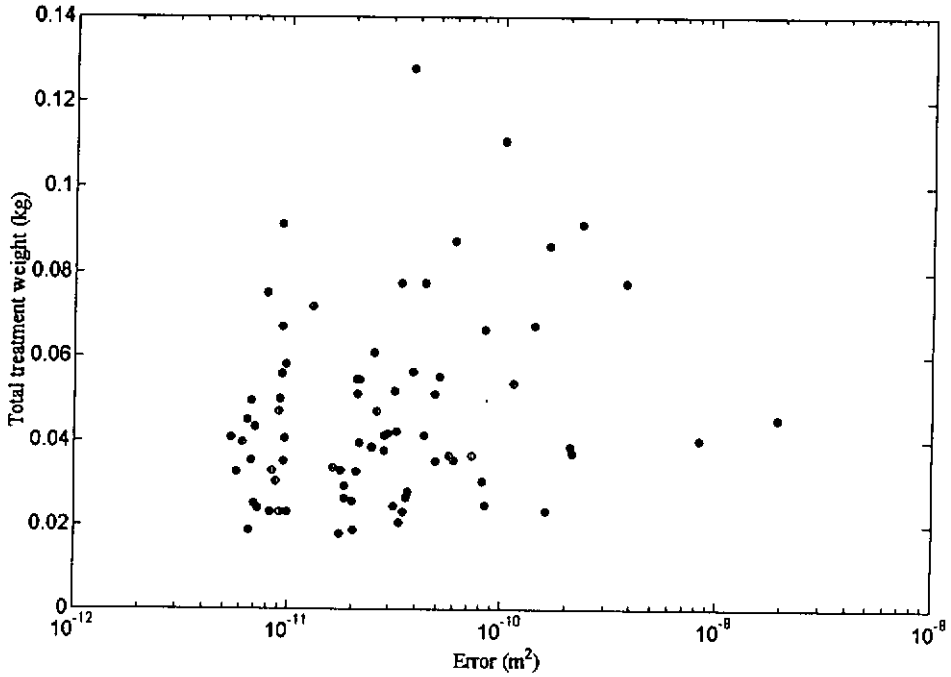

Figure 5-3 Projection of Pareto solutions on error and weight ($\Phi_1 - \Phi_2$) surfaces

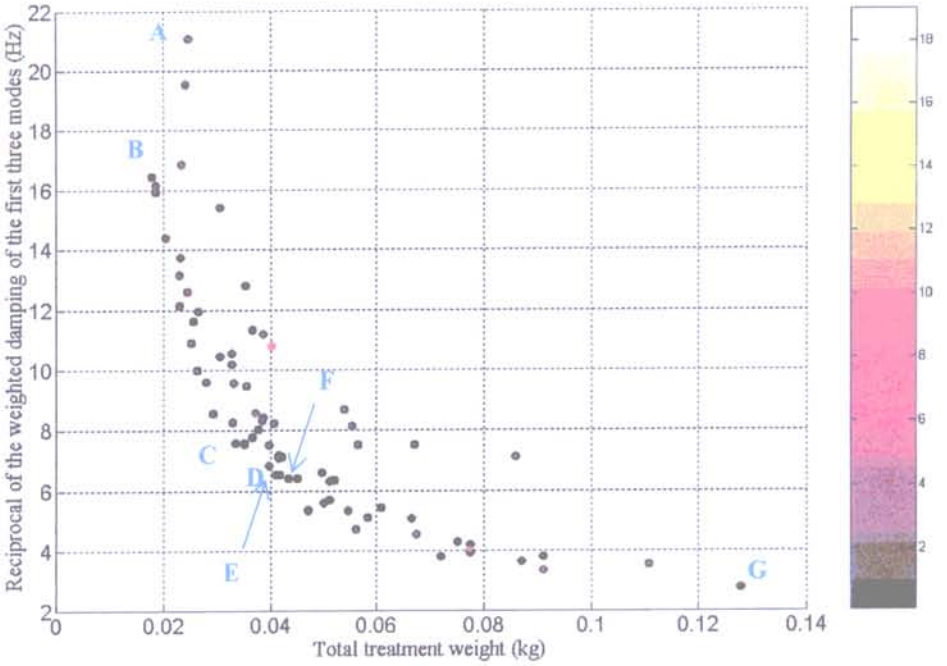

Figure 5-4 Pareto solutions and design candidates

The solutions that have the best and worst value of weight and damping objective functions, as shown in Figure 5-4 (A, B, and G), are given in Table 5-3 to 5-5. The different colors in the color bar represent the values of error for different solutions. The deepest (brown) represents small value of error, while the lightest (white) represents large value of error. In the solution with the smallest value of weight (solution B), the constraining layer is relatively thin. Also, the lengths of the patches are relatively short, so the damping is small. On the other hand, solution G, with the smallest value of the reciprocal of damping, both the piezoelectric constraining and viscoelastic layers are relatively thick (converging to the upper limit). Nevertheless, although A is a solution

that has the largest value of the reciprocal of damping, it does not represent the solution with the lightest weight. These can be due to the fact that the viscoelastic thickness contributes much to the weight, but damping does not monotonically increase with its thickness. Also, the patch locations have effects on the damping as well. Finally, solution C, D, E and F have relatively small values of error, as they are deep in color in Figure 5-4. Therefore, they all are reasonable choices for the present shape control system.

Table 5-3 Design values of solution A

Design variable	Value
P_1	0.05 (m)
S_2	0.1 (m)
S_3	0.2 (m)
L_1	0.15 (m)
L_2	0.2 (m)
L_3	0.1 (m)
t_p	0.257 (mm)
t_v	0.635 (mm)

Table 5-4 Design values of solution B

Design variable	Value
P_1	0 (m)
S_2	0.2 (m)
S_3	0.1 (m)
L_1	0.1 (m)
L_2	0.15 (m)
L_3	0.1 (m)
t_p	0.291 (mm)
t_v	0.282 (mm)

Table 5-5 Design values of solution G

Design variable	Value
P_1	0 (m)
S_2	0.1 (m)
S_3	0.05 (m)
L_1	0.25 (m)
L_2	0.25 (m)
L_3	0.25 (m)
t_p	0.965 (mm)
t_v	0.952 (mm)

Table 5-6 Design values of solution F

Design variable	Value	Design variable	Value
P_1	0 (m)	K_{P1}, K_{P2}, K_{P3}	47.506, 30.342, 44.565
S_2	0.15 (m)	K_{I1}, K_{I2}, K_{I3}	1.05, 4.456, 3.542
S_3	0.1 (m)	K_{D1}, K_{D2}, K_{D3}	200.9, 286.6, 183.76
L_1	0.2 (m)	k_{p1}, k_{p2}, k_{p3}	11.557, 24.299, 38.105
L_2	0.15 (m)	k_{i1}, k_{i2}, k_{i3}	4.301, 3.408, 3.824
L_3	0.15 (m)	k_{d1}, k_{d2}, k_{d3}	222.86, 436.69, 399.6
t_p	0.486 (mm)	t_v	0.512 (mm)

5.3 TRANSIENT ANALYSIS

To evaluate the shape change performance, solution F, with an error of 6.9622 x 10^{-12} m^2, is chosen. The values of other objective functions and design variables are listed in Table 5-6. Two cases are considered. CASE I refers to the situation that the beam changes from flat to the parabolic shape, while CASE II is the reverse situation; i.e. the beam changes from parabolic to flat shape.

5.3.1 CASE I: Flat to Parabolic Shape

Figures 5-5 to 5-8 are the results for CASE I. From Figure 5-5, it can be seen that the final achieved shape is close to the desired shape. Figure 5-6 shows the tip transverse displacement of the beam. It is clear that the tip of the beam settles down within three

seconds, thus satisfying the constraint on settling time. Also, the maximum overshoot is below 10 %. As shown in Figure 5-7, all the three input voltages to the piezoelectric constraining layers are below the break down value during the whole shape control process. Therefore, it can be concluded that the control gains obtained from solution D are effective.

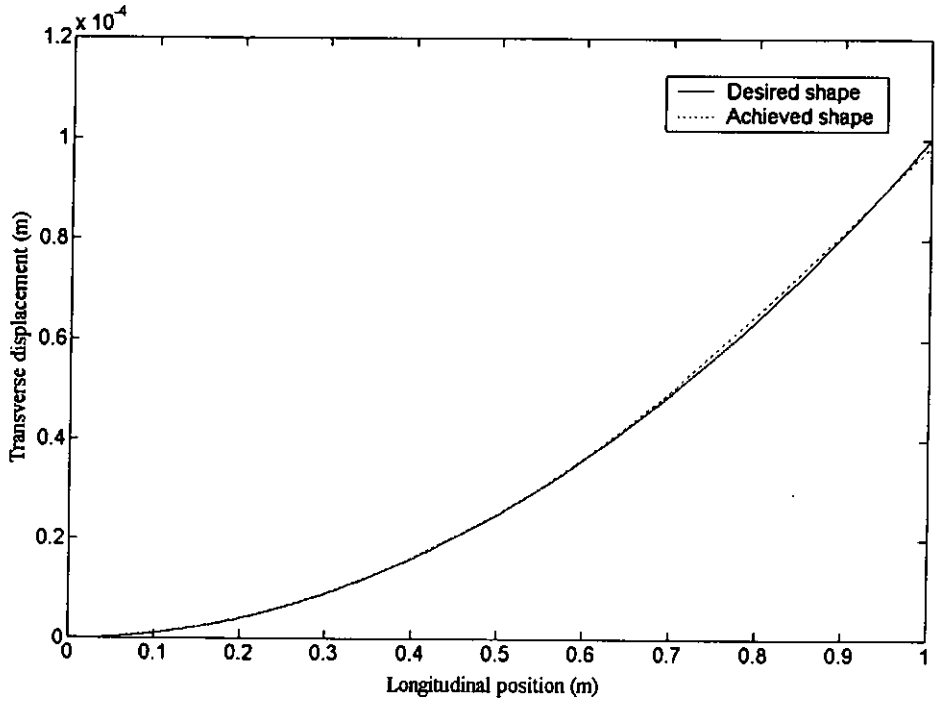

Figure 5-5 Desired and achieved shapes of the beam after 5 seconds – CASE I

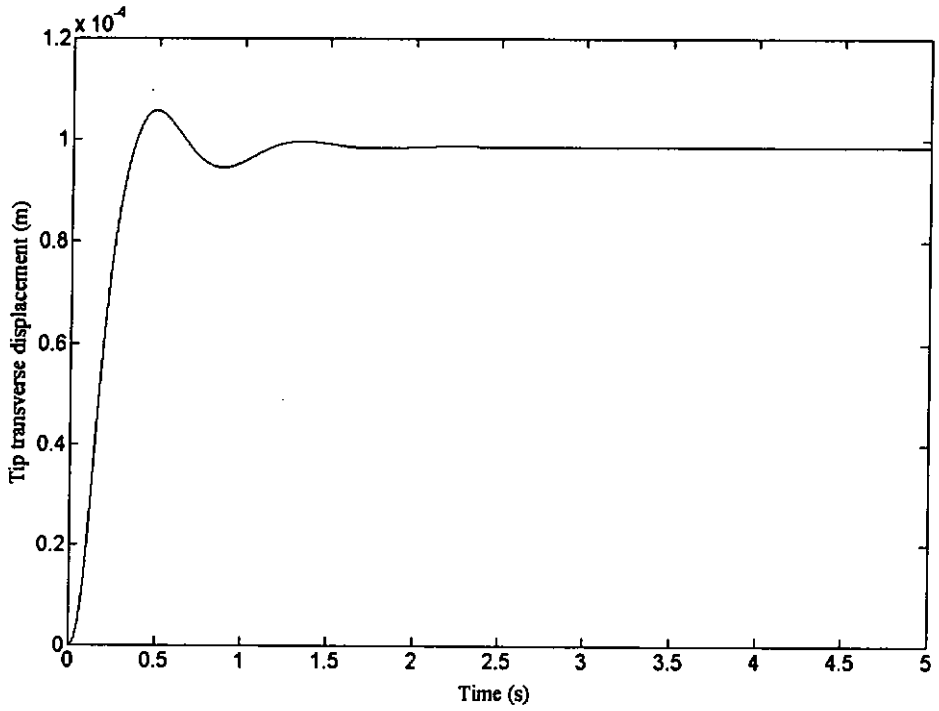

Figure 5-6 Tip transverse response of beam during shape control process – CASE I

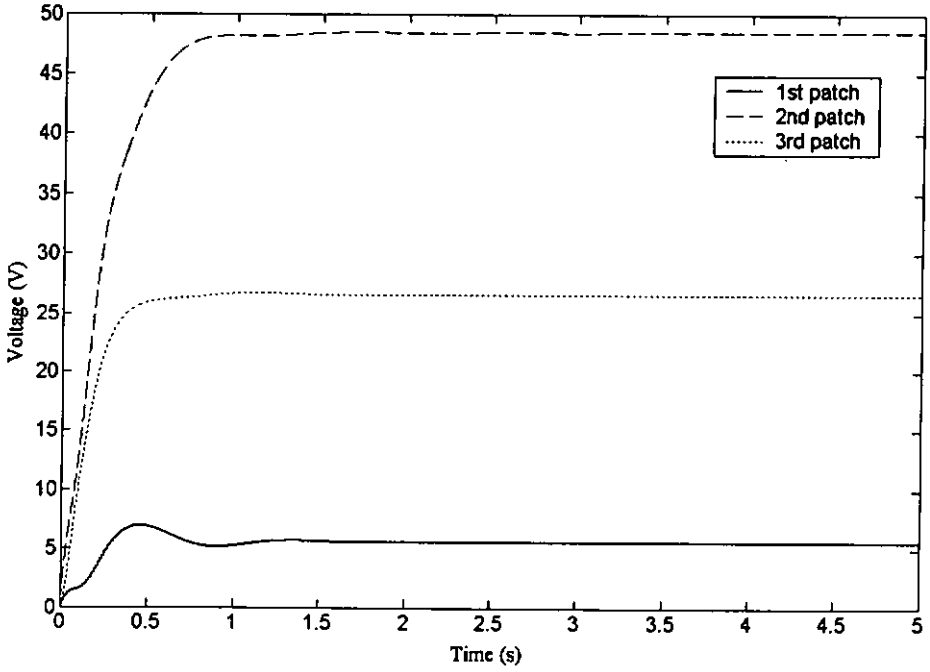

Figure 5-7 Time history of voltages applied to ACLD patches – CASE I

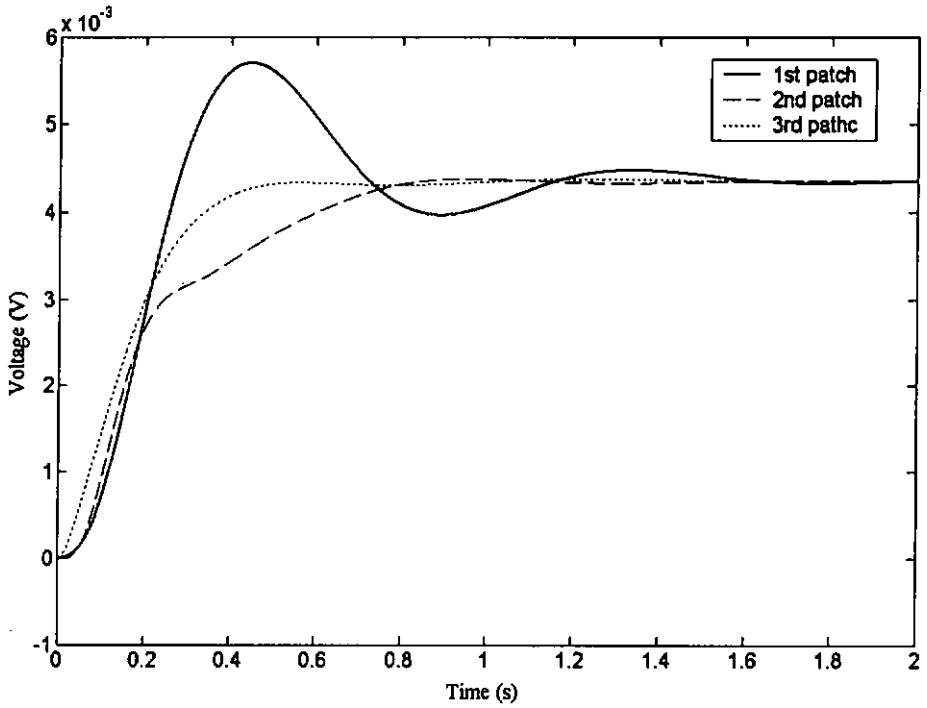

Figure 5-8 Time history of sensor output voltages of ACLD patches – CASE I

5.3.2 CASE II: Parabolic to Flat Shape

For CASE II, at the beginning, the shape is in parabolic form. After one second, the system is commanded to change to flat shape. Figures 5-9 to 5-12 show the transient behavior of the system during this process. It can be interpreted from these figures that, similar to CASE I, the system violates none of the constraints imposed on it. It is also obvious that the control system can bring the beam to the original shape smoothly.

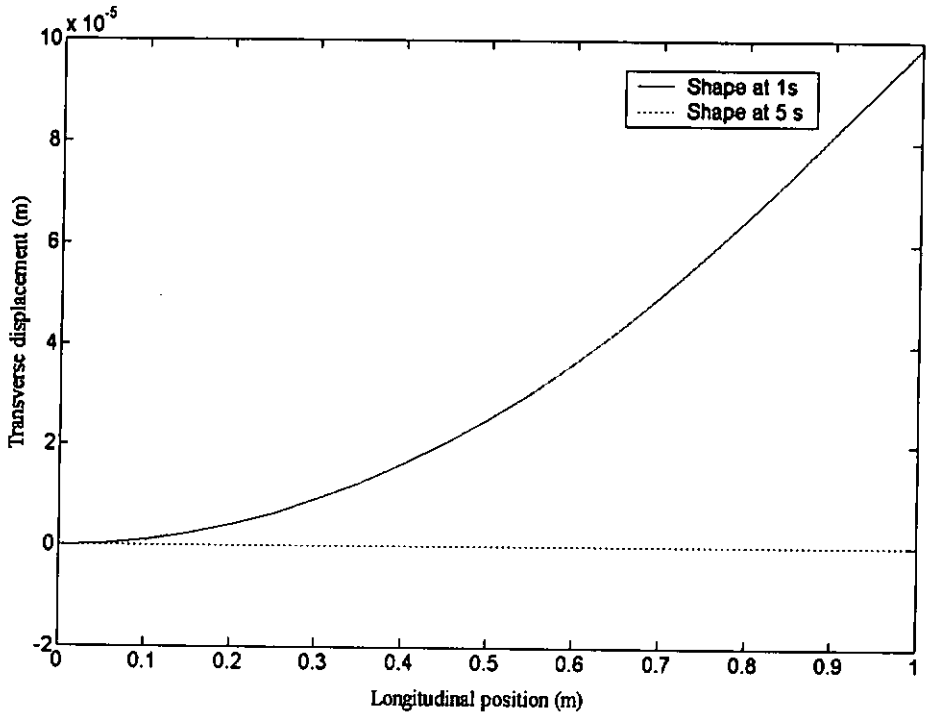

Figure 5-9 Initial and final shapes of the beam – CASE II

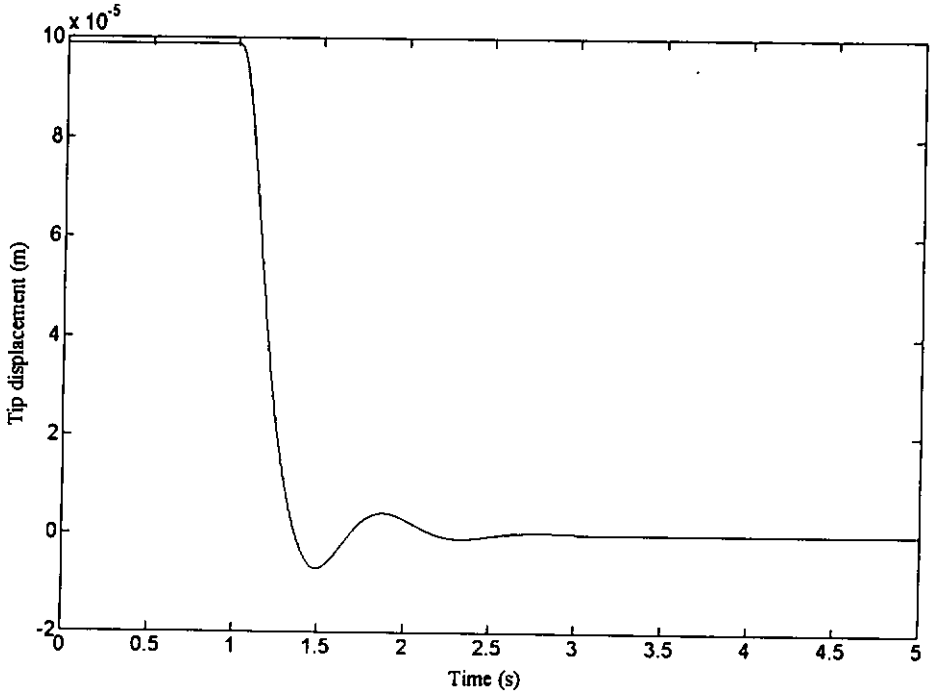

Figure 5-10 Tip transverse response of beam during shape control process – CASE II

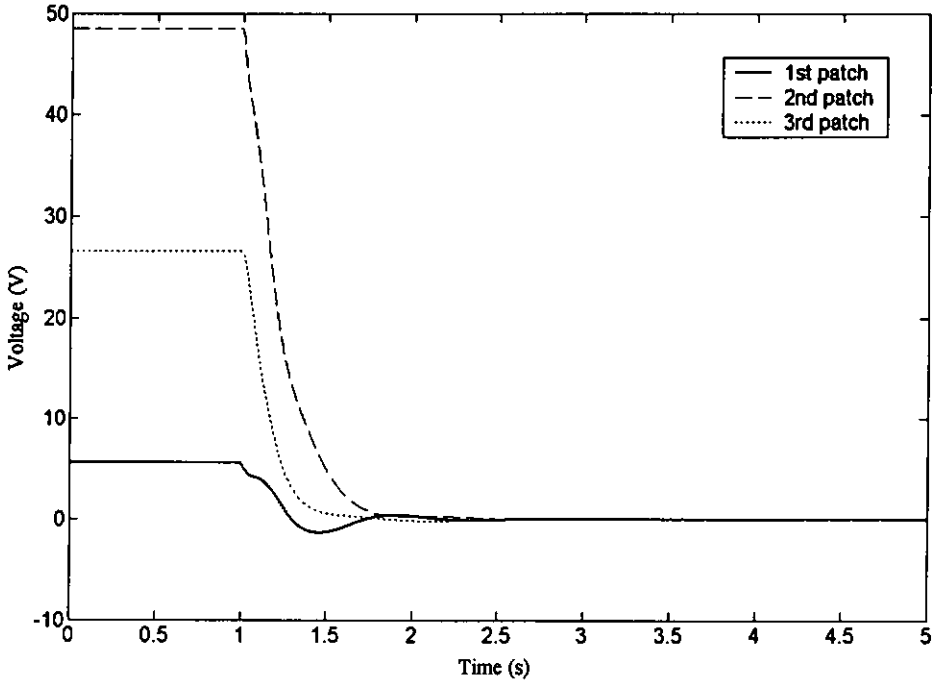

Figure 5-11 Time history of voltages applied to ACLD patches – CASE II

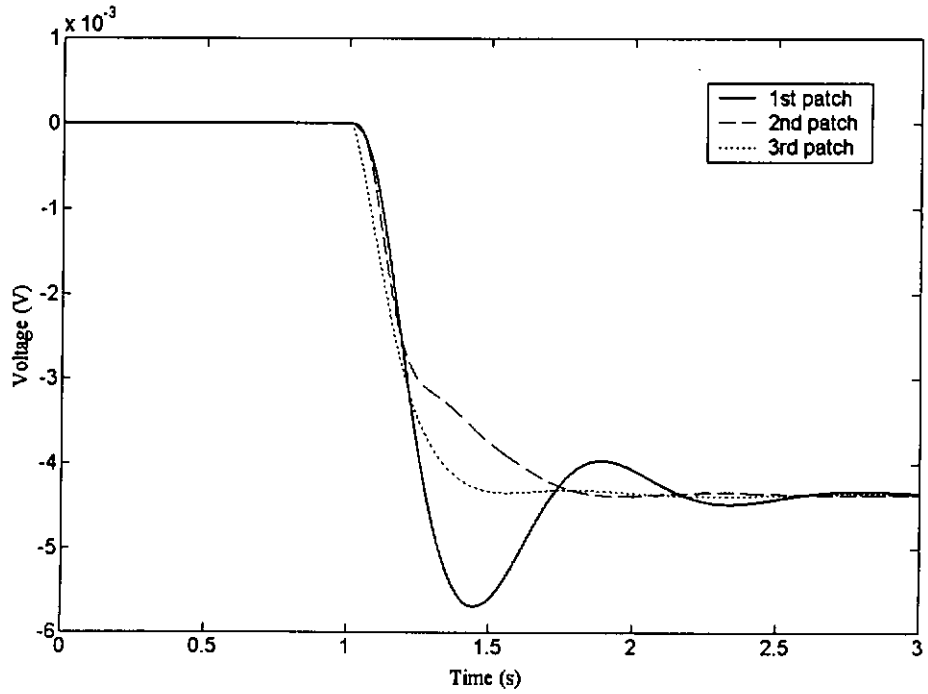

Figure 5-12 Time history of sensor output voltages of ACLD patches – CASE II

5.3.3 Comparison between Open and Closed Loops

In fact, in the absence of loading, both open and closed-loop controls can achieve the desired shape with no significant difference. The main discrepancy between open and closed loop controls is the time required to finish the process or the settling time. In the case of open-loop control, the beam vibrates rapidly and it takes a long time to settle down to the final status (the final achieved shape). This can be interpreted from the tip response of the beam (Figure 5-13), in which the steady-state control voltages (closed loop) are directly applied to the three actuators (for CASE I). Hence, compared with the short settling time (around 2.5 seconds) of the closed-loop control, it is clear that the performance of open-loop control is unsatisfactory.

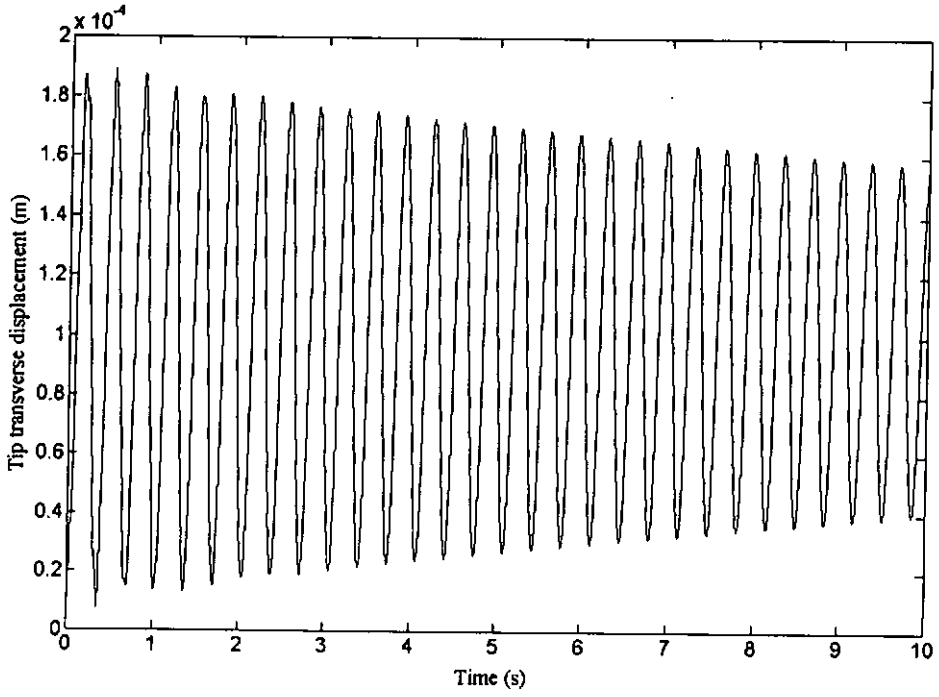

Figure 5-13 Tip transverse response of beam for open loop control – CASE I

5.3.4 Discussion on ACLD and AC for Shape Control

It is known that the vicoelastic layers of the ACLD patches deteriorate the control actions from the piezoelectric constraining layers to the host structure. It other words, more control voltages are required to obtain the same bending effect to the host structure, when compared with purely active control (AC) – the piezoelectric layers are directly bonded to the host structure. Therefore, it seems that AC is better than ACLD, when it comes to shape control of structures. However, when fail-safe issue is taken into account in the design, ACLD is obviously preferred. Consider a break down situation occurs, in the case of AC, the structure vibrates rapidly due to the flexible nature of the host structure. Yet, for ACLD, the passive damping introduced alleviates the vibration problem and thus minimizes the adverse effects.

5.4 EFFECT OF DISTURBANCE

Effects of external disturbances on the shape control system is also examined by applying various types of loadings (static/impulsive and point/distributed) at different occasions – (a) the shape change is in process, and (b) the shape change is finished.

5.4.1 Comparison between Static and Impulsive Loads

Firstly, a point load, with magnitude leading to around 0.01 (mm) tip deflection (when the beam is in flat shape), is acting at the middle to the beam at 0.5 second (when the structure is changing from flat to parabolic shape). For static case, the point load is always present once acting on. For impulse case, the point load acts on the beam for only 0.5 second. Figure 5-14 and 5-15 are the results given for the static case, while

figure 5-16 and 5-17 are those for the impulse case. For both cases, the shape can be recovered to the unloaded shape due to the closed loop control actions. However, with respect to the static case, the steady input voltages are increased in order to maintain the achieved shape. As shown in Figure 5-15, the input voltages of the first and second patches are also increased respectively from 5.59 V to 6.45 V and from 48.45 V to 51.71 V. Conversely, the input voltage of the third patch is decreased from 26.59 V to 25.40 V. For the impulse case, the input voltages increase initially due to the effect of impulsive load, but finally return to the unloaded level, as the load vanishes (Figure 5-17).

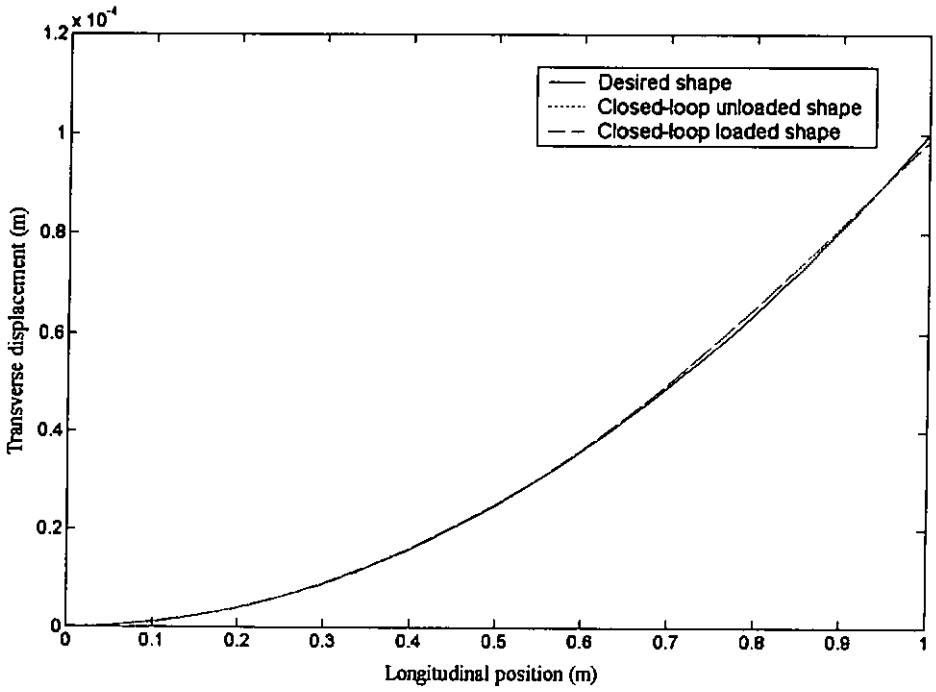

Figure 5-14 Closed loop loaded and unloaded shapes for static load

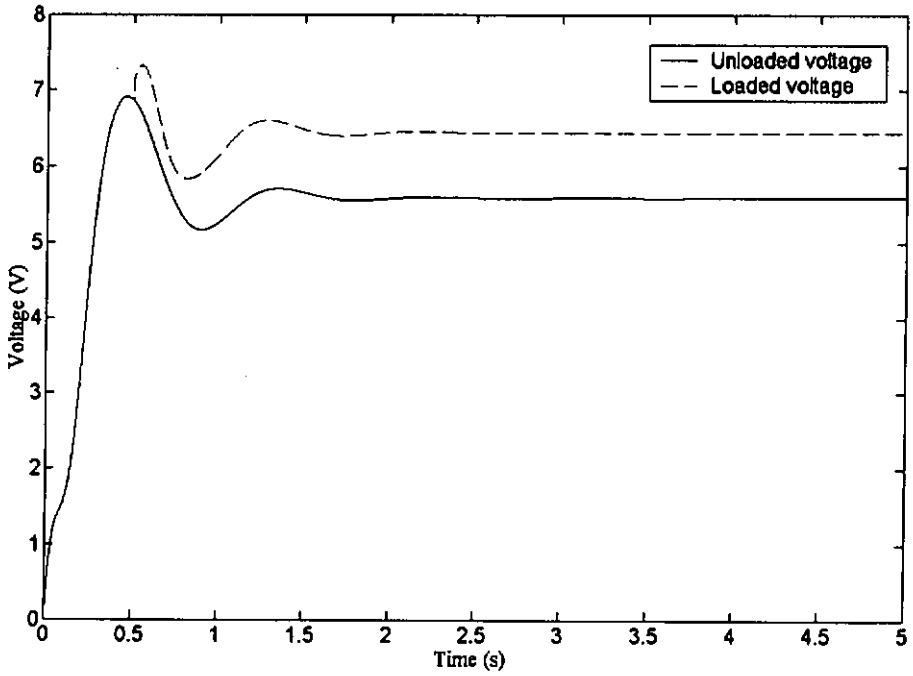

Figure 5-15(a) Comparison between loaded and unloaded applied voltages of 1st patch for static load

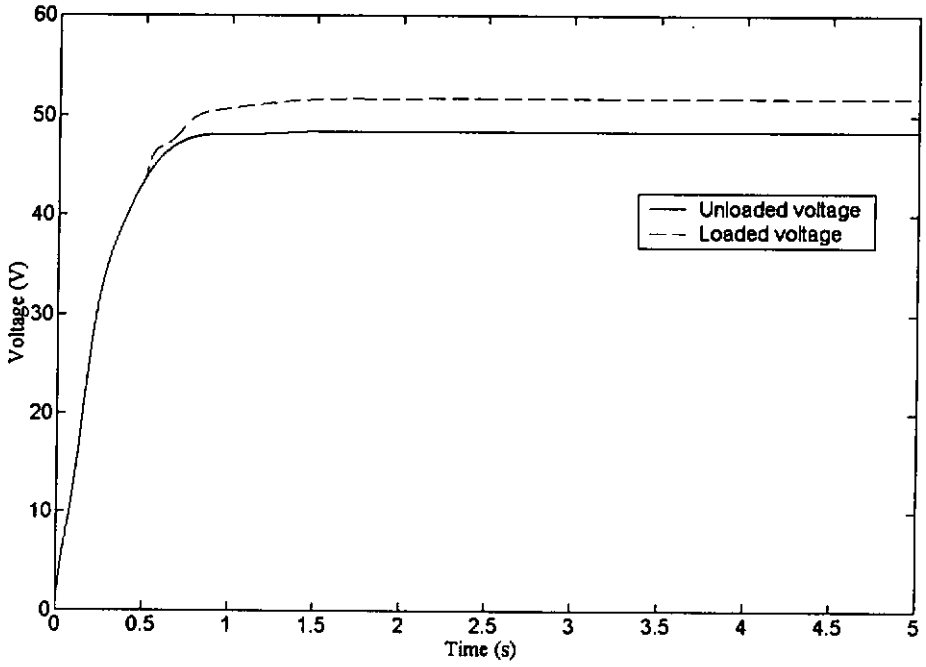

Figure 5-15(b) Comparison between loaded and unloaded applied voltages of 2nd patch for static load

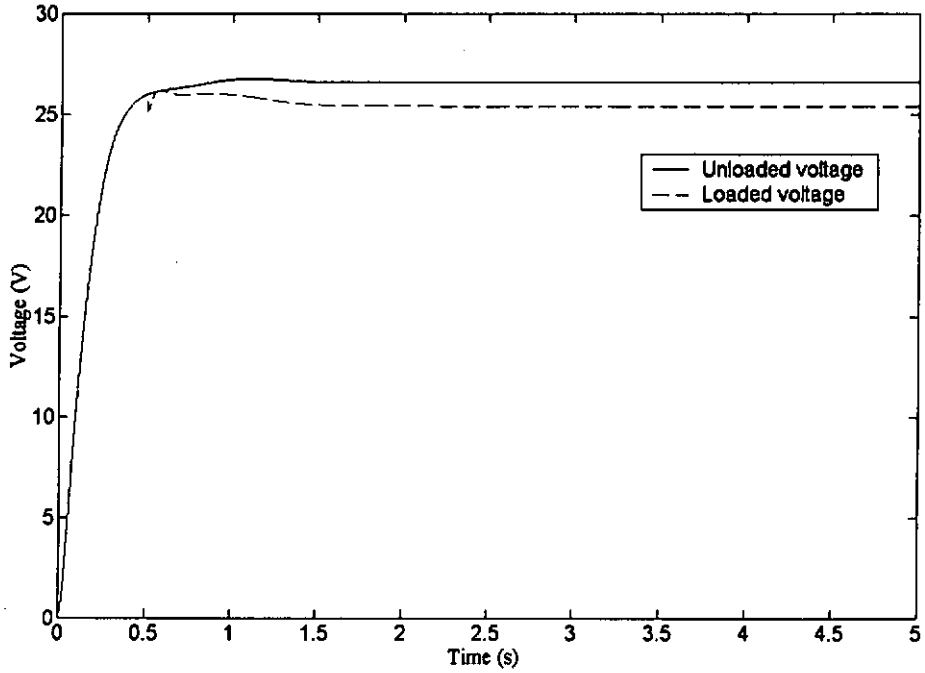

Figure 5-15(c) Comparison between loaded and unloaded applied voltages of 3rd patch for static load

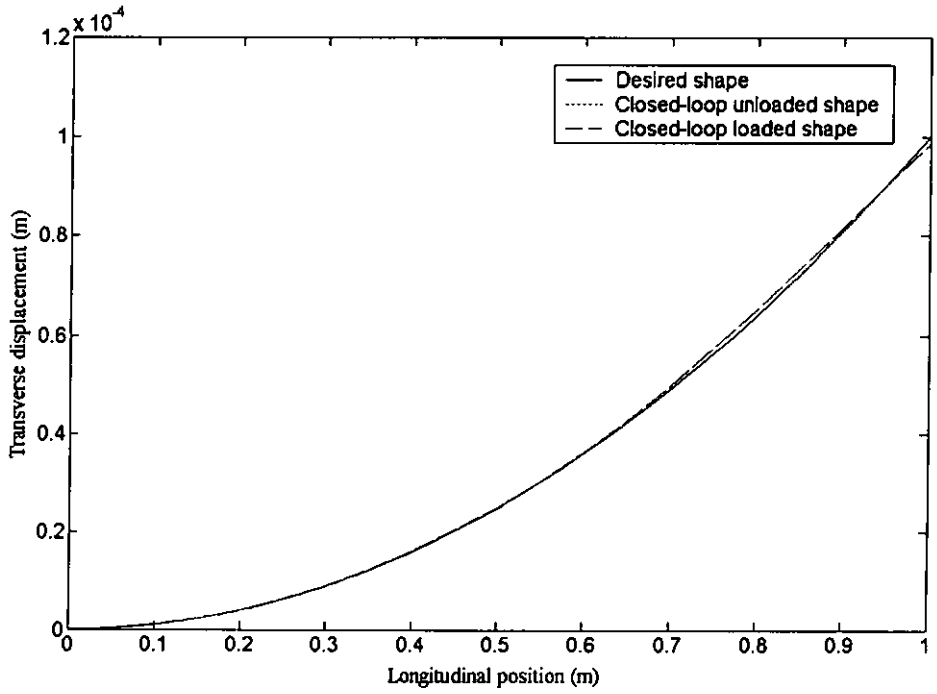

Figure 5-16 Closed loop loaded and unloaded shapes for impulsive load

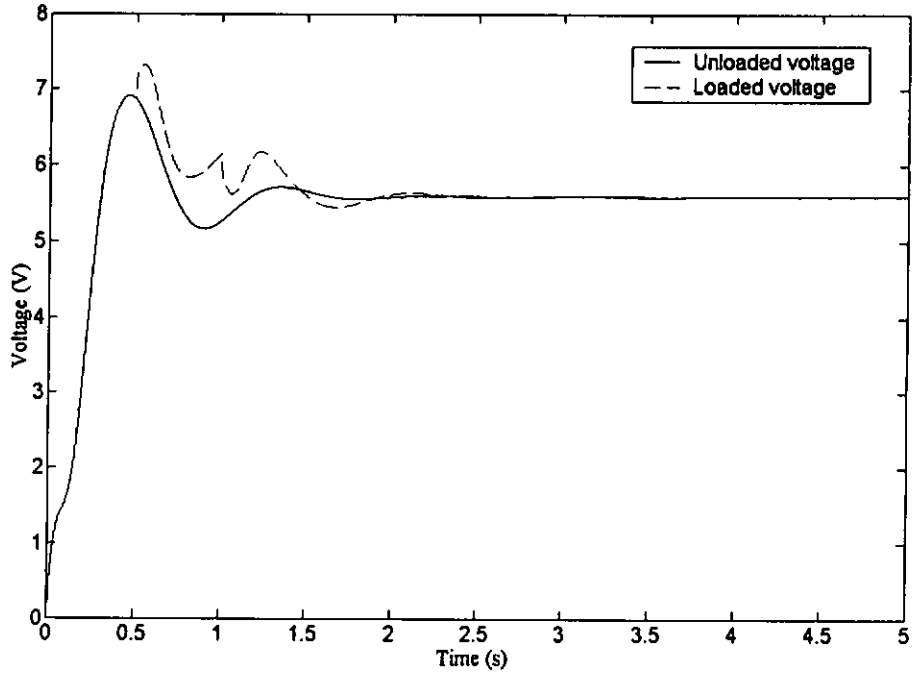

Figure 5-17(a) Comparison between loaded and unloaded applied voltages of 1st patch for impulsive load

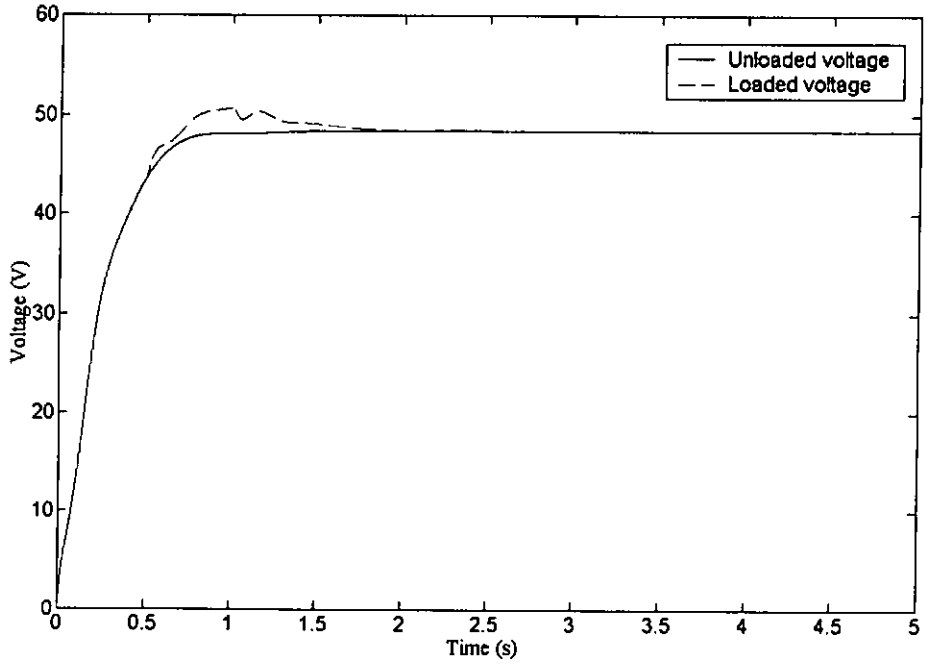

Figure 5-17(b) Comparison between loaded and unloaded applied voltages of 2nd patch for impulsive load

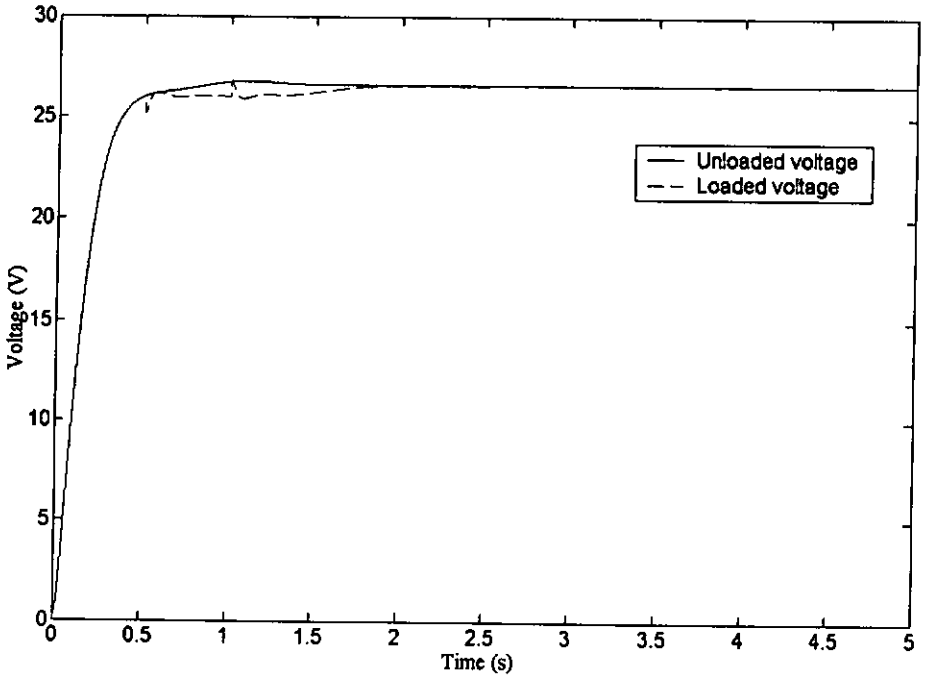

Figure 5-17(c) Comparison between loaded and unloaded applied voltages of 3rd patch for impulsive load

5.4.2 Comparison between Open and Closed Loops

On the other hand, the abilities of open and closed-loop control to maintain the achieved shape under the influence of external loading are compared. Figure 5-18 shows the open-loop loaded and closed-loop loaded shapes. A distributed load, which reduces the tip transverse displacement by about 0.01 (mm) (when the beam is in flat shape) is acting on the beam, when the beam is in parabolic shape. The errors of the open-loop loaded, closed-loop loaded and closed-loop unloaded shapes are summarized in Table 5-7. It can be seen that in the case of open-loop control, the external load deforms the achieved shape into the open-loop loaded shape. It is also found that the error is

increased substantially. However, when closed-loop control is used, the mismatch between the desired shape and distorted shape results in sensor output signals (both piezo-sensors and tip position sensor). These signals are fed to the control system, which will regulate the actuator, thus correcting the distorted shape. As shown in figure 5-19, all the three actuator voltages are increased. It is also evident from Figure 5-18 that the errors of the closed loop loaded (6.98×10^{-12} m^2) and unloaded (6.96×10^{-12} m^2) shapes are almost the same. On the whole, it can be concluded that the closed-loop system outperforms the open-loop system, as far as disturbance–rejection ability is concerned.

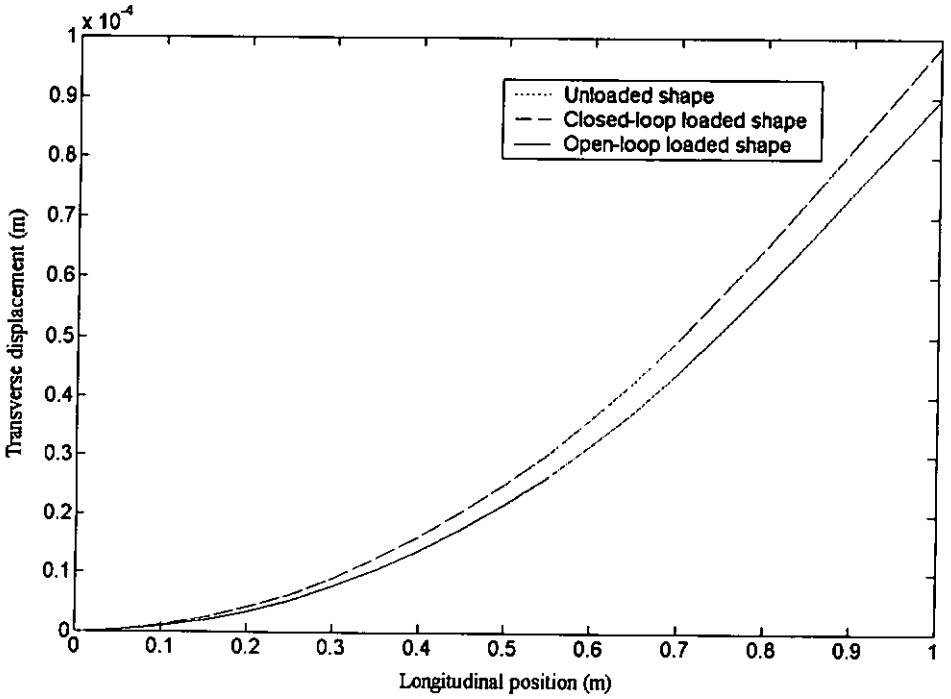

Figure 5-18 Comparison between open-loop loaded and closed-loop loaded and unloaded shapes for static distributed load – parabolic shape

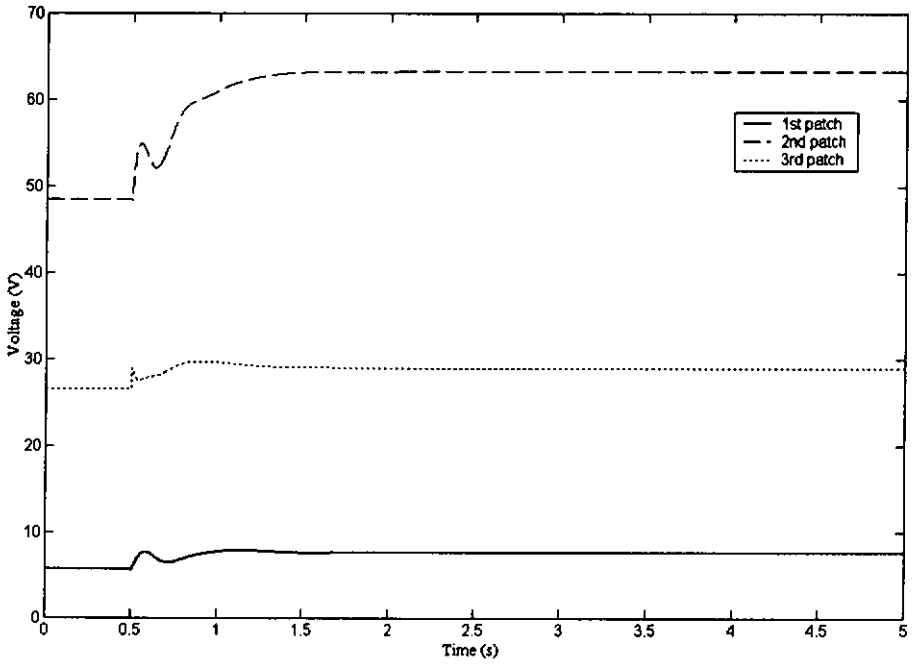

Figure 5-19 Effect of static distributed load on applied voltages of ACLD patches

Table 5-7 Summary of errors for static distributed load – parabolic shape

Node error	Open-loop loaded (m^2)	Closed-loop loaded (m^2)	Closed-loop unloaded (m^2)
δ_1^2	5.54×10^{-16}	4.92×10^{-16}	5.01×10^{-16}
δ_2^2	1.38×10^{-14}	3.48×10^{-15}	3.57×10^{-15}
δ_3^2	9.34×10^{-14}	6.13×10^{-15}	6.38×10^{-15}
δ_4^2	3.38×10^{-13}	6.83×10^{-15}	7.27×10^{-15}
δ_5^2	8.43×10^{-13}	8.93×10^{-15}	9.67×10^{-15}
δ_6^2	1.71×10^{-12}	1.30×10^{-14}	1.42×10^{-14}
δ_7^2	3.05×10^{-12}	1.71×10^{-14}	1.89×10^{-14}
δ_8^2	4.97×10^{-12}	1.83×10^{-14}	2.05×10^{-14}
δ_9^2	7.59×10^{-12}	1.52×10^{-14}	1.76×10^{-14}
δ_{10}^2	1.08×10^{-11}	1.46×10^{-14}	1.73×10^{-14}
δ_{11}^2	1.42×10^{-11}	3.04×10^{-14}	3.47×10^{-14}
δ_{12}^2	1.74×10^{-11}	9.84×10^{-14}	1.07×10^{-13}
δ_{13}^2	2.02×10^{-11}	2.81×10^{-13}	2.96×10^{-13}
δ_{14}^2	2.29×10^{-11}	6.05×10^{-13}	6.3×10^{-13}
δ_{15}^2	2.61×10^{-11}	9.96×10^{-13}	1.03×10^{-12}
δ_{16}^2	3.04×10^{-11}	1.26×10^{-12}	1.3×10^{-12}
δ_{17}^2	3.75×10^{-11}	1.09×10^{-12}	1.14×10^{-12}
δ_{18}^2	4.95×10^{-11}	4.39×10^{-13}	4.67×10^{-13}
δ_{19}^2	6.97×10^{-11}	1.52×10^{-14}	1.02×10^{-14}
δ_{20}^2	1.03×10^{-10}	1.90×10^{-12}	1.84×10^{-12}
$\max(\delta^2) = \delta_{20}^2$	1.03×10^{-10}	1.90×10^{-12}	1.84×10^{-12}
$e = \sum \delta^2$	4.20×10^{-10}	6.98×10^{-12}	6.96×10^{-12}

5.4.3 Discussion on ACLD and PCLD for Shape Control

When the beam is in flat shape, open-loop control refers to PCLD, while closed-loop control means ACLD. Consider a point load same as the one in Section 5.4.1. The errors of the open-loop loaded and closed-loop loaded are summarized in Table 5-8. The error of open-loop control is much larger than that of closed-loop control. Moreover, it can be seen from Figure 5-21 that for open-loop control, apart from the distortion of the achieved shape (Figure 5-20), the beam vibrates with a first mode damping ratio of 2.20 x 10^{-3} about its equilibrium position. Figure 5-22 and Table 5-8 reveal that when closed-loop control is used, the loaded shape can return to the original shape with negligible error (i.e. 2.61 x 10^{-22} m^2) and a settling time of less than 2.5 seconds.

The open-loop or PCLD can be regarded as the break down situation of the ACLD control system. The beam eventually settles down to an equilibrium position despite of damped oscillations. On the other hand, the break down of the AC beam will lead to sustained vibration due to the absence of the viscoelastic layer. This justifies the use of ACLD in the shape control application.

Table 5-8 Summary of errors for static distributed load – flat shape

Node error	Open-loop loaded (m^2)	Closed-loop loaded (m^2)
δ_1^2	2.55×10^{-15}	3.22×10^{-27}
δ_2^2	3.80×10^{-14}	4.45×10^{-26}
δ_3^2	1.80×10^{-13}	1.92×10^{-25}
δ_4^2	5.37×10^{-13}	5.19×10^{-25}
δ_5^2	1.25×10^{-12}	1.09×10^{-24}
δ_6^2	2.46×10^{-12}	1.94×10^{-24}
δ_7^2	4.29×10^{-12}	3.05×10^{-24}
δ_8^2	6.82×10^{-12}	4.38×10^{-24}
δ_9^2	1.01×10^{-11}	5.91×10^{-24}
δ_{10}^2	1.41×10^{-11}	7.60×10^{-24}
δ_{11}^2	1.89×10^{-11}	9.48×10^{-24}
δ_{12}^2	2.45×10^{-11}	1.16×10^{-23}
δ_{13}^2	3.08×10^{-11}	1.40×10^{-23}
δ_{14}^2	3.77×10^{-11}	1.68×10^{-23}
δ_{15}^2	4.53×10^{-11}	2.00×10^{-23}
δ_{16}^2	5.36×10^{-11}	2.37×10^{-23}
δ_{17}^2	6.25×10^{-11}	2.79×10^{-23}
δ_{18}^2	7.21×10^{-11}	3.25×10^{-23}
δ_{19}^2	8.23×10^{-11}	3.76×10^{-23}
δ_{20}^2	9.32×10^{-11}	4.31×10^{-23}
$\max(\delta^2) = \delta_{20}^2$	9.32×10^{-11}	4.31×10^{-23}
$e = \sum \delta^2$	5.61×10^{-10}	2.61×10^{-22}

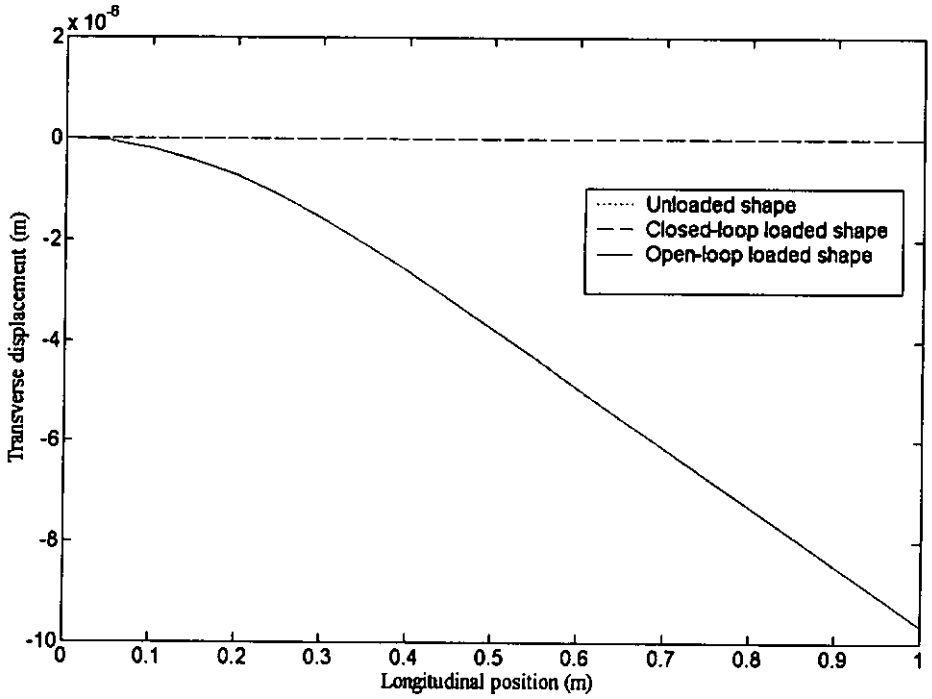

Figure 5-20 Comparison between open loop and closed loop loaded shapes for static distributes load – flat shape

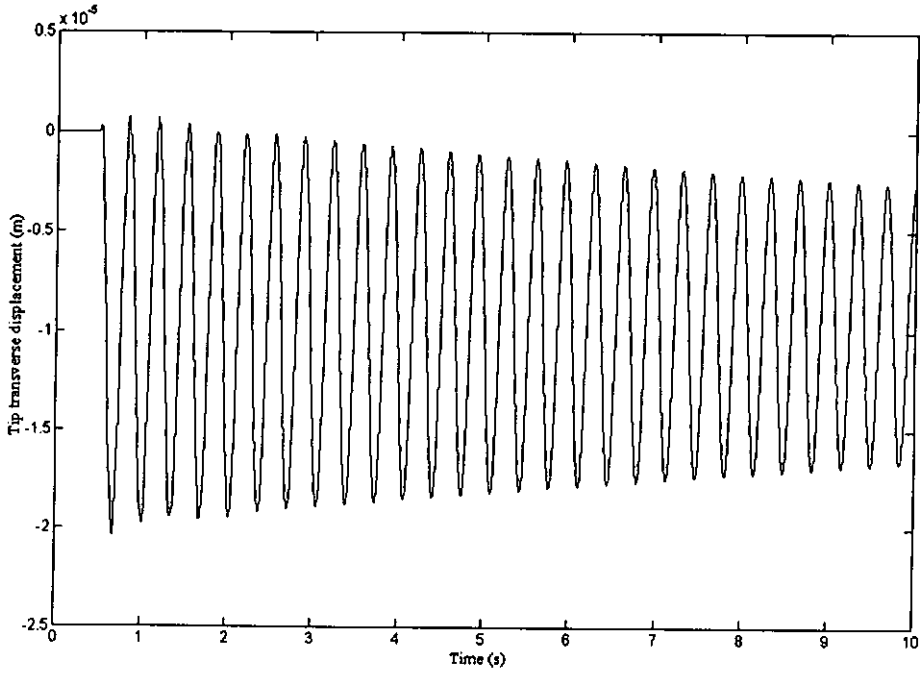

Figure 5-21 Effect of static distributed load on beam tip transverse displacement – open-loop

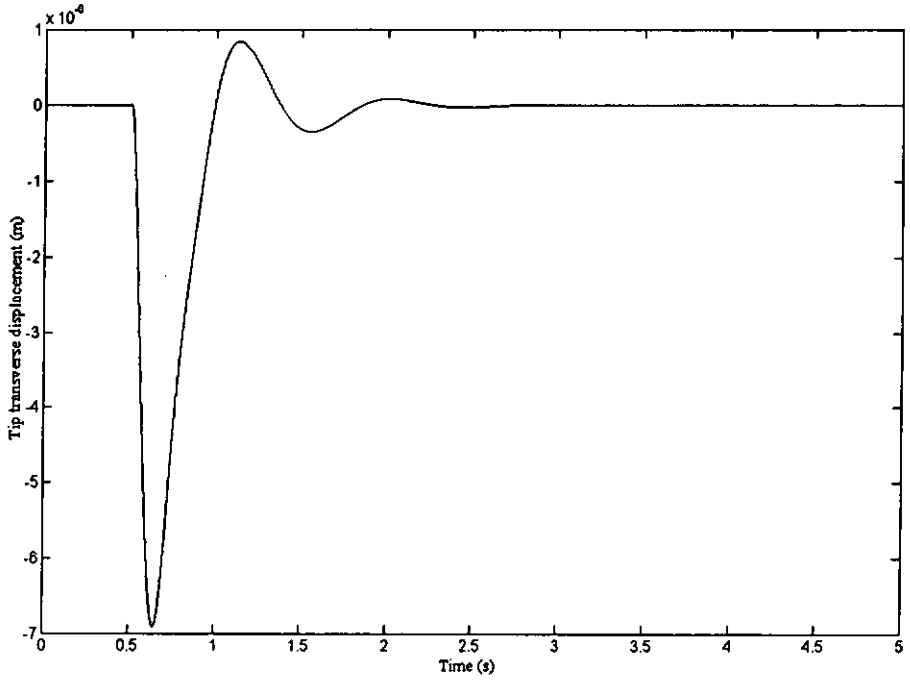

Figure 5-22 Effect of static distributed load on beam tip transverse displacement – closed-loop

5.5 DISCUSSION ON CONTROL VOLTAGE

It is clear that treating also the control energy (the total control voltages required to maintain the achieved shape at steady state) as another objective function makes the design more thorough, since both open and closed-loop performances can be optimized. Hence, a four-objective optimization is also performed, with the same MOGA parameters used before. The fourth objective function is:

(4) Minimizing the summation of the squares of control voltages at steady state.

Objective function4 Φ_4 : $V_{c1}^2 + V_{c2}^2 + V_{c3}^2$

The optimization results are given in Figures 5-23 to 5-26. It can be seen that the distribution of solutions (Figures 5-23 to 5-25) are similar to those in the three-objective case (Figures 5-1 to 5-3). As shown in Figure 5-26, reasonable Pareto solutions can be found in error and voltage surfaces. However, the error values become larger because of the inclusion of the control voltages in the objective functions. A solution, with the smallest value of error, is selected. It is shown, from Figure 5-27, that the achieved shape encounters a large derivation from the desired shape. Consequently, it can be concluded that considering the control voltages as one of the objective functions scarifies significantly the accuracy of the achieved shape.

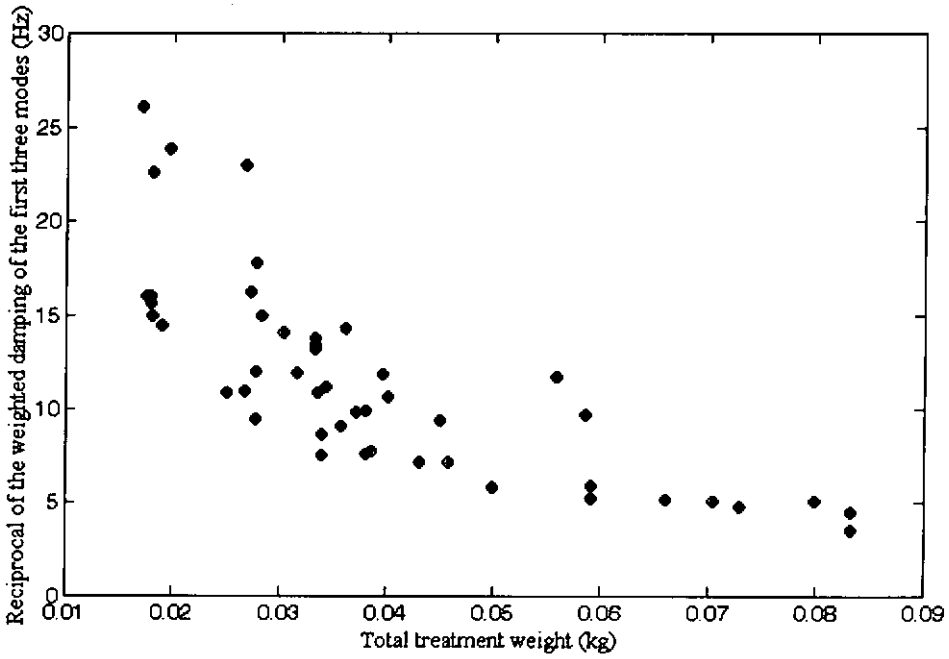

Figure 5-23 Projection of Pareto solutions on weight and damping surfaces: 4-objective case

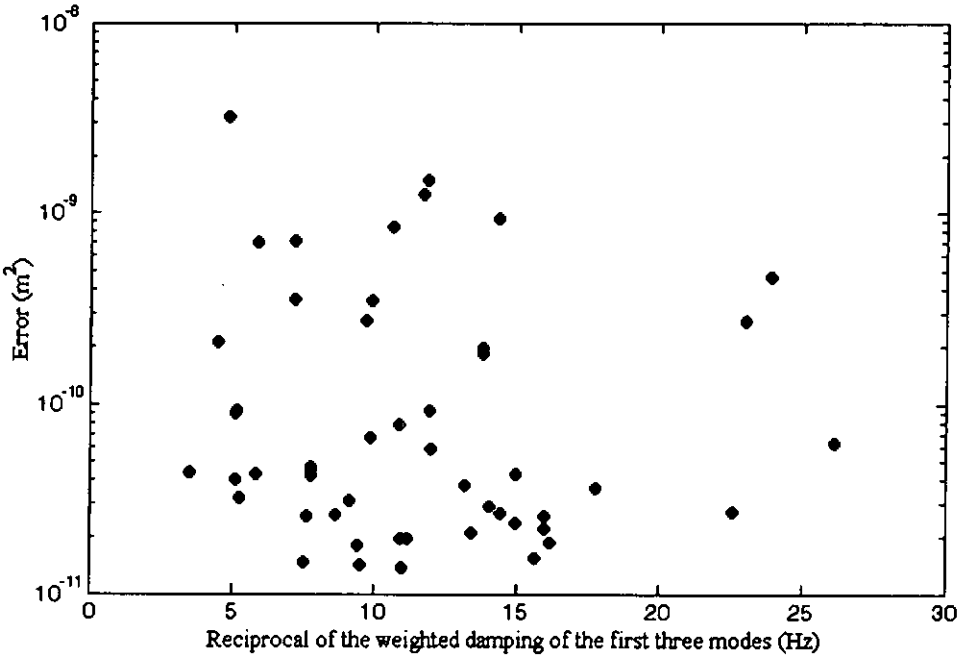

Figure 5-24 Projection of Pareto solutions on damping and error surfaces: 4-objective case

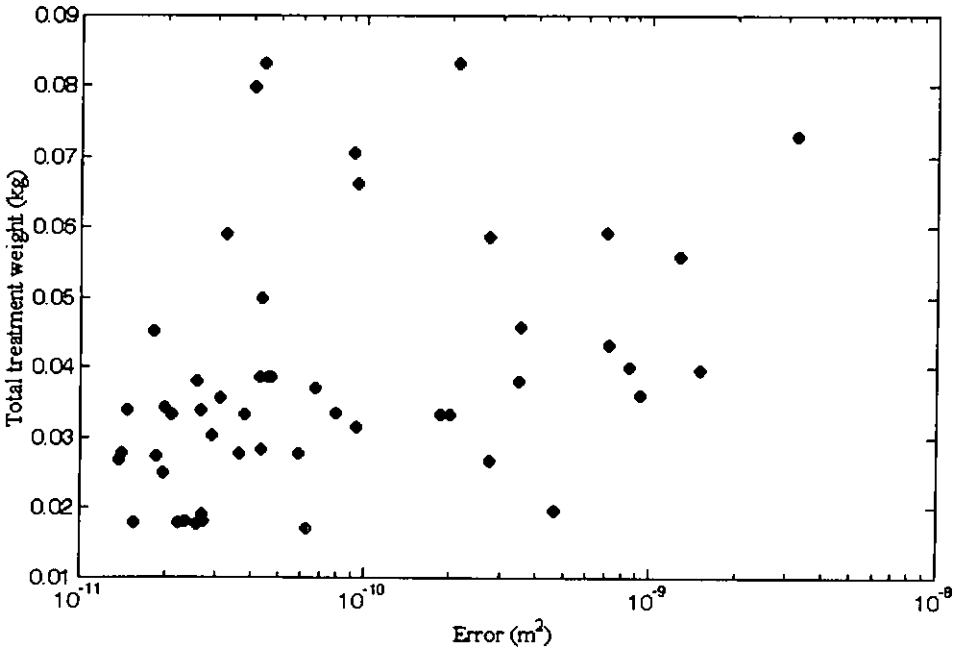

Figure 5-25 Projection of Pareto solutions on error and weight surfaces: 4-objective case

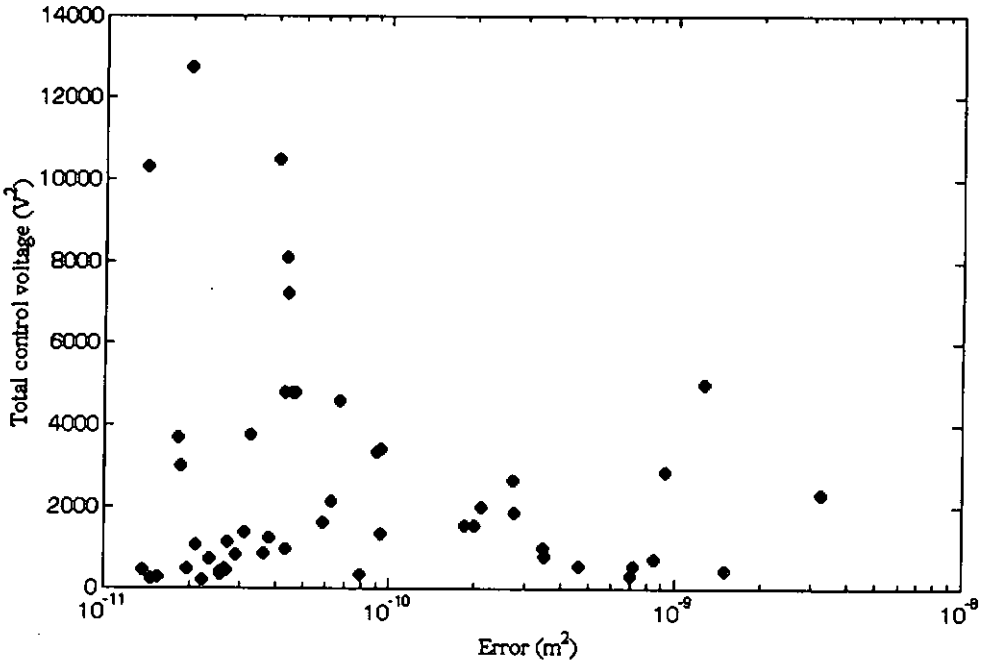

Figure 5-26 Projection of Pareto solutions on error and voltage surfaces: 4-objective case

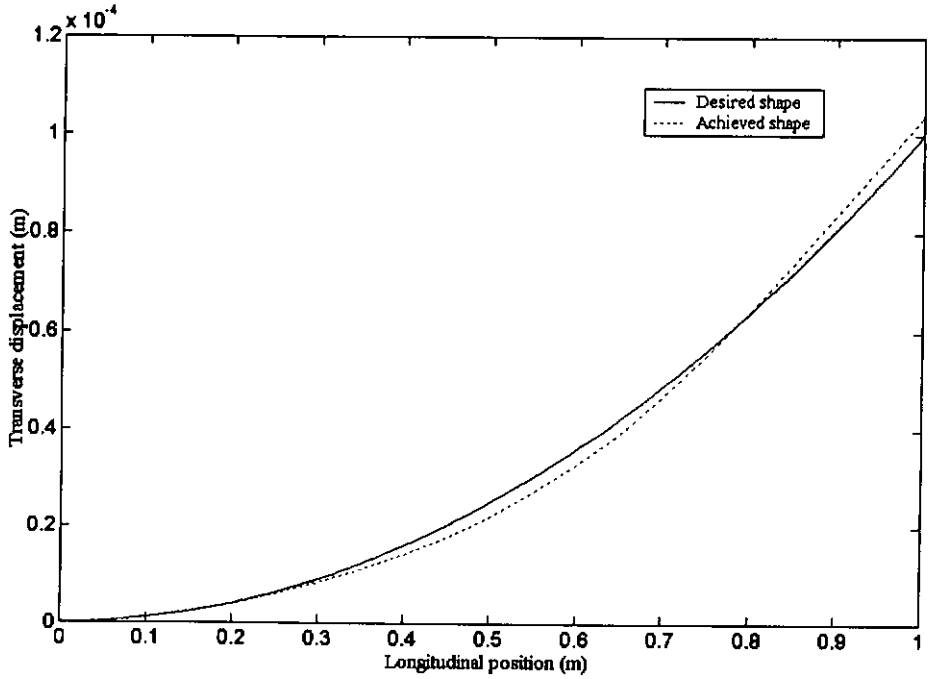

Figure 5-27 Desired and achieved shapes of the beam after 5 seconds: 4-objective case

5.6 SUMMARY

The above findings are summarized below.

(i) Pareto solutions for this multi-objective optimization problem are successfully found. There exists a clear tradeoff between the treatment weight and summation of passive damping.

(ii) ACLD patches can drive the structure to the desired shape smoothly.

(iii) For the loads under consideration in this study, the closed loop control outperforms the open loop control in terms of disturbance-rejection ability and settling time.

(iv) ACLD is better than AC for shape control of structures, when taking fail-safe issue into account in the design.

CHAPTER 6

CONCLUSIONS

6.1 CONCLUDING REMARKS

In this thesis, feasibility of utilizing ACLD treatments for shape control application was investigated, and results were presented. The studies of ACLD treatments for vibration suppression have shown promising results, but the application of such treatments for shape control is an unexplored topic. The optimization issue of such kind of system was addressed, and the performance was also evaluated numerically. The major work done in this thesis is summarized below.

(i) In order to predict the dynamic behavior of the flexible beam with distributed ACLD patches for design purpose, a mathematical model is required. In this model, some assumptions were made to simplify the complexity of the structure. Besides, considering the distributed nature of the ACLD patches, and to facilitate time-domain analysis, the finite element method (FEM), in conjunction with the Golla-Hughes-McTavish (GHM) viscoelastic model, was employed. Comparisons were made with other models available in the literature. It is shown that analysis results by the present model are in close agreement with those given by other models.

(ii) To obtain an overall view on the damping characteristic of the ACLD treated beam, a parametric study was conducted using the developed model. The objective was to identify the effects of treatment length and location, the layer physical and geometrical properties as well as the control gains on the damping performance. It is demonstrated that proper selections of control gains are crucial for active damping and system stabilization. The effective location is mode dependent. It is also found that, unlike the constraining layer thickness that the damping monotonically increases with it, both the viscoelastic layer thickness and shear modulus exhibit optimal values for maximum damping.

(iii) The shape control design problem was formulated. When selecting the proper design objectives, both open and closed-loop requirements were considered. With respect to open loop, certain amount of passive damping is necessary for stability and fail-safe consideration. Thus, it is reasonable that the maximization of the passive damping should be a design objective. Meanwhile, a heavy structure is undesirable, so the minimization of treatment weight is necessary. On the other hand, when it comes to closed loop, the minimization of the error between the desired and achieved shapes is another concern. Also, the transient behavior is specified by imposing the constraints on the settling time and maximum overshoot of the beam tip. Therefore, the design is no longer a single objective problem. Instead, it is treated as a multi-objective optimization problem. Appropriate design variables and constraints are identified as well, based on the study in (ii).

(iv) To solve the multi-objective optimization problem stated in (iii), the stochastic approach, MOGA, was used. A program was developed, with the aid of the commercial software package MATLAB, to implement the principle and philosophy of MOGA so that solutions can be obtained. A simple multi-objective engineering design problem was used to test and debug the developed program.

(v) The multi-objective design problem, described in (iv) was solved by the MOGA algorithm developed in the present work. Pareto solutions were successfully obtained. A clear conflict between the total treatment weight and summation of passive damping was found. They also exhibit a convex tradeoff relation. Since the most important aspect of multi-objective optimization problem is to provide alternatives, several Pareto solutions were chosen for the final evaluation based on their shape errors.

(vi) Lastly, the shape control problem was studied numerically by selecting a solution, with smallest value of error, obtained from the MOGA. The performance was evaluated by analyzing its transient behavior. Simulation results demonstrated the feasibility of using ACLD patches for the shape change of structure. Effects of external disturbances on the shape control were also examined. Several types of load, including static/impulsive and point/distributed loads (with magnitude leading to around 0.01 mm tip deflection), were applied on the structure under different occasions. It is shown that for the loads under consideration, the closed-loop control could regulate the actuator voltages to correct the distorted shape.

Finally, comparison was made between open and closed-loop controls. It is evident that the closed-loop control outperforms the open-loop one in terms of disturbance-rejection ability and settling time.

6.2 RECOMMENDATIONS

Although this work has shown encouraging results, more work is necessary to be done to make the proposed idea – utilizing ACLD treatments for shape control of structures, implement in real-life application. Some suggestions are listed below.

(i) Extending the application of the ACLD patches for shape control to other types of engineering structures is encouraged, such as plates, shells and curved structures. Besides, it is essential that models of the above structures be non-dimensionalized, so that the design results can be applicable to the general beam-like structures.

(ii) The control used in the present work is the common Proportional-Integral-Derivative (PID) control. In fact, with the rapid development in control techniques, more advanced controllers can be applied to the present shape control problem, such as the robust control, fuzzy-logic control, and variable-structure control. It is hoped that these can help to enhance the disturbance rejection ability of the system.

(iii) It is also recommended that more design variables and objectives be considered in the optimization problem. Environmental protection is now a global issue, and one of the philosophies of it is resource saving. Therefore, minimization of the voltages used during the control process should also be the design objective. Also, in terms of material saving, number of ACLD patches should also be considered as the design variables, which will inevitably lead to more complicated problems due to the interactions between the structural and control designs.

(iv) Experimental verification is expected to be performed in due course. The performance evaluation and analysis on the shape control problem are confined only in numerical work so far. It means that many factors, that may affect the implementation of the shape control, are ignored during the analysis. With experimental work, the difficulties associated with the real implementation of shape control of ACLD structure can be identified. Solutions can then be proposed to tackle the problems.

APPENDIX A

FREQUENCY RESPONSE RESULTS (LEE AND KIM, 2001)

The following frequency response functions are extracted from Lee and Kim [47].

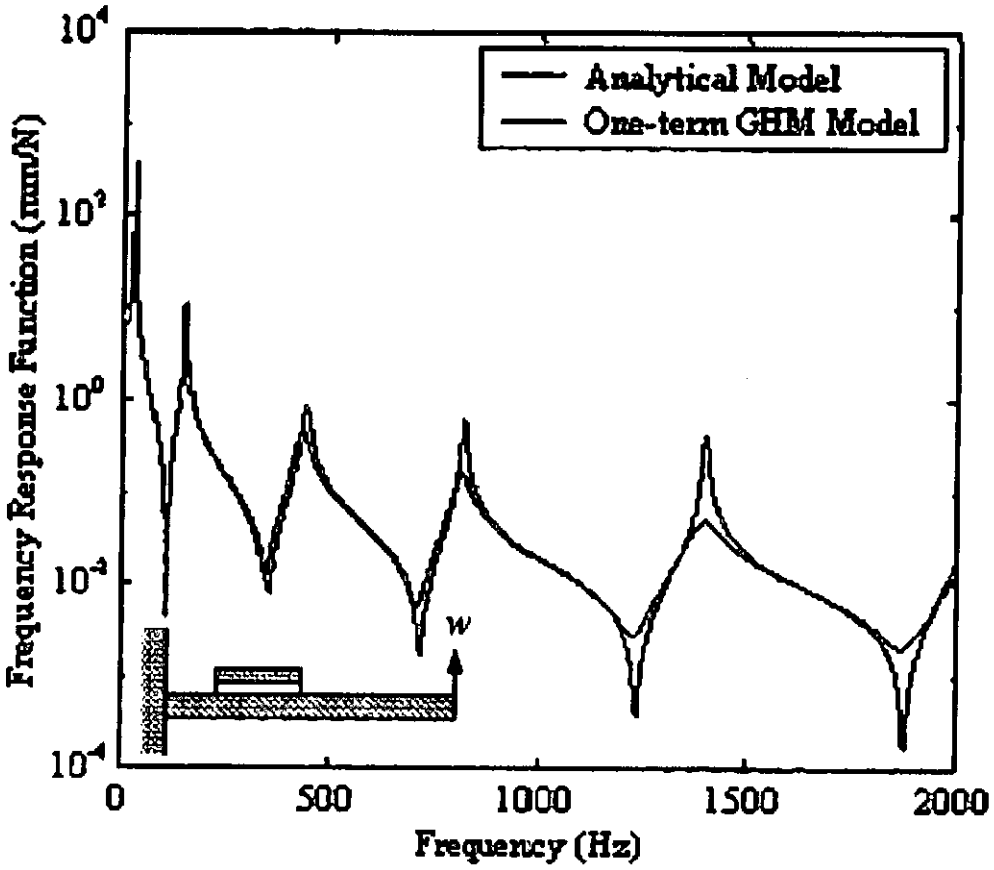

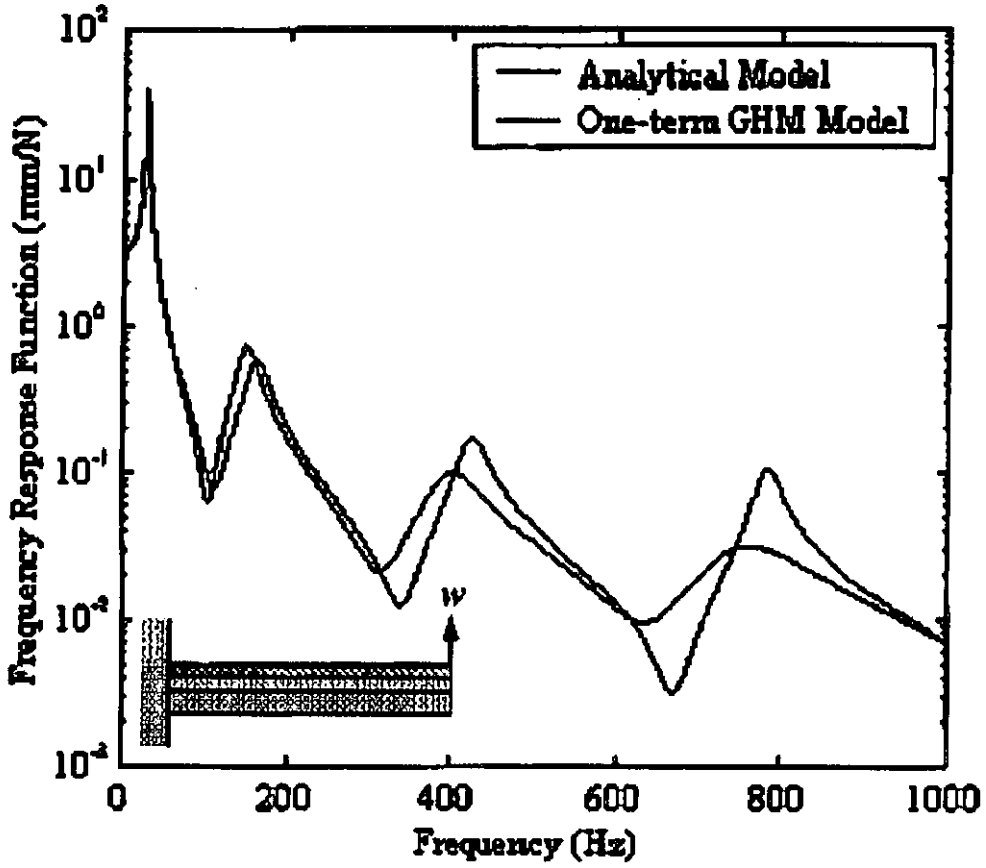
Analytical Model
One-term GHM Model
Frequency Response Function (mm/N)
Frequency (Hz)
w
10^{2}
10^{1}
10^{0}
10^{-1}
10^{-2}
10^{-3}
0
200
400
600
800
1000

APPENDIX B

PARETO-OPTIMAL SOLUTIONS (KALYANMOY, 2001)

The following Pareto-optimal solutions are extracted from Kalyanmoy [94].

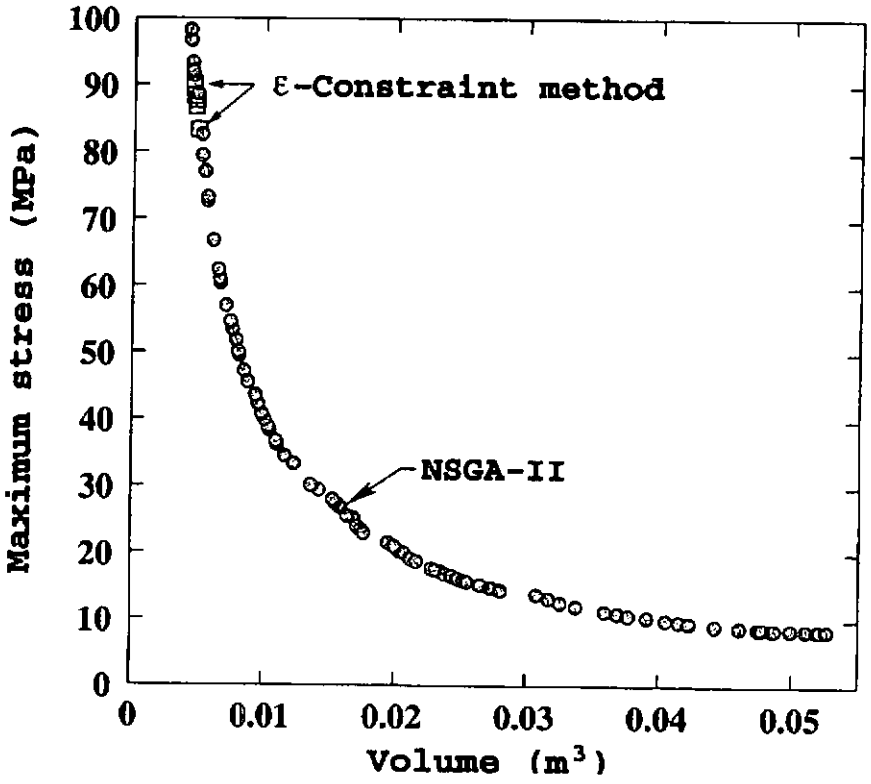

APPENDIX C

COMPUTER CODE OF MOGA

```
format short e

evo_no=200;

Unconstraint=zeros(evo_no,1);
Max_value=zeros(evo_no,3);
Min_value=zeros(evo_no,3);
Average_value=zeros(evo_no,3);

for Big_loop=1:evo_no

%************************%
% Loading I from Generation %
%************************%
load Generation;

Iold=I;

PI1=zeros(size(Iold,1),1);
PI2=zeros(size(Iold,1),1);
PI3=zeros(size(Iold,1),1);
Fitness=zeros(size(Iold,1),1);

%*********%
% Decoding %
%*********%
vlb=[1,1,1,2,2,2];
vub=[2,4,4,5,5,5];
bits=[1,2,2,2,2,2];

for i=1:sum(bits)
   Icode(:,i)=Iold(:,i);
end

[Idecode]=Decode(Icode,vlb,vub,bits);

for gen_no=1:size(Iold,1)
```

```
gen_no
  Out=0;

%*****************%
% Obtain Information %
%*****************%
  P1=round(Idecode(gen_no,1));
  S2=round(Idecode(gen_no,2));
  S3=round(Idecode(gen_no,3));
  L1=round(Idecode(gen_no,4));
  L2=round(Idecode(gen_no,5));
  L3=round(Idecode(gen_no,6));

  tc=Iold(gen_no,sum(bits)+1)*10^-3;
  tv=Iold(gen_no,sum(bits)+2)*10^-3;
  KI1=Iold(gen_no,sum(bits)+3);
  KI2=Iold(gen_no,sum(bits)+4);
  KI3=Iold(gen_no,sum(bits)+5);
  KD1=Iold(gen_no,sum(bits)+6);
  KD2=Iold(gen_no,sum(bits)+7);
  KD3=Iold(gen_no,sum(bits)+8);
  ki1=Iold(gen_no,sum(bits)+9);
  ki2=Iold(gen_no,sum(bits)+10);
  ki3=Iold(gen_no,sum(bits)+11);
  kd1=Iold(gen_no,sum(bits)+12);
  kd2=Iold(gen_no,sum(bits)+13);
  kd3=Iold(gen_no,sum(bits)+14);

  P2=P1+S2+L1;
  P3=P2+S3+L2;

  type=ones(1,20);
  for i=0:L1-1
    type(P1+i)=2;
  end
  for i=0:L2-1
    type(P2+i)=2;
  end
  for i=0:L3-1
    type(P3+i)=2;
  end

%*******************%
% Invaild Configuration %
%*******************%
  patch_no=0;
```

```
patch_length=zeros;
signal=0;
countL=1;
countN=1;

for i=1:20
  if (type(1,i)==1 & signal==1)
    signal=0;
    countL=1;
    countN=countN+1;
  elseif (type(1,i)==2)
    patch_length(countN)=countL;
    countL=countL+1;
    patch_no=countN;
    signal=1;
  end
end

if (patch_no~=3)
  Fitness(gen_no,1)=0.2;
  Out=1;
end
if (P3+(L3-1)>20)
  Fitness(gen_no,1)=0.2;
  Out=1;
end

if (Out==0)

%**************%
% FEM Analysis %
%**************%

    [Error,Weight,Sum_damping]=FEM(type,tc,tv,KI1,KI2,KI3,KD1,KD2,KD3,ki1,
    ki2,ki3,kd1,kd2,kd3,P1,P2,P3,L1,L2,L3);

PI1(gen_no,1)=Error;
PI2(gen_no,1)=Weight;
PI3(gen_no,1)=Sum_damping;

  if (PI1(gen_no,1)~=0 & PI2(gen_no,1)~=0 & PI3(gen_no,1)~=0)
    Fitness(gen_no,1)=1.2-((0.4*((0.5*size(Iold,1))-1))/(size(Iold,1)-1));
  else
    Fitness(gen_no,1)=1.2-((0.4*((0.95*size(Iold,1))-1))/(size(Iold,1)-1));
  end
```

```
    end

  end

  %******************%
  % Fitness Assignment %
  %******************%
  %--------------------------------%
  % Identifying Feasible Gene %
  %--------------------------------%
  feasible=zeros;
  s=1;

  for i=1:size(Iold,1)
    if (Fitness(i,1)==1.2-((0.4*((0.5*size(Iold,1))-1))/(size(Iold,1)-1)))
      feasible(s)=i;
      s=s+1;
    end
  end

  if (feasible~=0)

  %------------%
  % Ranking %
  %------------%
    domainance=0;

    for i=1:length(feasible)
      for j=1:length(feasible)
        if (feasible(i)~=feasible(j))
          if                    (PI1(feasible(j),1)<=PI1(feasible(i),1)                    &
        PI2(feasible(j),1)<=PI2(feasible(i),1) & PI3(feasible(j),1)<=PI3(feasible(i),1))
            domainance=domainance+1;
          end
        end
      end
      if (domainance==0)
        Fitness(feasible(i),1)=1.2;
      end
      domainance=0;
    end

  end
```

```
%**************%
% Saving I to Evo %
%**************%
Irecord=Iold;

if (feasible~=0)
   Unconstraint(Big_loop,1)=length(feasible);
   Max_value(Big_loop,1)=max(PI1(feasible,1));
   Max_value(Big_loop,2)=max(PI2(feasible,1));
   Max_value(Big_loop,3)=max(PI3(feasible,1));
   Min_value(Big_loop,1)=min(PI1(feasible,1));
   Min_value(Big_loop,2)=min(PI2(feasible,1));
   Min_value(Big_loop,3)=min(PI3(feasible,1));
   Average_value(Big_loop,1)=mean(PI1(feasible,1));
   Average_value(Big_loop,2)=mean(PI2(feasible,1));
   Average_value(Big_loop,3)=mean(PI3(feasible,1));
   else
   Unconstraint(Big_loop,1)=0;
   Max_value(Big_loop,1)=0;
   Max_value(Big_loop,2)=0;
   Max_value(Big_loop,3)=0;
   Min_value(Big_loop,1)=0;
   Min_value(Big_loop,2)=0;
   Min_value(Big_loop,3)=0;
   Average_value(Big_loop,1)=0;
   Average_value(Big_loop,2)=0;
   Average_value(Big_loop,3)=0;
end

save Evo200 Irecord PI1 PI2 PI3 Fitness feasible

feasible
Iga=Iold;

%*******%
% MOGA %
%*******%
[Inew]=MOGA(Iga,Fitness);

%*******************%
% Saving I to Generation %
%*******************%
I=Inew;
save Generation I

end
```

```
save Data Unconstraint Max_value Min_value Average_value
function[Error,Weight,Sum_damping]=FEM(type,tc,tv,KI1,KI2,KI3,KD1,KD2,KD3,ki
        1,ki2,ki3,kd1,kd2,kd3,P1,P2,P3,L1,L2,L3);

KP1=0;
KP2=0;
KP3=0;
kp1=0;
kp2=0;
kp3=0;

KP=[KP1,0,0;0,KP2,0;0,0,KP3];
KI=[KI1,0,0;0,KI2,0;0,0,KI3];
KD=[KD1,0,0;0,KD2,0;0,0,KD3];
kp=[kp1,0,0;0,kp2,0;0,0,kp3];
ki=[ki1,0,0;0,ki2,0;0,0,ki3];
kd=[kd1,0,0;0,kd2,0;0,0,kd3];

Out=0;

%***************%
% Node Estimation %
%***************%
node=zeros(1,20);
if (type(1)==1)
   countn=2;
else countn=8;
end
for i=1:20
  if (i<20)
     node(i)=countn;
     if (type(i)==1)
        if (type(i+1)==1)
           countm=3;
        else countm=10;
        end
        countn=countn+countm;
     else
        if (type(i+1)==1)
           countm=4;
        else countm=10;
        end
        countn=countn+countm;
     end
  else
```

```
      if (type(20)==1)
         node(20)=countn;
      else node(20)=countn;
      end
   end
end

%*******************************%
%  Material and Geometric Properties %
%*******************************%
%%% Height & Width %%%
tb=0.002;
ts=0.000028;
b=0.020;
Ls1=0.05*L1;
Ls2=0.05*L2;
Ls3=0.05*L3;

%%% Young's Modulus %%%
Eb=150*10^9;
Ec=64.9*10^9;

%%% Desity %%%
pb=1600;
pv=1250;
pc=7600;

%%% GHM Parameters %%%
Gv=5*10^5;
parw1=6502.9;
parw2=50618.8;
parw3=352782;
parz1=6.97;
parz2=5.38;
parz3=2.56;
paralpha1=0.742;
paralpha2=3.237;
paralpha3=41.654;
d31=-1.75*10^-10;
K3t=1.5*10^-8;

%*****************%
% Moment of Inertia %
%*****************%
Ib=(b*(tb^3))/12;
Iv=(b*(tv^3))/12;
```

```
Ic=(b*(tc^3))/12;

%*************************%
% Compute tnel, type & length %
%*************************%
tnel=20;
length=0.05*ones(1,20);

%***********************%
%  Calculation of Vsd & Wd %
%***********************%
Vsd1=-((Ec*d31*ts*(ts+(tb/2)))/(K3t*Ls1))*(0.0002*Ls1);
Vsd2=-((Ec*d31*ts*(ts+(tb/2)))/(K3t*Ls2))*(0.0002*Ls2);
Vsd3=-((Ec*d31*ts*(ts+(tb/2)))/(K3t*Ls3))*(0.0002*Ls3);
Wsd=0.0001;

%********************%
% Compute OriginalSize %
%********************%
TempSize=0;
OriginalSize=0;
for n=1:tnel-1
  if (type(n)==1)
    TempSize=TempSize+3;
  else
    if (type(n+1)==1)
      TempSize=TempSize+11;
    else
      TempSize=TempSize+10;
    end
  end
end
if (type(tnel)==1)
  OriginalSize=TempSize+6;
else
  OriginalSize=TempSize+14;
end
MM=zeros(OriginalSize,OriginalSize);
DD=zeros(OriginalSize,OriginalSize);
KK=zeros(OriginalSize,OriginalSize);
BBc1=zeros(OriginalSize,1);
BBc2=zeros(OriginalSize,1);
BBc3=zeros(OriginalSize,1);
BBc=zeros(OriginalSize,3);
CCc1=zeros(1,OriginalSize);
CCc2=zeros(1,OriginalSize);
```

```
CCc3=zeros(1,OriginalSize);
CCc=zeros(3,OriginalSize);

%***************%
% Obtaine M D K %
%***************%
Ls=Ls1;
row=0;
flag=0;
i=1;
for m=1:tnel
  j=i;

  if (type(m)==1)
    L=length(m);

%*******************%
% Case I: Pure Element %
%*******************%
[Mbeam,Dbeam,Kbeam,BBcbeam,CCcbeam]=Beam_Matrix(Eb,pb,tb,Ib,b,L);

  else
    L=length(m);

%***********************%
% Case II: ACLD Element %
%***********************%
[Macld,Kacld,KacldV]=ACLD_Matrix(Eb,Ec,Gv,pb,pc,pv,tb,tc,tv,Ib,Ic,b,L);

%%%% Spectral Decomposition %%%%
[Ae,Re]=Decomposition(Gv,KacldV);

%***********************%
% Rearrange for Assembly %
%***********************%
[MMacld,DDacld,KKacld]=Arrange(Macld,Kacld,KacldV,parw1,parz1,paralpha1,parw
      2,parz2,paralpha2,parw3,parz3,paralpha3,Gv,Ae,Re);
BBcacld=[-Ec*d31*b;0;Ec*d31*b*(tv+((tb+tc)/2));-
      Ec*d31*b*tv;0;0;0;0;0;0;Ec*d31*b;0;-
      Ec*d31*b*(tv+((tb+tc)/2));Ec*d31*b*tv];
CCcacld=[0,0,(Ec*d31*ts*(ts+(tb/2)))/(K3t*Ls),0,0,0,0,0,0,0,0,0,-
      (Ec*d31*ts*(ts+(tb/2)))/(K3t*Ls),0];

  end
```

```
%********************%
% Assembly M D and K %
%********************%
  if (type(m)==1)
          index(1)=j;
          index(2)=j+1;
          index(3)=j+2;
     index(4)=j+3+flag;
     index(5)=j+4+flag;
     index(6)=j+5+flag;
          edof=6;
          for ir=1:edof;
          irs=index(ir);
       for ic=1:edof;
          ics=index(ic);
          KK(irs,ics)=KK(irs,ics)+Kbeam(ir,ic);
          DD(irs,ics)=DD(irs,ics)+Dbeam(ir,ic);
          MM(irs,ics)=MM(irs,ics)+Mbeam(ir,ic);
       end
       if (row==0)
          BBc1(irs,1)=BBc1(irs,1)+BBcbeam(ir,1);
          CCc1(1,irs)=CCc1(1,irs)+CCcbeam(1,ir);
       elseif (row==1)
          BBc2(irs,1)=BBc2(irs,1)+BBcbeam(ir,1);
          CCc2(1,irs)=CCc2(1,irs)+CCcbeam(1,ir);
       else
          BBc3(irs,1)=BBc3(irs,1)+BBcbeam(ir,1);
          CCc3(1,irs)=CCc3(1,irs)+CCcbeam(1,ir);
       end
    end
  else
     index(1)=j;
          index(2)=j+1;
          index(3)=j+2;
          index(4)=j+3;
          index(5)=j+4;
          index(6)=j+5;
          index(7)=j+6;
     index(8)=j+7;
     index(9)=j+8;
     index(10)=j+9;
     index(11)=j+10;
     index(12)=j+11;
     index(13)=j+12;
     index(14)=j+13;
     edof=14;
```

```
      for ir=1:edof;
          irs=index(ir);
          for ic=1:edof;
             ics=index(ic);
          KK(irs,ics)=KK(irs,ics)+KKacld(ir,ic);
          DD(irs,ics)=DD(irs,ics)+DDacld(ir,ic);
          MM(irs,ics)=MM(irs,ics)+MMacld(ir,ic);
        end
        if (row==0)
          BBc1(irs,1)=BBc1(irs,1)+BBcacld(ir,1);
          CCc1(1,irs)=CCc1(1,irs)+CCcacld(1,ir);
        elseif (row==1)
          BBc2(irs,1)=BBc2(irs,1)+BBcacld(ir,1);
          CCc2(1,irs)=CCc2(1,irs)+CCcacld(1,ir);
        else
          BBc3(irs,1)=BBc3(irs,1)+BBcacld(ir,1);
          CCc3(1,irs)=CCc3(1,irs)+CCcacld(1,ir);
        end
      end
    end

      if (type(m)==1)
        if (flag==1)
          i=i+4;
          flag=0;
        else
              i=i+3;
        end
      else
        if (m<tnel)
          if (type(m+1)==2)
            i=i+10;
          else
            i=i+10;
            flag=1;
            row=row+1;
            if (row==1)
               Ls=Ls2;
            else Ls=Ls3;
            end
          end
        end
      end

end
```

```
BBc(:,1)=BBc1;
BBc(:,2)=BBc2;
BBc(:,3)=BBc3;
CCc(1,:)=CCc1;
CCc(2,:)=CCc2;
CCc(3,:)=CCc3;

%******************%
% Boundary Conditions %
%******************%
if (type(1)==1)
   bound=3;
else
   bound=4;
end

BoundarySize=OriginalSize-bound;

M=zeros(BoundarySize,BoundarySize);
D=zeros(BoundarySize,BoundarySize);
K=zeros(BoundarySize,BoundarySize);
Bc=zeros(BoundarySize,3);
Bd=zeros(BoundarySize,1);
Cc=zeros(3,BoundarySize);
Cd=zeros(1,BoundarySize);

for i=1:BoundarySize
  for j=1:BoundarySize
    M(i,j)=MM(i+bound,j+bound);
    D(i,j)=DD(i+bound,j+bound);
    K(i,j)=KK(i+bound,j+bound);
    Bc(i,1)=BBc(i+bound,1);
    Bc(i,2)=BBc(i+bound,2);
    Bc(i,3)=BBc(i+bound,3);
    Cc(1,i)=CCc(1,i+bound);
    Cc(2,i)=CCc(2,i+bound);
    Cc(3,i)=CCc(3,i+bound);
  end
end

Bd(node,1)=1;
Cd(1,node(20))=1;

A=[0*eye(BoundarySize),eye(BoundarySize);-inv(M)*K,-inv(M)*D];
B1=[0*ones(BoundarySize,3);(inv(M)*Bc)];
B2=[0*ones(BoundarySize,1);(inv(M)*Bd)];
```

```
C1=[Cc,0*ones(3,BoundarySize)];
C2=[Cd,0*ones(1,BoundarySize)];

%*********%
%  (Weight) %
%*********%
Weight=(pv*b*tv*(Ls1+Ls2+Ls3))+(pc*b*tc*(Ls1+Ls2+Ls3));

%**************%
% (Sum_damping) %
%**************%
Osys=ss(A,B1,C1,0);
[Wn,Z,P]=damp(Osys);

count_damp=0;
i=1;

for j=1:size(P,1)
   if (count_damp<3)
      if (Z(i)==1)
         i=i+1;
      else damping_ratio(count_damp+1)=(Z(i)*100)/(Wn(i)/(2*pi));
         i=i+2;
         count_damp=count_damp+1;
      end
   end
end

Sum_damping=1/sum(damping_ratio);

%*****************%
% Trainsient Analysis %
%*****************%
[V,W]=eig(K,M);
U=zeros(BoundarySize,3);
U(:,1)=V(:,1);
U(:,2)=V(:,2);
U(:,3)=V(:,3);
%U(:,4)=V(:,4);
%U(:,5)=V(:,5);

Mbar=U'*M*U;
Dbar=U'*D*U;
Kbar=U'*K*U;
Bcbar=U'*Bc;
Bdbar=U'*Bd;
```

```
Ccbar=Cc*U;
Cdbar=Cd*U;

Abar=[0*eye(3),eye(3);-inv(Mbar)*Kbar,-inv(Mbar)*Dbar];
B1bar=[0*ones(3,3);(inv(Mbar)*Bcbar)];
B2bar=[0*ones(3,1);(inv(Mbar)*Bdbar)];
C1bar=[Ccbar,0*ones(3,3)];
C2bar=[Cdbar,0*ones(1,3)];

[n,m]=size(B1bar);
time=0:0.0001:3.1-0.0001;
nc=max(size(time));
Ts=time(2)-time(1);
Phi=expm(Abar*Ts);
Gamma1=inv(Abar)*(Phi-eye(n))*B1bar;
Gamma2=inv(Abar)*(Phi-eye(n))*B2bar;

x=zeros(nc,n);
tx=zeros(n,1);
x0=zeros(n,1);
xi=x0;
tx=xi;

Vs=zeros(3,nc);
VsDot=zeros(3,nc);
DeltaVs=zeros(3,nc);
DeltaVsDot=zeros(3,nc);
InDeltaVs1=0;
InDeltaVs2=0;
InDeltaVs3=0;

Ws=zeros(3,nc);
WsDot=zeros(3,nc);
DeltaWs=zeros(3,nc);
DeltaWsDot=zeros(3,nc);
InDeltaWs=0;

Vc=zeros(3,nc);

Vsd=[Vsd1;Vsd2;Vsd3];
Fd=0;

Transfer=[U,0*eye(BoundarySize,3);0*eye(BoundarySize,3),U];

for i=1:nc
  x(i,:)=tx';
```

```
    Temp=Transfer*tx;
    Vs(:,i)=[Cc,0*ones(3,BoundarySize)]*Temp;
    VsDot(:,i)=[0*ones(3,BoundarySize),Cc]*Temp;
    DeltaVs(:,i)=Vsd-Vs(:,i);
    DeltaVsDot(:,i)=-VsDot(:,i);
    InDeltaVs1=InDeltaVs1+DeltaVs(1,i);
    InDeltaVs2=InDeltaVs2+DeltaVs(2,i);
    InDeltaVs3=InDeltaVs3+DeltaVs(3,i);
    Ws(:,i)=[Cd,0*ones(1,BoundarySize)]*Temp;
    WsDot(:,i)=[0*ones(1,BoundarySize),Cd]*Temp;
    DeltaWs(:,i)=Wsd-Ws(:,i);
    DeltaWsDot(:,i)=-WsDot(:,i);
    InDeltaWs=InDeltaWs+DeltaWs(:,i);

        Vc(:,i)=((KP*DeltaVs(:,i))+(KD*DeltaVsDot(:,i))+(KI*[InDeltaVs1;InDeltaVs2
        ;InDeltaVs3]))+((kp*DeltaWs(:,i))+(kd*DeltaWsDot(:,i))+(ki*InDeltaWs));
    tx=Phi*tx+Gamma1*Vc(:,i)+Gamma2*Fd;
end

p=Transfer*x';


for i=1:1000
    ts1=(abs(Vs(1,30000)-Vs(1,30000+i)))/Vs(1,30000);
    if (abs(ts1)<=0.001)
        good1=1;
    else good1=0;
    end
end
for j=1:1000
    ts2=(abs(Vs(2,30000)-Vs(2,30000+j)))/Vs(2,30000);
    if (abs(ts2)<=0.001)
        good2=1;
    else good2=0;
    end
end
for k=1:1000
    ts3=(abs(Vs(3,30000)-Vs(3,30000+k)))/Vs(3,30000);
    if (abs(ts3)<=0.001)
        good3=1;
    else good3=0;
    end
end

if (max(abs(Vs(1,:)))>=1000000)
    good1=0;
```

```
end
if (max(abs(Vs(2,:)))>=1000000)
   good2=0;
end
if (max(abs(Vs(3,:)))>=1000000)
   good3=0;
end

if (good1==0 | good2==0 | good3==0)
   Out=1;
end

if (Out==0)

%*******%
% (Error) %
%*******%
   node_error=zeros(20,1);

  for i=1:20
     node_error(i,1)=((0.0001*(0.05*i)^2)-(p(node(i),nc)))^2;
   end
   total_error=sum(node_error);
   Error=total_error;

else
   Weight=0;
   Sum_damping=0;
   Error=0;
end

function[Macld,Kacld,KacldV]=ACLD_Matrix(Eb,Ec,Gv,pb,pc,pv,tb,tc,tv,Ib,Ic,b,L);

KacldUb=Eb*tb*b*[1/L,0,0,0,-1/L,0,0,0;
            0,0,0,0,0,0,0,0;
            0,0,0,0,0,0,0,0;
            0,0,0,0,0,0,0,0;
            -1/L,0,0,0,1/L,0,0,0;
            0,0,0,0,0,0,0,0;
            0,0,0,0,0,0,0,0;
            0,0,0,0,0,0,0,0];
KacldWb=Eb*Ib*[0,0,0,0,0,0,0,0;
          0,12/L^3,6/L^2,0,0,-12/L^3,6/L^2,0;
          0,6/L^2,4/L,0,0,-6/L^2,2/L,0;
          0,0,0,0,0,0,0,0;
          0,0,0,0,0,0,0,0;
```

```
          0,-12/L^3,-6/L^2,0,0,12/L^3,-6/L^2,0;
          0,6/L^2,2/L,0,0,-6/L^2,4/L,0;
          0,0,0,0,0,0,0,0];
MacldUb=pb*tb*b*[1/3*L,0,0,0,1/6*L,0,0,0;
          0,0,0,0,0,0,0,0;
          0,0,0,0,0,0,0,0;
          0,0,0,0,0,0,0,0;
          1/6*L,0,0,0,1/3*L,0,0,0;
          0,0,0,0,0,0,0,0;
          0,0,0,0,0,0,0,0;
          0,0,0,0,0,0,0,0];
MacldWb=pb*tb*b*[0,0,0,0,0,0,0,0;
          0,13/35*L,11/210*L^2,0,0,9/70*L,-13/420*L^2,0;
          0,11/210*L^2,1/105*L^3,0,0,13/420*L^2,-1/140*L^3,0;
          0,0,0,0,0,0,0,0;
          0,0,0,0,0,0,0,0;
          0,9/70*L,13/420*L^2,0,0,13/35*L,-11/210*L^2,0;
          0,-13/420*L^2,-1/140*L^3,0,0,-11/210*L^2,1/105*L^3,0;
          0,0,0,0,0,0,0,0];

KacldUc=Ec*tc*b*[1/L,0,-1/L*(1/2*tb+tv+1/2*tc),tv/L,-1/L,0,1/L*(1/2*tb+tv+1/2*tc),-
      tv/L;
         0,12*(1/2*tb+tv+1/2*tc)^2/L^3,6*(1/2*tb+tv+1/2*tc)^2/L^2,0,0,-
      12*(1/2*tb+tv+1/2*tc)^2/L^3,6*(1/2*tb+tv+1/2*tc)^2/L^2,0;
         -
      1/L*(1/2*tb+tv+1/2*tc),6*(1/2*tb+tv+1/2*tc)^2/L^2,4*(1/2*tb+tv+1/2*tc)^2/L,
      -tv/L*(1/2*tb+tv+1/2*tc),1/L*(1/2*tb+tv+1/2*tc),-
      6*(1/2*tb+tv+1/2*tc)^2/L^2,2*(1/2*tb+tv+1/2*tc)^2/L,tv/L*(1/2*tb+tv+1/2*tc);
         tv/L,0,-tv/L*(1/2*tb+tv+1/2*tc),tv^2/L,-tv/L,0,tv/L*(1/2*tb+tv+1/2*tc),-
      tv^2/L;
         -1/L,0,1/L*(1/2*tb+tv+1/2*tc),-tv/L,1/L,0,-1/L*(1/2*tb+tv+1/2*tc),tv/L;
         0,-12*(1/2*tb+tv+1/2*tc)^2/L^3,-
      6*(1/2*tb+tv+1/2*tc)^2/L^2,0,0,12*(1/2*tb+tv+1/2*tc)^2/L^3,-
      6*(1/2*tb+tv+1/2*tc)^2/L^2,0;

      1/L*(1/2*tb+tv+1/2*tc),6*(1/2*tb+tv+1/2*tc)^2/L^2,2*(1/2*tb+tv+1/2*tc)^2/L,t
      v/L*(1/2*tb+tv+1/2*tc),-1/L*(1/2*tb+tv+1/2*tc),-
      6*(1/2*tb+tv+1/2*tc)^2/L^2,4*(1/2*tb+tv+1/2*tc)^2/L,-
      tv/L*(1/2*tb+tv+1/2*tc);
         -tv/L,0,tv/L*(1/2*tb+tv+1/2*tc),-tv^2/L,tv/L,0,-
      tv/L*(1/2*tb+tv+1/2*tc),tv^2/L];
KacldWc=Ec*Ic*[0,0,0,0,0,0,0,0;
         0,12/L^3,6/L^2,0,0,-12/L^3,6/L^2,0;
         0,6/L^2,4/L,0,0,-6/L^2,2/L,0;
         0,0,0,0,0,0,0,0;
         0,0,0,0,0,0,0,0;
```

```
        0,-12/L^3,-6/L^2,0,0,12/L^3,-6/L^2,0;
        0,6/L^2,2/L,0,0,-6/L^2,4/L,0;
        0,0,0,0,0,0,0,0];
MacldUc=pc*tc*b*[1/3*L,1/4*tb+1/2*tv+1/4*tc,11/12*(1/2*tb+tv+1/2*tc)*L-
      1/2*tb*L-L*tv-1/2*tc*L,1/3*L*tv,1/6*L,-1/4*tb-1/2*tv-
      1/4*tc,1/12*(1/2*tb+tv+1/2*tc)*L,1/6*L*tv;

      1/4*tb+1/2*tv+1/4*tc,6/5*(1/2*tb+tv+1/2*tc)^2/L,1/10*(1/2*tb+tv+1/2*tc)^2,1/
      2*(1/2*tb+tv+1/2*tc)*tv,1/4*tb+1/2*tv+1/4*tc,-
      6/5*(1/2*tb+tv+1/2*tc)^2/L,1/10*(1/2*tb+tv+1/2*tc)^2,1/2*(1/2*tb+tv+1/2*tc)
      *tv;
         11/12*(1/2*tb+tv+1/2*tc)*L-1/2*tb*L-L*tv-
      1/2*tc*L,1/10*(1/2*tb+tv+1/2*tc)^2,2/15*(1/2*tb+tv+1/2*tc)^2*L,-
      1/12*(1/2*tb+tv+1/2*tc)*L*tv,1/12*(1/2*tb+tv+1/2*tc)*L,-
      1/10*(1/2*tb+tv+1/2*tc)^2,-
      1/30*(1/2*tb+tv+1/2*tc)^2*L,1/12*(1/2*tb+tv+1/2*tc)*L*tv;
         1/3*L*tv,1/2*(1/2*tb+tv+1/2*tc)*tv,-
      1/12*(1/2*tb+tv+1/2*tc)*L*tv,1/3*tv^2*L,1/6*L*tv,-
      1/2*(1/2*tb+tv+1/2*tc)*tv,1/12*(1/2*tb+tv+1/2*tc)*L*tv,1/6*tv^2*L;
         1/6*L,1/4*tb+1/2*tv+1/4*tc,1/12*(1/2*tb+tv+1/2*tc)*L,1/6*L*tv,1/3*L,-
      1/4*tb-1/2*tv-1/4*tc,-1/12*(1/2*tb+tv+1/2*tc)*L,1/3*L*tv;
         -1/4*tb-1/2*tv-1/4*tc,-6/5*(1/2*tb+tv+1/2*tc)^2/L,-
      1/10*(1/2*tb+tv+1/2*tc)^2,-1/2*(1/2*tb+tv+1/2*tc)*tv,-1/4*tb-1/2*tv-
      1/4*tc,6/5*(1/2*tb+tv+1/2*tc)^2/L,-1/10*(1/2*tb+tv+1/2*tc)^2,-
      1/2*(1/2*tb+tv+1/2*tc)*tv;
         1/12*(1/2*tb+tv+1/2*tc)*L,1/10*(1/2*tb+tv+1/2*tc)^2,-
      1/30*(1/2*tb+tv+1/2*tc)^2*L,1/12*(1/2*tb+tv+1/2*tc)*L*tv,-
      1/12*(1/2*tb+tv+1/2*tc)*L,-
      1/10*(1/2*tb+tv+1/2*tc)^2,2/15*(1/2*tb+tv+1/2*tc)^2*L,-
      1/12*(1/2*tb+tv+1/2*tc)*L*tv;

      1/6*L*tv,1/2*(1/2*tb+tv+1/2*tc)*tv,1/12*(1/2*tb+tv+1/2*tc)*L*tv,1/6*tv^2*L,
      1/3*L*tv,-1/2*(1/2*tb+tv+1/2*tc)*tv,-
      1/12*(1/2*tb+tv+1/2*tc)*L*tv,1/3*tv^2*L];
MacldWc=pc*tc*b*[0,0,0,0,0,0,0,0;
        0,13/35*L,11/210*L^2,0,0,9/70*L,-13/420*L^2,0;
        0,11/210*L^2,1/105*L^3,0,0,13/420*L^2,-1/140*L^3,0;
        0,0,0,0,0,0,0,0;
        0,0,0,0,0,0,0,0;
        0,9/70*L,13/420*L^2,0,0,13/35*L,-11/210*L^2,0;
        0,-13/420*L^2,-1/140*L^3,0,0,-11/210*L^2,1/105*L^3,0;
        0,0,0,0,0,0,0,0];

KacldVv=Gv*tv*b*[0,0,0,0,0,0,0,0;
        0,0,0,0,0,0,0,0;
        0,0,0,0,0,0,0,0;
```

```
            0,0,0,1/3*L,0,0,0,1/6*L;
            0,0,0,0,0,0,0,0;
            0,0,0,0,0,0,0,0;
            0,0,0,0,0,0,0,0;
            0,0,0,1/6*L,0,0,0,1/3*L];
MacldUv=pv*tv*b*[1/3*L,1/4*tb+1/4*tv,11/12*(1/2*tb+1/2*tv)*L-1/2*tb*L-
        1/2*L*tv,1/6*L*tv,1/6*L,-1/4*tb-1/4*tv,1/12*(1/2*tb+1/2*tv)*L,1/12*L*tv;

        1/4*tb+1/4*tv,6/5*(1/2*tb+1/2*tv)^2/L,1/10*(1/2*tb+1/2*tv)^2,1/4*(1/2*tb+1/2
        *tv)*tv,1/4*tb+1/4*tv,-
        6/5*(1/2*tb+1/2*tv)^2/L,1/10*(1/2*tb+1/2*tv)^2,1/4*(1/2*tb+1/2*tv)*tv;
           11/12*(1/2*tb+1/2*tv)*L-1/2*tb*L-
        1/2*L*tv,1/10*(1/2*tb+1/2*tv)^2,2/15*(1/2*tb+1/2*tv)^2*L,-
        1/24*(1/2*tb+1/2*tv)*L*tv,1/12*(1/2*tb+1/2*tv)*L,-1/10*(1/2*tb+1/2*tv)^2,-
        1/30*(1/2*tb+1/2*tv)^2*L,1/24*(1/2*tb+1/2*tv)*L*tv;
           1/6*L*tv,1/4*(1/2*tb+1/2*tv)*tv,-
        1/24*(1/2*tb+1/2*tv)*L*tv,1/12*tv^2*L,1/12*L*tv,-
        1/4*(1/2*tb+1/2*tv)*tv,1/24*(1/2*tb+1/2*tv)*L*tv,1/24*tv^2*L;
           1/6*L,1/4*tb+1/4*tv,1/12*(1/2*tb+1/2*tv)*L,1/12*L*tv,1/3*L,-1/4*tb-
        1/4*tv,-1/12*(1/2*tb+1/2*tv)*L,1/6*L*tv;
          -1/4*tb-1/4*tv,-6/5*(1/2*tb+1/2*tv)^2/L,-1/10*(1/2*tb+1/2*tv)^2,-
        1/4*(1/2*tb+1/2*tv)*tv,-1/4*tb-1/4*tv,6/5*(1/2*tb+1/2*tv)^2/L,-
        1/10*(1/2*tb+1/2*tv)^2,-1/4*(1/2*tb+1/2*tv)*tv;
           1/12*(1/2*tb+1/2*tv)*L,1/10*(1/2*tb+1/2*tv)^2,-
        1/30*(1/2*tb+1/2*tv)^2*L,1/24*(1/2*tb+1/2*tv)*L*tv,-
        1/12*(1/2*tb+1/2*tv)*L,-1/10*(1/2*tb+1/2*tv)^2,2/15*(1/2*tb+1/2*tv)^2*L,-
        1/24*(1/2*tb+1/2*tv)*L*tv;

        1/12*L*tv,1/4*(1/2*tb+1/2*tv)*tv,1/24*(1/2*tb+1/2*tv)*L*tv,1/24*tv^2*L,1/6*
        L*tv,-1/4*(1/2*tb+1/2*tv)*tv,-1/24*(1/2*tb+1/2*tv)*L*tv,1/12*tv^2*L];
MacldWv=pv*tv*b*[0,0,0,0,0,0,0,0;
            0,13/35*L,11/210*L^2,0,0,9/70*L,-13/420*L^2,0;
            0,11/210*L^2,1/105*L^3,0,0,13/420*L^2,-1/140*L^3,0;
            0,0,0,0,0,0,0,0;
            0,0,0,0,0,0,0,0;
            0,9/70*L,13/420*L^2,0,0,13/35*L,-11/210*L^2,0;
            0,-13/420*L^2,-1/140*L^3,0,0,-11/210*L^2,1/105*L^3,0;
            0,0,0,0,0,0,0,0];

KacId=(KacldUb+KacldUc)+(KacldWb+KacldWc);
MacId=(MacldUb+MacldUv+MacldUc)+(MacldWb+MacldWv+MacldWc);
KacldV=KacldVv;

function[Mbeam,Dbeam,Kbeam,BBcbeam,CCcbeam]=Beam_Matrix(Eb,pb,tb,Ib,b,L);

KbeamU=Eb*tb*b*[1/L,0,0,-1/L,0,0;
```

```
            0,0,0,0,0,0;
            0,0,0,0,0,0;
            -1/L,0,0,1/L,0,0;
            0,0,0,0,0,0;
            0,0,0,0,0,0];
KbeamW=Eb*Ib*[0,0,0,0,0,0;
          0,12/L^3,6/L^2,0,-12/L^3,6/L^2;
          0,6/L^2,4/L,0,-6/L^2,2/L;
          0,0,0,0,0,0;
          0,-12/L^3,-6/L^2,0,12/L^3,-6/L^2;
          0,6/L^2,2/L,0,-6/L^2,4/L];
MbeamU=pb*tb*b*[1/3*L,0,0,1/6*L,0,0;
            0,0,0,0,0,0;
            0,0,0,0,0,0;
            1/6*L,0,0,1/3*L,0,0;
            0,0,0,0,0,0;
            0,0,0,0,0,0];
MbeamW=pb*tb*b*[0,0,0,0,0,0;
            0,13/35*L,11/210*L^2,0,9/70*L,-13/420*L^2;
            0,11/210*L^2,1/105*L^3,0,13/420*L^2,-1/140*L^3;
            0,0,0,0,0,0;
            0,9/70*L,13/420*L^2,0,13/35*L,-11/210*L^2;
            0,-13/420*L^2,-1/140*L^3,0,-11/210*L^2,1/105*L^3];

Kbeam=KbeamU+KbeamW;
Mbeam=MbeamU+MbeamW;
Dbeam=zeros(6,6);
BBcbeam=zeros(6,1);
CCcbeam=zeros(1,6);

function[Ae,Re]=decomposition(Gv,KacldV);

KacldVbar=(1/Gv)*KacldV;

[U,S,V]=svd(KacldVbar);

Abar=S;
Rbar=U;

lamda=diag(Abar);

count=0;
flag=1;

for i=1:8;
  if (lamda(i)<=0)
```

```
    count=count;
  else
    Ae(flag,flag)=lamda(i);
    Re(:,flag)=Rbar(:,i);
  end
    count=count+1;
    flag=flag+1;
end

function[MMacld,DDacld,KKacld]=arrange(Macld,Kacld,Kacldv,parw1,parz1,paralpha
        1,parw2,parz2,paralpha2,parw3,parz3,paralpha3,Gv,Ae,Re);

MMacld=zeros(14,14);
DDacld=zeros(14,14);
KKacld=zeros(14,14);

w1=parw1;
w2=parw2;
w3=parw3;
z1=parz1;
z2=parz2;
z3=parz3;
ar1=paralpha1;
ar2=paralpha2;
ar3=paralpha3;

A=Gv*Ae;
R=Re*A;
Rt=R';

KK=Kacld+(1+ar1+ar2+ar3)*Kacldv;

%%% Compute MMacld %%%
for ir=1:2;
   irs=ir+4;
  for ic=1:2;
     ics=ic+4;
    MMacld(irs,ics)=MMacld(irs,ics)+((ar1/w1^2)*A(ir,ic));
  end
end
for ir=1:2;
   irs=ir+6;
  for ic=1:2;
     ics=ic+6;
    MMacld(irs,ics)=MMacld(irs,ics)+((ar2/w2^2)*A(ir,ic));
  end
```

```
 end
 for ir=1:2;
    irs=ir+8;
   for ic=1:2;
      ics=ic+8;
     MMacld(irs,ics)=MMacld(irs,ics)+((ar3/w3^2)*A(ir,ic));
   end
 end

 for ir=1:4;
   for ic=1:4;
     MMacld(ir,ic)=MMacld(ir,ic)+Macld(ir,ic);
   end
 end

 for ir=1:4;
   for ic=5:8;
     ics=ic+6;
     MMacld(ir,ics)=MMacld(ir,ics)+Macld(ir,ic);
   end
 end

 for ir=5:8;
  irs=ir+6;
 for ic=1:4;
   MMacld(irs,ic)=MMacld(irs,ic)+Macld(ir,ic);
 end
 end

 for ir=5:8;
   irs=ir+6;
  for ic=5:8;
    ics=ic+6;
    MMacld(irs,ics)=MMacld(irs,ics)+Macld(ir,ic);
  end
 end

 %%% Compute DDacld %%%
 for ir=1:2;
    irs=ir+4;
   for ic=1:2;
      ics=ic+4;
     DDacld(irs,ics)=DDacld(irs,ics)+((2*ar1*z1/w1)*A(ir,ic));
   end
 end
 for ir=1:2;
```

```
   irs=ir+6;
  for ic=1:2;
     ics=ic+6;
    DDacld(irs,ics)=DDacld(irs,ics)+((2*ar2*z2/w2)*A(ir,ic));
  end
end
for ir=1:2;
   irs=ir+8;
  for ic=1:2;
     ics=ic+8;
    DDacld(irs,ics)=DDacld(irs,ics)+((2*ar3*z3/w3)*A(ir,ic));
  end
end

%%% Compute KKacld %%%
for ir=1:2;
   irs=ir+4;
  for ic=1:2;
     ics=ic+4;
    KKacld(irs,ics)=KKacld(irs,ics)+(ar1*A(ir,ic));
  end
end
for ir=1:2;
   irs=ir+6;
  for ic=1:2;
     ics=ic+6;
    KKacld(irs,ics)=KKacld(irs,ics)+(ar2*A(ir,ic));
  end
end
for ir=1:2;
   irs=ir+8;
  for ic=1:2;
     ics=ic+8;
    KKacld(irs,ics)=KKacld(irs,ics)+(ar3*A(ir,ic));
  end
end

for ir=1:4;
  for ic=1:4;
    KKacld(ir,ic)=KKacld(ir,ic)+KK(ir,ic);
  end
end
for ir=1:4;
  for ic=5:8;
    ics=ic+6;
    KKacld(ir,ics)=KKacld(ir,ics)+KK(ir,ic);
```

```
    end
  end
  for ir=5:8;
   irs=ir+6;
  for ic=1:4;
    KKacld(irs,ic)=KKacld(irs,ic)+KK(ir,ic);
  end
  end
  for ir=5:8;
    irs=ir+6;
   for ic=5:8;
     ics=ic+6;
     KKacld(irs,ics)=KKacld(irs,ics)+KK(ir,ic);
   end
  end


  for ir=1:4;
    for ic=1:2;
      ics=ic+4;
      KKacld(ir,ics)=KKacld(ir,ics)-(ar1*R(ir,ic));
    end
  end
  for ir=1:4;
    for ic=1:2;
      ics=ic+6;
      KKacld(ir,ics)=KKacld(ir,ics)-(ar2*R(ir,ic));
    end
  end
  for ir=1:4;
    for ic=1:2;
      ics=ic+8;
      KKacld(ir,ics)=KKacld(ir,ics)-(ar3*R(ir,ic));
    end
  end

  for ir=5:8;
    irs=ir+6;
    for ic=1:2;
      ics=ic+4;
      KKacld(irs,ics)=KKacld(irs,ics)-(ar1*R(ir,ic));
    end
  end
  for ir=5:8;
   irs=ir+6;
   for ic=1:2;
```

```
      ics=ic+6;
      KKacld(irs,ics)=KKacld(irs,ics)-(ar2*R(ir,ic));
    end
  end
  for ir=5:8;
    irs=ir+6;
    for ic=1:2;
      ics=ic+8;
      KKacld(irs,ics)=KKacld(irs,ics)-(ar3*R(ir,ic));
    end
  end

  for ir=1:2;
    irs=ir+4;
    for ic=1:4;
      KKacld(irs,ic)=KKacld(irs,ic)-(ar1*Rt(ir,ic));
    end
  end
  for ir=1:2;
    irs=ir+6;
    for ic=1:4;
      KKacld(irs,ic)=KKacld(irs,ic)-(ar2*Rt(ir,ic));
    end
  end
  for ir=1:2;
    irs=ir+8;
    for ic=1:4;
      KKacld(irs,ic)=KKacld(irs,ic)-(ar3*Rt(ir,ic));
    end
  end

  for ir=1:2;
    irs=ir+4;
    for ic=5:8;
      ics=ic+6;
      KKacld(irs,ics)=KKacld(irs,ics)-(ar1*Rt(ir,ic));
    end
  end
  for ir=1:2;
    irs=ir+6;
    for ic=5:8;
      ics=ic+6;
      KKacld(irs,ics)=KKacld(irs,ics)-(ar2*Rt(ir,ic));
    end
  end
  for ir=1:2;
```

```
  irs=ir+8;
  for ic=5:8;
    ics=ic+6;
    KKacld(irs,ics)=KKacld(irs,ics)-(ar3*Rt(ir,ic));
  end
end

function[Inew]=MOGA(Iga,Fitness);

%--------------------------------%
% Selection for reproduction %
%--------------------------------%
norm_fit=Fitness/sum(Fitness);
selected=rand(size(Iga,1),1);
sum_fit=0;

for i=1:length(Fitness)
  sum_fit=sum_fit+norm_fit(i);
  index=find(selected<sum_fit);
  selected(index)=i*ones(size(index));
end

Iselected=Iga(selected,:);

%--------------------------------%
% Reordering for Crossover %
%--------------------------------%
[juck,order]=sort(rand(size(Iga,1),1));
Iordered=Iselected(order,:);

%-------------%
% Crossover %
%-------------%
sites=ceil(rand((size(Iga,1)/2),1)*(size(Iga,2)-1));
sites=sites.*(rand(size(sites))<0.8);
for i=1:length(sites);
  if (sites(i)<=11 & sites(i)~=0)
Icrossed([(2*i)-1    2*i],:)=[Iordered([(2*i)-1    2*i],1:sites(i)),Iordered([2*i    (2*i)-
      1],sites(i)+1:size(Iga,2))];
  elseif (sites(i)>11 & sites(i)~=0)
Icrossed([(2*i)-1    2*i],:)=[Iordered([(2*i)-1    2*i],1:sites(i)),Iordered([2*i    (2*i)-
      1],sites(i)+1:size(Iga,2))];
V1=rand(1);
V2=rand(1);
Icrossed((2*i)-1,sites(i))=(V1*Iordered((2*i)-1,sites(i)))+((1-
      V1)*Iordered(2*i,sites(i)));
```

```
Icrossed(2*i,sites(i))=(V2*Iordered(2*i,sites(i)))+((1-V2)*Iordered((2*i)-1,sites(i)));
   else
Icrossed((2*i)-1,:)=Iordered(2*i,:);
Icrossed(2*i,:)=Iordered((2*i)-1,:);
   end
end
Icrossed;

%------------%
% Mutation %
%------------%
Imutated=Icrossed;

mutate=find(rand(size(Iga))<0.05);

for i=1:length(mutate)
   if (mutate(i)<=2200)
     Imutated(mutate)=1-Icrossed(mutate);
   end
   V=rand(1);
   if (mutate(i)>=2201 & mutate(i)<=2400)
     Imutated(mutate(i))=(V*(1-0.01))+0.01;
   end
   if (mutate(i)>=2401 & mutate(i)<=2600)
     Imutated(mutate(i))=(V*(1-0.01))+0.01;
   end
   if (mutate(i)>=2601 & mutate(i)<=3200)
     Imutated(mutate(i))=(V*(3-0))+0;
   end
   if (mutate(i)>=3201 & mutate(i)<=3800)
     Imutated(mutate(i))=(V*(500-100))+100;
   end
   if (mutate(i)>=3801 & mutate(i)<=4400)
     Imutated(mutate(i))=(V*(20-0))+0;
   end
   if (mutate(i)>=4401 & mutate(i)<=5000)
     Imutated(mutate(i))=(V*(500-100))+100;
  end
end

%--------------------%
% New Generation %
%--------------------%
Inew=Imutated;
```

REFERENCES

[1] Frost, P. "Smart materials provide for self-adjusting satellite antennas". *Science Daily News Releases*, (1998)

[2] Baz, A. "Active constrained layer damping". U.S. Patent, 5,485,053, Jan. (1996)

[3] Austin, F., Rossi, M. J., Jameson, A., Van Nostrand, W., Su, J. and Knowles, G. "Active rib experiment for adaptive conformal wing". *Proceedings of the Third International Conference on Adaptive Structures*, San Diego, CA, pp.43-55 (1992)

[4] Austin, F., Van Nostrand, W. and Rossi, M. J. "Shape control of structures with semi-definite stiffness matrices for adaptive wings". *Proceedings of the Smart Structures and Materials 1993*, Bellingham, WA, pp.419-425 (1993)

[5] Austin, F., Rossi, M. J., Van Nostrand, W. and Knowles, G. "Static shape control for adaptive wings". *AIAA Journal*, Vol. 32, pp.1895-1901 (1994)

[6] Ananthasuresh, G. K. and Kota, S. "Designing compliant mechanism". *Mechanical Engineering*, Vol. 117, pp.93-96 (1995)

[7] Saggere, L. and Kota, S. "Static shape control of smart structures using compliant mechanisms". *AIAA Journal*, Vol. 37, pp.572-578 (1999)

[8] Lu, K. J. and Kota, S. "Compliant mechanisms synthesis for shape-change applications: preliminary results". *Proceedings of SPIE*, pp.161-172 (2002)

[9] Chaudhry Z. and Rogers C. A. "Bending and shape control of beams using SMA actuators". *Journal of Intelligent Material Systems and Structures*, Vol. 2, pp.581-602 (1991)

[10] Baz, A., Chen, T. and Ro., J. "Shape control of nitinol-reinforced composite beams". *Journal of Composite Engineering: Part B*, Vol. 31, pp.631-642, (2000)

[11] Song, G., Kelly, B. and Agrawal, B.N. "Active position control of a shape memory alloy wire actuated composite beam". *Smart Materials and Structures*, Vol. 9, pp.711-716 (2000)

[12] Oh, J. T., Park, H. C. and Hwang W. "Active shape control of a double-plate structures using piezoceramics and SMA wires". *Smart Materials and Structures*, Vol. 10, pp.1100-1106 (2001)

[13] Irschik, H. "A review on static and dynamic shape control of structures by piezoelectric actuation". *Engineering Structures*, Vol. 24, pp.5-11 (2002)

[14] Donthireddy, P. and Chandrashekhara, K. "Modeling and shape control of composite beams with embedded piezoelectric actuators". *Composite Structures*, Vol. 35, pp.237-244 (1996)

[15] Jenkins, C. H., Kalanovic, V. D., Padmanabhan, K. and Faisal S. M. "Intelligent shape control for precision membrane antennae and reflectors in space". *Smart Materials and Structures*, Vol. 8, pp.857-867 (1999)

[16] Yang, S. and Ngoi, B. "Shape control of beams by piezoelectric actuators". *AIAA Journal*, Vol. 38, pp.2292-2298 (2000)

[17] Kekana, M., Tabakov, P. and Walker, M. "A shape control model for piezo-elastic structures based in divergence free electric displacement". *International Journal of Solids and Structures*, Vol. 40, pp.715-727 (2003)

[18] Wang, Z., Chen, S. and Han, W. "The static shape control for intelligent structures". *Finite Elements in Analysis and Design*, Vol. 26, pp.303-314 (1997)

[19] Tong, D., Williams II, R. L. and Agrawal, S. K. "Optimal shape control of composite thin plates with piezoelectric actuators". *Journal of Intelligent Material Systems and Structures*, Vol. 9, pp.458-467 (1998)

[20] Lin, C. C. and Hsu, C. Y. "Static shape control of smart beam plates laminated with sine sensors and actuators" *Smart Materials and Structures*, Vol. 8, pp.519-530 (1999)

[21] Bruch, J. C., Sloss, J. M., Adali, S. and Sadek, I. S. "Optimal piezo-actuator locations/lengths and applied voltage for shape control of beams". *Smart Materials and Structures*, Vol. 9, pp.205-211 (2000)

[22] Adali, S., Bruch, J. C., Sadek, I. S. and Sloss J. M. "Robust shape control of beams with load uncertainties by optimally placed piezo actuators". *Structural and Multidisciplinary Optimization*, Vol. 19, pp.274-281 (2000)

[23] Sheng, L. and Kapania, R. K. "Genetic algorithms for optimization of piezoelectric actuator locations". *AIAA Journal*, Vol. 39, pp.1818-1822 (2001)

[24] Chandrashekhara, K. and Varadarajan, S. "Adaptive shape control of composite beams with piezoelectric actuators". *Journal of Intelligent Material Systems and Structures*, Vol. 8, pp.112-124 (1997)

[25] Varadarajan, S., Chandrashekhara, K. and Agarwal, S. "Adaptive shape control of laminated composite plates using piezoelectric materials". *AIAA Journal*, Vol. 36, pp.1694-1698 (1998)

[26] Agrawal, B. N. and Treanor K. E. "Shape control of a beam using piezoelectric actuators". *Smart Materials and Structures*, Vol. 8, pp.729-740 (1999)

[27] Wang, C. M., Ang, K. K. and Ajit, A. "Shape control of laminated cantilevered beams with piezoelectric actuators". *Journal of Intelligent Material Systems and Structures*, Vol. 10, pp.164-175 (1999)

[28] Fitzpatrick, B. G. "Shape matching with smart material structures using piezoceramic actuators". *Journal of Intelligent Material Systems and Structures*, Vol. 8, pp.876-882 (1997)

[29] Kalaycioglu, S. and Silva D. "Minimization of vibration of spacecraft appendages during shape control using smart structures". *Journal of Guidance, control and dynamics*, Vol. 23, pp.558-561 (2000)

[30] Benjeddou, A. "Advances in hybrid active-passive vibration and noise control via piezoelectric and viscoelastic constrained layer treatments". *Journal of Vibration and Control*, Vol. 7, pp.565-602 (2001)

[31] Plump, J. M. and Hubbard, J. E. "Modeling of an active constrained layer damper". *Proceedings of 12th International Congress on Acoustics*, Toronto, Canada, Paper D4-1 (1996)

[32] Agnes, G. and Napolitano, K. "Active constrained layer viscoelastic damping". *Proceedings of 34th AIAA/ASME/ASCE/AHS/ASC Structures, Structural Dynamics and Materials Conference*, pp.3499-3506 (1993)

[33] Baz, A. and Ro, J. "The concept and performance of active constrained layer damping treatment". *Sound and Vibration Magazine*, March issue, pp.18-21 (1994)

[34] Baz, A. and Ro, J. "Performance characteristics of active constrained layer damping". *Journal of Shock and Vibration*, Vol. 2, pp.33-42 (1995)

[35] Baz, A. and Ro, J. "Partial treatment of flexible beams with active constrained layer damping". *Journal of Sound and Vibration*, Vol. 52, pp.269-997 (1993)

[36] Ray, M. C. and Baz, A. "Control of nonlinear vibration of beams using active constrained layer damping". *Journal of Vibration and Control*, Vol. 7, pp.539-549 (2001)

[37] Shen, I. Y. "Hybrid damping through intelligent constrained layer treatments". *ASME Journal of Vibration and Acoustics*, Vol. 116, pp.341-349 (1994a)

[38] Shen, I. Y. "Bending vibration control of composites and isotropic plates through intelligent constrained layer treatments". *Smart Material and Structures*, Vol. 3, pp.59-70 (1994b)

[39] Shen, I. Y. "Stability and controllability of Euler-Bernoulli beams with intelligent constrained layer treatments". *ASME Journal of Vibration and Acoustics*, Vol. 118, pp.70-77 (1996)

[40] Nostrand, V. and Inman, D.J. "Finite element model for active constrained layer damping". *SPIE in Active Materials and Smart Structures*, Vol. 2427, pp.124-139 (1995)

[41] Lesieutre, G. A. and Lee, U. "A finite element for beams having segmented active constrained layers with frequency-dependent viscoelastic". *Smart Materials and Structures*, Vol. 5, pp.615-627 (1996)

[42] Trindade, M. A., Benjeddou, A. and Ohayon, R. "Modeling of frequency-dependent viscoelastic materials for active-passive vibration damping". *ASME Journal of Vibration and Acoustics*, Vol. 122, pp.169-174 (2000)

[43] Trindade, M. A., Benjeddou, A. and Ohayon, R. "Piezoelectric active vibration control of damped sandwich beams". *Journal of Sound and Vibration*, Vol. 246, pp.653-677 (2001)

[44] Lam, M. J., Saunders, W. R., and Inman, D. J. "Modeling active constrained layer damping using Golla-Hughes-McTavish approach". *Proceedings of Conference on Smart Structures and Materials*, SPIE Vol. 2445, pp.86-97 (1995)

[45] Liao, W. H. and Wang, K. W. "On the analysis of viscoelastic materials for active constrained layer damping treatments". *Journal of Sound and Vibration*, Vol. 207, pp.319-334 (1997a)

[46] Lim, Y. H., Varadan, V. V. and Varadan V. K. "Closed loop finite-element modeling of active constrained layer damping in the time domain analysis". *Smart Materials and Structures*, Vol. 11, pp.89-97 (2002)

[47] Lee, U. and Kim, J. "Spectral element modeling for the beams treated with active constrained layer damping". *International Journal of Solids and Structures*, Vol. 38, pp.5679-5702 (2001)

[48] Azvine, B., Tomlinson, G. R. and Wynne, R, J. "Use of active constrained layer damping for controlling resonant vibration". *Smart Materials and Structures*, Vol. 4, pp.1-6 (1995)

[49] Veley, D. E. and Rao, S. S. "A comparison of active, passive and hybrid damping in structural design". *Smart Materials and Structures*, Vol. 5, pp.660-671 (1996)

[50] Lam, M. J., Inman, D. J. and Saunders, W. R. "Vibration control through passive constrained layer damping and active control". *Journal of Intelligent Material Systems and Structures*, Vol. 8, pp.663-677 (1997)

[51] Lam, M. J., Inman, D. J. and Saunders, W. R. "Hybrid damping models using the Golla-Hughes-McTavish method with internally balanced model reduction and output feedback". *Smart Material and Structures*, Vol. 9, pp.362-371 (2000)

[52] Yellin, J. M. and Shen, I. Y. "A self-Sensing active constrained layer damping treatment for Euler-Bernoulli beam," *Smart Materials and Structures*, Vol. 5, pp.628-637 (1996)

[53] Dosch, J. J., and Inman, D. J. "A self-sensing piezoelectric actuator for collocated control". *Journal of Intelligent Material Systems and Structures*, Vol. 3, pp.166-185 (1992)

[54] Liao, W. H. and Wang, K. W. "On the active-passive hybrid control actions of active constrained layers". *ASME Journal of Vibration and Acoustics,* Vol. 119, pp.563-572 (1997b)

[55] Liao, W. H. and Wang, K. W. "A new active constrained layer configuration with enhanced boundary actions". *Smart Materials and Structures*, Vol. 5, pp.638-648 (1996)

[56] Liu, Y. and Wang, K. W. "A non-dimensional parametric study of enhanced active constrained layer damping treatments". *Journal of Sound and Vibration,* Vol. 233, pp.611-644 (1999)

[57] Marcelin, J. L., Trompette, P. and Smati, A. "Optimal constrained layer damping with partial coverage". *Finite Elements in Analysis and Design*, Vol. 12, pp.273-280 (1992)

[58] Marcelin, J. L., Shakhesi, S. and Pourroy, F. "Optimal constrained layer damping of beams: experimental and numerical studies". *Shock and Vibration*, Vol. 2, pp.445-450 (1995)

[59] Chen, Y, C. and Huang, S. C. "An optimal placement of CLD treatment for vibration suppression of plates". *International Journal of Mechanical Sciences*, Vol. 44, pp.1801-1821 (2002)

[60] Pau, G. S. H., Zheng, H. and Liu, G. R. "A comparative study on optimization of constrained layer damping for vibration control of beams". *High Performance Computation for Engineered Systems*, (2003)

[61] Baz, A. and Ro, J. "Optimum design and control of active constrained layer damping". *ASME Special 50th Anniversary Design Issue*, Vol. 117, pp.135-144 (1995)

[62] Ro, J. and Baz, A. "Optimum design and control of partial active constrained layer damping treatments". *Proceedings of the American Control Conference*, Settle, Washington, (1995)

[63] Huang, S. C., Inman, D. J. and Austin, E. M. "Some design considerations for active and passive constrained layer damping treatments". *Smart Materials and Structures*, Vol. 5, pp.301-313 (1996)

[64] Clark, R. L. and Fuller, C. R. "Optimal placement of piezoelectric actuators and polyvinylidenefluoride error sensors in active structural acoustic control approaches". *Journal of the Acoustical Society of America*, Vol. 92, pp.1521-1533 (1992)

[65] Devasia, S. Meressi, T., Paden, B. and Bayo, E. "Piezoelectric actuator design for vibration suppression: placement and sizing". *Journal of Guidance, Control, and Dynamics*, Vol. 16, pp.859-864 (1993).

[66] Wang, B. T., Burdisso, R. A. and Fuller, C. R. "Optimal placement of piezoelectric actuators for active structural acoustic control" *Journal of Intelligent Material Systems and Structures*, Vol. 5, pp.67-77 (1994)

[67] Main, J. A., Garcia, E. and Howars, D. "Optimal placement and sizing of paired piezoactuators in beams and plates". *Smart Materials and Structures*, Vol. 3, pp.373-381 (1994)

[68] Nam, C., Kim, Y. and Weisshaar, T. A. "Optimal sizing and placement of piezo-actuators for active flutter suppression". *Smart Materials and Structures*, Vol. 5, pp.216-224 (1996)

[69] Kapania, R. K. and Sheng, L. "Toward more effective genetic algorithms for the optimization of piezoelectric actuator locations". *AIAA Journal*, Vol. 40, pp.1246-1250 (2002)

[70] Kim, J., Varadan, V. V. and Varadan, V. K. "Finite element-optimization methods for the active control of radiated sound from a plate structure". *Smart Materials and Structures*, Vol. 4, pp.318-326 (1995)

[71] Varadan, V. V., Kim, J. and Varadan, V. K. "Optimal placement of piezoelectric actuators for active noise control" *AIAA Journal*, Vol. 35, pp.526-33 (1997)

[72] Kim, J. and Ko, B. "Optimal design of a piezoelectric smart structure for noise control". *Smart Materials and Structures*, Vol. 7, pp.801-808 (1998)

[73] Yousefi-koma, A. and Vukovich, G. "Optimization of piezoactuator configuration in control of flexible structures". *Journal of Intelligent Material Systems and Structures*, Vol. 10, pp.787-796 (1999)

[74] Wang, Z., Chen, S. and Han, W. "Integrated structural and control optimization of intelligent structures". *Engineering Structures*, Vol. 21, pp.183-191 (1999)

[75] Zhang, H., Lennox, B., Goulding, P. R. and Leung, A. Y. T. "A float-encoded genetic algorithm technique for integrated optimization of piezoelectric actuator and sensor placement and feedback gains". *Smart Materials and Structures*, Vol. 9, pp.552-557 (2000)

[76] Beri. R., Chattopadhyay, A. and Nam, C. "Integrated structures/controls optimization of a smart composite plate with segmented active constrained layer damping". *Proceedings of*, SPIE Vol. 3985 (2000)

[77] Liu, Y. and Wang, K. W. "Damping optimization by integrating enhanced active constrained layer and active-passive hybrid constrained layer treatments". *Journal of Sound and Vibration*, Vol. 255, pp.763-775 (2002)

[78] Maxwell N. D. and Asokanthan, S. F. "Optimally distributed actuator placement and control for a slewing single-link flexible manipulator". *Smart Materials and Structures*, Vol. 12, pp.287-296 (2003)

[79] ANSI-IEEE Std 176-1987 *IEEE Standard on Piezoelectricity* (1987)

[80] Golla, D. F. and Hughes, P. C. "Dynamics of viscoelastic structures - a time domain finite element formulation". *Journal of Applied Mechanics*, Vol. 52, pp.897-906 (1985)

[81] McTavish, D. J. and Hughes, P. C. "Modeling of linear viscoelastic space structures". *ASME Journal of Vibration and Acoustics*, Vol. 115, pp.103-110 (1993)

[82] Christensin, R. M. "Theory of Viscoelasticity: an Introduction" New York: Academic Press; second edition (1971)

[83] Shi, Y. M., Li, Z. F., Hua, H. X. and Fu, Z. F. "The modeling and vibration control of beams with active constrained layer damping". *Journal of Sound and Vibration*, Vol. 245, pp.785-800 (2001)

[84] Soovere, J. and Drake, M. L. "Aerospace structures technology damping design guide" Vol. III (1985)

[85] Liao, W. H. "An enhanced self-sensing piezoelectric actuator" *International Conference on Mechatronics and Machine Vision in Practice*, pp.201-206 (1998)

[86] Veley, D. E. and Rao, S. S. "Two-dimensional finite element modeling of constrained layer damping". *Proceedings of SPIE Smart Structures and Materials*, Vol. 52193 pp.276-283 (1994)

[87] Fonseca, C. M. and Fleming, P. J. "Multiobjective optimization and multiple constraint handling with evolutionary algorithms – Part I: a unified formulation" *IEEE Transactions on System, Man and Cybernetics*, Vol. 28, pp.26-37 (1998)

[88] Treanor, K. E. "Performance and optimal placement of piezoelectric actuators for shape control of a cantilever beam". MSc Thesis, Naval Postgraduate School (1996)

[89] Davis, L. "Handbook of genetic algorithm". Van Nostrand Reinhold, New York (1991)

[90] Goldberg, D. E. "Genetic algorithm in search, optimization and machine learning". Reading, Mass: Addison Wesley, (1989)

[91] Michalewics, Z. "Genetic algorithms + data structures = evolution program". Berlin: Springer, (1996)

[92] Kurpati, A., Azarm, S. and Wu, J. "Constraint handling improvements for multiobjective genetic algorithms". *Structural Multidisciplinary Optimization*, Vol. 23, pp.204-213 (2002)

[93] Kim, J. W., Kim, S. W., Park, P. G. and Park, T. J. "On the similarities between binary-coded GA and real-coded GA in wide search space". *IEEE*, pp.681-686 (2002)

[94] Kalyanmoy, D. "Multi-objective optimization using evolutionary algorithms". New York: John Wiley and Sons, (2001)